NOAA Technical Memorandum, OAR-AOML-104
Prepared for the South Florida Water Management District
Under contract C-10806

Investigation of Intra-seasonal to Multi-decadal Variability in South Florida Rainfall

Alberto M. Mestas-Nuñez
David B. Enfield

Atlantic Oceanographic and Meteorological Laboratory
Miami, Florida
March 2003

noaa NATIONAL OCEANIC AND ATMOSPHERIC ADMINISTRATION / Oceanic and Atmospheric Research Laboratories

Investigation of Intra-seasonal to Multi-decadal Variability in South Florida Rainfall

Final Report

Alberto M. Mestas-Nuñez [(1)] and David B. Enfield [(2)]

[(1)] Cooperative Institute for Marine and Atmospheric Studies (CIMAS), U. of Miami
[(2)] NOAA, Atlantic Oceanographic and Meteorological Laboratory (AOML)

March 2003

Abstract

We investigated different climatic factors affecting South Florida (climate divisions 4, 5 and 6) precipitation. The climatic indexes used here are based on over a century of global sea surface temperature anomalies. The climatic associations are studied for different seasons and in three frequency bands (intra-seasonal, inter-annual and decadal). We found that the known ENSO relationship for winter/spring (wetter than normal South Florida rainfall anomalies during El Niño) does not hold during the summer. We attribute this to an opposite relationship on intra-seasonal South Florida precipitation (dry during El Niño) that exists during that season. The ENSO associations with South Florida unfiltered precipitation depend on the different phases of the North Atlantic and Eastern North Pacific decadal variability. In general, decadal warming of the Eastern North Pacific and North Atlantic are associated with wetter decades of south Florida precipitation. Seasonal outlooks of south Florida precipitation ought to consider SST variability associated with ENSO, and from decadal modes of variability in the Pacific and the Atlantic.

Table of Contents

Acknoweledgements

We thank Paul Trimble and Chris Landsea for helpful discussions. Jay Harris helped with the preparation of the datasets and Gail Derr with the production of this report. Funding came from the South Florida Water Management District (contract C-10806) and the National Oceanic and Atmospheric Administration.

1. Introduction

This report summarizes the results of an investigation into the climate factors affecting South Florida rainfall supported by a research contract between the NOAA Atlantic Oceanographic and Meteorological Laboratory (AOML) and the South Florida Water Management District (SFWMD). The work was started on May of 2000 and involved collaborations with Chris Landsea (AOML) and Paul Trimble (SFWMD).

In our preliminary work we used a variety of climatic indices from our previous and ongoing work on global SST modes of variability (Enfield and Mestas-Nuñez 1999; Mestas-Nuñez and Enfield 1999; Mestas-Nuñez and Enfield 2001) to explore correlations with precipitation over South Florida and the Caribbean Ocean. Precipitation came from a 40-yr monthly gridded precipitation dataset. We were able to reproduce the know El Niño/Southern Oscillation (ENSO) relationship that affects South Florida precipitation during winter (e.g. Hanson and Maul 1991) and explored new associations with the Atlantic Multidecadal Oscillation (AMO). Our results for the AMO were published in *Geophysical Research Letters* (Enfield et al. 2001).

In this final report we focus on south Florida precipitation at three climatic divisions 4-6 (Fig.1). Of these divisions, division 4 includes the entire catchment for Lake Okeechobee inflow in south-central Florida. The association of precipitation with SST variability is investigated using correlations with global SST. Compared to our preliminary work, we know use a longer temporal record (over 100 years) and explore the associations for each season and in different frequency bands. This report is organized as follows: In section 2 we present the data and methods, in section 3 we present the results, in section 4 we give our conclusions and in section 5 we make some final remarks. Additional useful information is given in the appendices, which include the summary of the AMO paper (Appendix A), and a list of scientific presentations of this work (Appendix B).

2. Data and Methods

This study is based on two datasets: an updated (1856-2001) version of the Kaplan et al. (1998) monthly analyses of global SST anomalies and monthly rainfall over South Florida climate divisions 4-6 (National Climatic Data Center). The Kaplan SST anomalies were calculated as deviations from the 1951-80 monthly climatology. Divisions 4-6 (hereafter, D4-D6) precipitation anomalies were calculated as deviations from a long-term monthly climatology (Fig. 2) estimated for the same (1951-80) period used for SST. Because in this study we focus on multi-decadal and shorter time scales we removed a linear trend from the precipitation anomaly time series to eliminate any secular trends. The spatial patterns of association between South Florida precipitation and SST were estimated from linear correlations analysis between the D4-D6 time series and the unfiltered Kaplan SST anomalies for the period 1895-1998.

The temporal-scale dependence of the associations was studied by dividing the D4-D6 precipitation anomaly time series in three frequency bands: intra-seasonal ($T< 1.5$ yr), interannual ($1.5 < T < 8$ yr) and decadal ($T > 8$ yr). The separation of the signal into these three respective high pass, band pass and low pass frequency bands was performed using a one-dimensional locally weighted regression (loess) algorithm (Cleveland and Devlin 1988). With this filter, each smoothed estimate is obtained by a weighted least square fit of a quadratic curve to the raw data near the estimation point. The degree of smoothing of the loess algorithm is determined by half the temporal width or span of the regression region around the estimation point. The smoothing of a loess filter with half span equal to1.5 (8) yr is roughly equivalent to what would be obtained from a 0.9 (4.8) yr running mean (Chelton et al. 1990). Seasonal dependences of the associations in each frequency band were studied from 3-month averages of the data for November-December-January (NDJ), February-March-April (FMA), May-June-July (MJJ) and August-September-October (ASO). Thus the Florida wet (dry) season is described by the periods MJJ-ASO (NDJ-FMA).

The changes in precipitation probability associated with the relevant SST modes were studied using three SST-based indexes: an ENSO index (Nino3), an Eastern North Pacific

(ENP) index and a North Atlantic (NA) index. These indexes were computed by averaging the Kaplan monthly SST anomalies in three rectangular areas bounded by 90-150ºW, 5ºS-5ºN for Nino3; 115-135ºW, 15-35ºN for ENP and 20-60ºW, 45-65ºN for NA. The same processing used with the precipitation time series was applied to the SST indexes. Briefly, a linear trend was removed, the three components of the variability (intra-seasonal, inter-annual and decadal) were separated using the loess filter, and the three-month seasonal averages (NDJ, FMA, MJJ and ASO) were computed.

The probability analysis is based on building seasonal contingency tables using the three-month averaged time series of unfiltered and filtered South Florida precipitation and the three-month averaged SST indexes. For South Florida precipitation variability, wet, neutral and dry conditions are defined by precipitation values falling in the upper, middle and lower tercile, respectively. In the case of ENSO variability, El Niño, neutral and La Niña conditions are defined by three-month averaged unfiltered Nino3 values falling in the upper, middle and lower tercile, respectively. The respective lower and upper Niño3 threshold values are –0.57 and 0.24 ºC for DJF, –0.37 and 0.16 ºC for FMA, -0.30 and 0.26 ºC for MJJ, and –0.45 and 0.20 ºC for ASO. For Pacific decadal variability associations, warm (cold) conditions are defined by positive (negative) values of the low-passed ENP SST index. For Atlantic decadal variability, warm (cold) conditions are defined by positive (negative) values of the low-passed NA SST index.

3. Results

a. Annual space patterns associated with south Florida precipitation variability

The time series for Raw, high pass (HP), band pass (BP) and low pass (LP) D4 precipitation anomalies are shown in Fig. 3. For graphical purposes, the time series were divided by their standard deviation (SD) because of the large discrepancy in the amplitude of the variability in the different frequency bands. The SD of Raw D4 precipitation is 1.98 in. The SD's of the filtered time series in decreasing order are 1.84 in for HP (intraseasonal), 0.6 in for BP (interannual), and 0.25 for LP (decadal). The ranges of variation of the time series are about ± 2 times the SD's.

The global SST patterns associated with these time series are shown in Fig. 4. The black box in the BP panel is the Niño-3 region and the boxes in the Pacific and Atlantic sectors of the in LP panel are the regions used for Pacific and Atlantic decadal variability indexes, respectively. The association of south Florida precipitation with ENSO is evident in the Raw and BP patterns because they look like the typical ENSO patterns. In the North Atlantic, the LP pattern shows high correlations over most of the basin, consistent with the results for the AMO (Enfield et al. 2001). In the Pacific, the LP pattern shows some indication of the known Pacific decadal pattern (which is similar to the ENSO pattern but has off equatorial maximum amplitudes in the eastern tropical Pacific). The HP pattern shows low correlations everywhere.

The time series for Raw, HP, BP and LP D5 precipitation anomalies are shown in Fig. 5. The SD of these time series are 1.95 in for Raw, 1.83 in for HP (intraseasonal), 0.56 in for BP (interannual), and 0.25 for LP (decadal). The global SST patterns associated with these time series are shown in Fig. 6. These patterns are similar to the ones for D4.

The time series for Raw, HP, BP and LP D6 precipitation anomalies are shown in Fig. 7. The SD of these time series are 2.52 in for Raw, 2.36 in for HP (intraseasonal), 0.71 in for BP (interannual), and 0.38 for LP (decadal). The global SST patterns associated with these time series are shown in Fig. 8. These patterns are similar to the ones for D4 and D5, except the LP pattern has smaller values of the correlation in the Atlantic sector suggesting a weaker association of D6 precipitation with Atlantic decadal variability.

b. Seasonal space patterns associated with south Florida precipitation variability

When the time series of D4 precipitation are averaged over 3-month seasons (Figs. 9, 11, 13 and 15) and the spatial patterns are calculated (Figs. 10, 12, 14 and 16) the major differences with the annual patterns are for HP and therefore also for Raw (because the raw variability is dominated by HP intraseasonal variability these patterns always look alike). For NDJ and FMA the Raw and HP patterns are similar to the ENSO pattern. For MJJ the HP pattern is strongly anti-correlated with Atlantic sector variability with larger

correlations over the tropical North Atlantic. For ASO the HP pattern is strongly anti-correlated with tropical Pacific variability with a pattern similar to ENSO. The implication is that during MJJ and ASO the interannual and intraseasonal patterns associated with Florida rainfall interfere with each other resulting in Raw patterns that look like weak HP patterns.

The 3-month averaged time series of D5 precipitation are shown in Figs. 17, 19, 21 and 23 and their associated spatial patterns of SST correlations are shown in Figs. 18, 20, 22 and 24. These seasonal patterns associated with D5 are very similar to the ones for D4.

The 3-month averaged time series of D6 precipitation are shown in Figs. 25, 27, 29 and 31 and their associated spatial patterns of SST correlations are shown in Figs. 26, 28, 30 and 32. These seasonal patterns associated with D6 are very similar to the ones for D4 and D5 but, as in the case of the annual patterns, the LP pattern has smaller correlations in the Atlantic sector.

c. Comparison of division 4-6 precipitation and SST indexes

The comparisons of D4 precipitation with SST indexes over the regions shown in Fig. 4 are shown in Fig. 33. The top panel shows the comparison with Niño-3 when both time series are band-passed in the 1.5-8 yr interannual band. The correlation between the two time series is 0.44 (maximum at zero lag) and is statistically significant with greater than 95% confidence accounting for serial correlations. This significant association illustrates the ENSO-related variability in South-Central Florida precipitation.

The middle panel shows the comparison of D4 precipitation with the North Atlantic index when both time series are low-passed to remove scales shorter than 8 yr. This correlation (0.31) is not statistically significant. Enfield et al. (2001) found a significant relationship with Atlantic SSTs when focusing on the multidecadal time scales. They applied a 10 yr running mean compared to the equivalent 4.8 yr running mean used here. Thus our representation of Atlantic decadal variability combines decadal and multidecadal variations.

The bottom panel shows the comparison with the Eastern North Pacific index when both time series are LP. The correlation is 0.51 and is statistically significant with greater than 95% confidence. This suggests an association between south Florida precipitation and Pacific decadal variability. The period of the oscillations is about 10 yr but the presence of longer period variations is evident from the 1920s to the 1950s. The correlation is weaker for the first half of the record, particularly from the 1920s to the 1950s when the Atlantic multidecadal signal was in its warm phase. The record is too short, however, to study the interaction between the Atlantic and Pacific decadal signals with statistical reliability. The discrepancies at both ends of the records may be associated with edge effects of the filtering.

The comparisons of Florida D5 precipitation with the SST indexes are shown in Fig. 34. The correlations of the BP Niño 3 and LP eastern North Pacific time series are respectively 0.42 and 0.41 and are significant with greater than 95% confidence. The BP correlation has a maximum at zero lag. The correlation with LP North Atlantic time series is 0.19 and it is not statistically significant.

The comparisons of Florida D6 precipitation with the SST indexes are shown in Fig. 35. The BP D6 precipitation is significantly correlated with BP Niño 3 SST (0.38, maximum at zero lag) with greater than 95% confidence. There is no statistically significant correlation with LP North Atlantic SST (0.16). The correlation with ENP SST is 0.31 and is statistically significant with greater than 90% confidence.

d. Changes in D4 precipitation probability associated with climatic shifts

To study the changes in D4 precipitation probability associated with ENSO we constructed contingency plots using terciles of precipitation and Niño-3. The lower, middle, and upper terciles of precipitation represent dry (brown), normal (white) and wet (green) conditions, respectively. The lower, middle and upper terciles of Niño-3 represent La Niña, neutral and El Niño conditions, respectively. We also investigated

changes of the contingency plots for the warm and cold phases of the Atlantic and Pacific decadal indexes.

The seasonal contingency plots illustrating the ENSO effects on raw D4 precipitation are shown in Fig. 36 and the corresponding contingency tables in Table 1. Only concurrent seasons are considered because as shown in section 3.3 the maximum correlation between ENSO and south Florida precipitation occurs at zero lag. The changes in the ENSO relationship in the interannual (BP) and intraseasonal (HP) bands are shown in in Figs. 37 (Table 2) and 38 (Table 3), respectively. The know relation, wet (dry) winter/spring during El Niño (La Niña) events, is clearly seen in the upper NDJ-FMA panels of Fig. 36. This is consistent with the patterns in the top panels of Figs. 10 and 12. This relation does not hold for the MJJ and ASO seasons. In fact an opposite relation is seen during ASO, consistent with the pattern in the top panel of Fig. 16. The contingency plot for the BP component of D4 precipitation (Fig. 37) shows that the ENSO relation holds for all seasons in the interannual band. This relation breaks down during ASO because of the opposite ENSO effects on intraseasonal precipitation shown in Fig. 38 (lower right panel).

The changes in the ENSO-D4 contingency plots during the warm and cold phases of the decadal North Atlantic index is shown in Figs. 39 (Table 4) and 40 (Table 5), respectively. Some changes in the associations during the warm and cold phases of the Atlantic decadal signal are apparent in these figures. For example, during the warm phase of the Atlantic decadal index the ENSO effect is reinforced during FMA giving wetter conditions than normally expected for ENSO years – the probability of wet FMA shifts from 35% to about 80%. Also for neutral ENSO years, the probability of wet MJJ and ASO seasons nearly doubles from cold to warm phases of the Atlantic decadal signal.

The changes in the ENSO-D4 contingency plots during the warm and cold phases of the decadal Pacific index are shown in Figs. 41 (Table 6) and 42 (Table 7), respectively. There some changes in unfiltered D4 precipitation probabilities during both phases of the Pacific decadal variability. For example, during warm ENSO years the FMA and MJJ seasons are somewhat wetter during warm phases of the Pacific decadal signal.

e. Changes in D5 precipitation probability associated with climatic shifts

The seasonal contingency plots illustrating the ENSO effects on raw D5 precipitation are shown in Fig. 43 and the corresponding contingency tables in Table 8. The changes in the ENSO relationship in the interannual (BP) and intraseasonal (HP) bands are shown in in Figs. 44 (Table 9) and 45 (Table 10), respectively. Similarly to the case of D4, the know relation, wet (dry) winter/spring during El Niño (La Niña) events, is clearly seen in the upper NDJ-FMA panels of Fig. 43. This is consistent with the patterns in the top panels of Figs. 18 and 20. This relation does not hold for the MJJ and ASO seasons. The contingency plot for the BP component of D5 precipitation (Fig. 44) shows that the ENSO relation holds for all seasons in the interannual band.

The changes in the ENSO-D5 contingency plots during the warm and cold phases of the decadal North Atlantic index is shown in Figs. 46 (Table 11) and 47 (Table 12), respectively. Except during NDJ, D5 is wetter during the warm phase of the Atlantic decadal signal.

The changes in the ENSO-D5 contingency plots during the warm and cold phases of the decadal Pacific index are shown in Figs. 48 (Table 13) and 49 (Table 14), respectively. In general there are little change in unfiltered D5 precipitation probabilities during both phases of the Pacific decadal variability except during the FMA season with wetter neutral and El Niño events during the warm phase of the Pacific decadal signal.

f. Changes in D6 precipitation probability associated with climatic shifts

The seasonal contingency plots illustrating the ENSO effects on raw D6 precipitation are shown in Fig. 50 and the corresponding contingency tables in Table 15. The changes in the ENSO relationship in the interannual (BP) and intraseasonal (HP) bands are shown in in Figs. 51 (Table 16) and 52 (Table 17), respectively. Similarly to D4 and D5, the know relation, wet (dry) winter/spring during El Niño (La Niña) events, is clearly seen in the upper NDJ-FMA panels of Fig. 50. This is consistent with the patterns in the top panels of Figs. 26 and 28. Similarly to D4 and D5, the ENSO relation does not hold for the MJJ

and ASO seasons. The contingency plot for the BP component of D6 precipitation (Fig. 51) shows that the ENSO relation holds for all seasons in the interannual band.

The changes in the ENSO-D6 contingency plots during the warm and cold phases of the decadal North Atlantic index is shown in Figs. 53 (Table 18) and 54 (Table 19), respectively. Except during NDJ, D6 is wetter during the warm phase of the Atlantic decadal signal.

The changes in the ENSO-D6 contingency plots during the warm and cold phases of the decadal Pacific index are shown in Figs. 55 (Table 20) and 56 (Table 21), respectively. In general there are little change in unfiltered D6 precipitation probabilities during both phases of the Pacific decadal variability except during the FMA season with wetter neutral ENSO events during the warm phase of the Pacific decadal signal.

g. Changes in LP precipitation probabilities associated with climatic shifts

The changes in the low-passed D4 precipitation probabilities (in terciles) during the warm and cold phases of the Atlantic decadal and Eastern Pacific decadal indexes are shown in Fig. 57 (Table 22). As in the figures for ENSO, the lower tercile of precipitation is indicated with brown, the middle with white and the upper with green. The relation seen in Fig. 57 is similar for both decadal indexes and is independent of the seasons. When the decadal indexes are warm (cold) the decadally smoothed D4 precipitation probabilities are higher (lower). In particular, the probability of a wet D4 decade changes from about 20% to 40% when the decadal indexes change from their cold to their warm phase.

The changes in the low-passed D5 precipitation probabilities during the warm and cold phases of the Atlantic multidecadal and Eastern North Pacific decadal indexes are shown in Fig. 58 (Table 23). The changes in the low-passed D6 precipitation probabilities during the warm and cold phases of the Atlantic multidecadal and Eastern North Pacific decadal indexes are shown in Fig. 59 (Table 24). The decadal changes of D5 and D6 precipitation probability are similar to D4 in general weaker.

4. Conclusions

We have investigated the effects of ENSO and decadal climate variability in south Florida (D4-D6) precipitation. Our approach here has been to determine the climatic patterns of SST variability that are associated with D4-D6 precipitation variability. We also looked at how these patterns vary when the precipitation variability is decomposed into intraseasonal, interannual and decadal frequency bands.

For ENSO, we showed that the known winter/spring relation (50% probability of wet NDJ and FMA during El Niño) does not hold during the summer. We demonstrated that this relation breaks down because of the opposite effect (smaller during warm ENSO phase) that ENSO has on the dominant intraseasonal precipitation variability during that season. Regarding the effect of the Atlantic decadal variability we showed that the most sensitive season is FMA when the probability of a wet D4 season during ENSO increases from about 35% to 80%. Also for neutral ENSO years, the probability of wet MJJ and ASO seasons nearly doubles from cold to warm phases of the Atlantic decadal signal. During El Niño years the FMA and MJJ seasons of D4 are about 20% wetter during warm phases of the Pacific decadal signal.

Regarding the effect of the decadal SST variability on the low-pass D4 precipitation, our results show that in general decadally warm Atlantic is associated with decadally wet South Florida – as was already discussed by Enfield et al. (2001) for the multidecadal scales. On decadal scale, we found a similar association with Pacific decadal variability. This association modulates the ENSO response and affects the precipitation probability in south Florida. Precipitation outlooks in south Florida should consider the effects of ENSO and the decadal Pacific and Atlantic variabilities.

5. Diagnostic of the statistical relationships

a. ENSO winters

On interannual time scales the link between South Florida rainfall and ENSO is related to latitudinal shifts in the subtropical jet stream and associated storm track activity over the eastern Pacific Ocean (e.g. Trenberth et al. 1998). This is especially clear during El Niño where a deepened Aleutian Low increases the baroclinicity of the storm track entering the US and shunts the track farther south. Because of the greater tropical humidity and the farther penetration of the storm systems into the more humid tropical regions, more moisture is entrained into these more energetic storms. The storms track preferentially across the southern tier states and pick up additional moisture from the Gulf of Mexico and Caribbean as they cross the Gulf States. The southern tier states (including Florida) are dry by contrast when La Niña conditions prevail and these mechanisms are absent.

This mechanism for increased precipitation over the southern U.S. has been postulated primarily for winter conditions and they are important in determining the cumulative hydrological setup (during the dry season) as the wet season onset approaches. Exceptions to the typical ENSO behavior are not uncommon. December and January of the 2002-2003 El Niño winter were a case in point. Instead of seeing a series of wet storms propagating eastward across the southern tier, there were a long series of strong polar fronts that expanded south across the great plains bringing cold Canadian air masses to Florida, but very little rain. This may have been related to the confounding effect of the Atlantic state on the ridge-trough structure across the US. Once better understood, this winter may be a good example of how a contrary Atlantic configuration can trump a weak El Niño.

b. ENSO summers

Our tercile probabilities hint at different mechanisms for summer rainfall in El Niño years. When Florida rainfall is compared against the terciles of NINO3 SST we find that warm SST anomalies in the equatorial Pacific are associated with lower rainfall in the

intraseasonal band. This suggests that tropical storm activity is less prevalent, in agreement with relevant hurricane research. The effect of ENSO variability on Atlantic tropical storm activity is opposite to that of the winter storm track activity shifts over the Pacific. During El Niño (La Niña) there is an increase (decrease) in the vertical shear of the horizontal wind over the Atlantic caused primarily by an increase (decrease) in the climatological westerly winds in the upper troposphere (Landsea 2000). This increase (decrease) in the shear leads directly to reduced (increased) Atlantic tropical storm activity.

The shear effect is probably related to the disruption of the Walker & Hadley circulations in the Atlantic sector (Wang and Enfield, 2003) and careful examination of hurricane frequencies reveals that the effect is mainly prevalent in the summer of the El Niño onset year [EN-0] and not of the following year [EN+1]. During the EN+1 years, the El Niño peak is most often followed by the development of a larger-than-normal Atlantic warm pool, which is now partially understood (Wang and Enfield, 2001, 2003). During these summers the Atlantic SST favors tropical storm development and the Caribbean experiences greater rainfall, which may extend to Florida or it may remove moisture from the air masses affecting Florida and thus lead to drier conditions. Unfortunately, our tercile analysis does not separate warm summers according the El Niño phase because this would greatly reduce the degrees of freedom and reliability of the analysis. A very important topic for future research is to understand better the difference between both the rainfall probabilities and the mechanisms that affect rainfall and tropical storms during onset summers vis-à-vis following-year summers. For the present, SFWMD must be aware of this distinction in its approach to developing El Niño scenarios.

c. Decadal variability

On decadal and longer time scales, South Florida precipitation is modulated by Pacific and Atlantic variability. Both Pacific and Atlantic decadal modulations are similar in the sense that warm (cold) eastern/tropical Pacific and North Atlantic lead to increased (decreased) South Florida precipitation independent of the season. The way in which these teleconnections occur, however, appear to be quite different.

As seen in Fig. 60, the winter 500 mb pattern associated with the Pacific decadal variability shows good correspondence with the Pacific-North American (PNA) pattern (Enfield and Mestas-Nuñez 1999). This is not surprising since although there are regional differences the large-scale structure of the decadal Pacific SST mode is similar to ENSO, which commonly excites the PNA pattern. Based on this analogy with the PNA pattern one can infer that the warm phase of the Pacific decadal variability is also associated with southward displacements of the subtropical storm track activity resulting in decadal wetter conditions over the southern U.S. including South Florida. Analysis of the ENSO and non-ENSO 500 mb vertical velocity patterns associated with Pacific SST variability confirms this suggestion showing anomalous ENSO and Pacific decadal vertical velocity fluctuations over South Florida that are in phase with each other (Mestas-Nuñez and Enfield 2001).

Figure 61 shows that the winter 500 mb pattern associated with the Atlantic decadal SST variability is similar to the North Atlantic Oscillation pattern (Enfield and Mestas-Nuñez 1999, their Fig. 8). This pattern shows that during the warm phase of the Atlantic decadal variability (especially the Atlantic Multidecadal Oscillation, hereafter AMO) the usual winter trough over the southeastern U.S. (which includes South Florida) also strengthens, while eastern Canada lies under higher pressures that favor cold air mass development there. This results in decreased winter cyclonic activity in the southwest and increased winter cyclonic activity in the southeast. But because the fronts bring in cold Canadian air masses from the north, these effects oppose the ENSO-related wet subtropical storm tendency when they occur in conjunction with El Niño. We note that this ENSO-Atlantic interaction scenario is consistent with the results of Enfield et al. (2001) who showed that when the North Atlantic is multi-decadally warm the southeastern states are less rainy during El Niño, and vice-versa for a cool North Atlantic (see Fig. 62). By the same reasoning, one would anticipate that a cold North Atlantic would reinforce the prototypical El Niño pattern, which is what Fig. 4 of Enfield et al. (2001) also shows. This interpretation of ENSO-AMO interactions is consistent with our tercile conditional-probability analysis for ENSO-AMO during El Niño DJF conditions, more noticeable for South Florida Divisions 5 and 6. The opposite scenario during La Niña winters, however, is not supported buy our analysis. We caution, however, that these are linear notions of

how ENSO and Atlantic variability may interact and that further research will be needed to understand these scenarios better.

6. Final remarks

The goal of this contract was to "identify links between various modes of ocean variability to that of the climatic and hydrologic variability in South Florida". The focus of the study was to estimate in a probabilistic sense the effects of the global climate on the hydrology of South Florida.

We performed exploratory analyses (Task 1) to determine what modes of global SST variability described in our previous work using Empirical Orthogonal Function (EOF) analysis are associated with south Florida hydrology. The result of this preliminary work allowed confirming that the main signal in south Florida hydrological variables comes from the ENSO mode. We were also able to determine that on multidecadal time scales the Atlantic multidecadal mode played a role and this led to a peer reviewed article (Enfield et al. 2001) where we described the associations of this index with U.S. precipitation (an abstract of this publication is included in Appendix A). In this final report we performed a correlation analysis of south Florida D4-D6 on global SST to determine the patterns associated with precipitation variability in three frequency bands (intraseasonal, interannual and decadal). The space patterns allowed determining the signature of the corresponding global modes that are involved. These patterns were used to define three indexes that capture the main global modes (ENSO, Atlantic decadal and Pacific decadal modes). The significance level of the correlation of these indexes with south Florida precipitation was also estimated taking into account serial correlations.

The three indexes of global SST variability were used to estimate the changes of probability distribution associated with the climatic signals (Task 2). The approach we undertook was a practical one based on terciles of the distribution of the variables in a manner similar to what is used by the Climate Prediction Center. The changes of probability distributions of South Florida D4-D6 precipitation associated with changes in the climatic indexes were studied taking into account conditional probabilities (e.g. how

does the ENSO associations change as a function of the phases of the decadal Pacific and Atlantic variability).

A diagnostic of the atmospheric mechanisms behind the statistical associations between South Florida precipitation and the interannual and decadal modes of SST variability (Task 3) is included in section 5. There we summarize of our present understanding of the mechanisms behind these relationships. These ideas are the focus of active research in the community and although some of the proposed mechanisms during winter are partially accepted, there is little understanding for the summer and on the non-linear interaction among the relevant modes of variability.

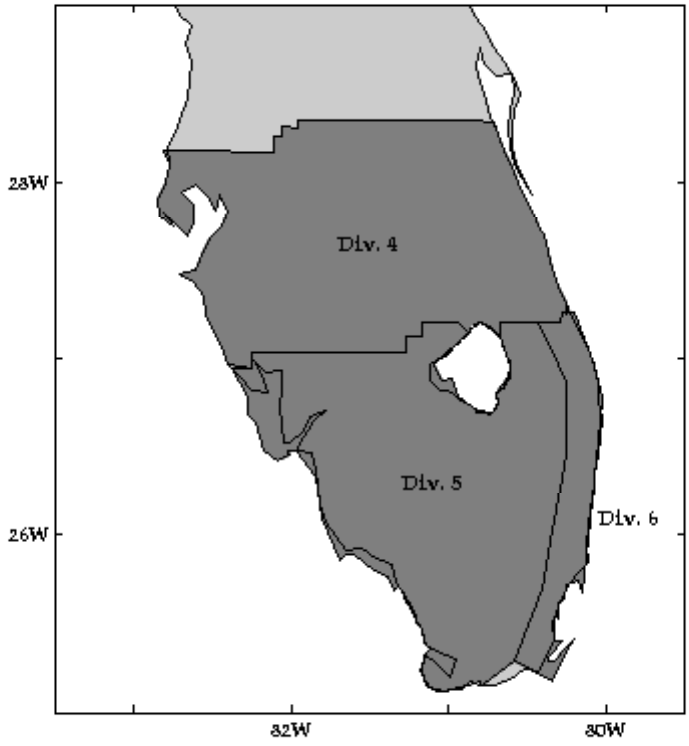

Fig. 1. Map of Florida showing the locations of Lake Okeechobee and climate divisions 4, 5 and 6.

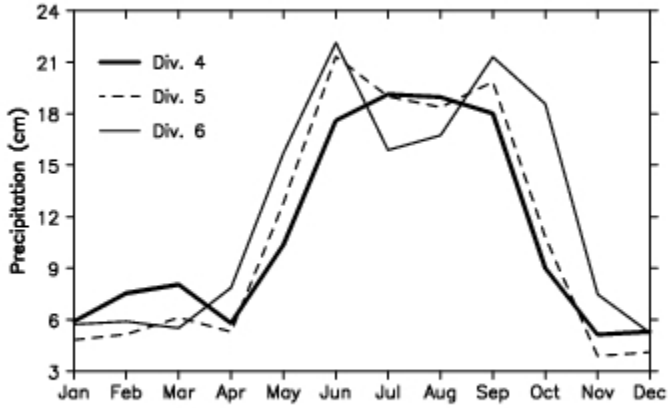

Fig. 2. Long-term average seasonal cycle of monthly precipitation in Florida climate divisions 4 (thick solid), 5 (dashed), and 6 (thin solid) estimated for the 1951-80 period.

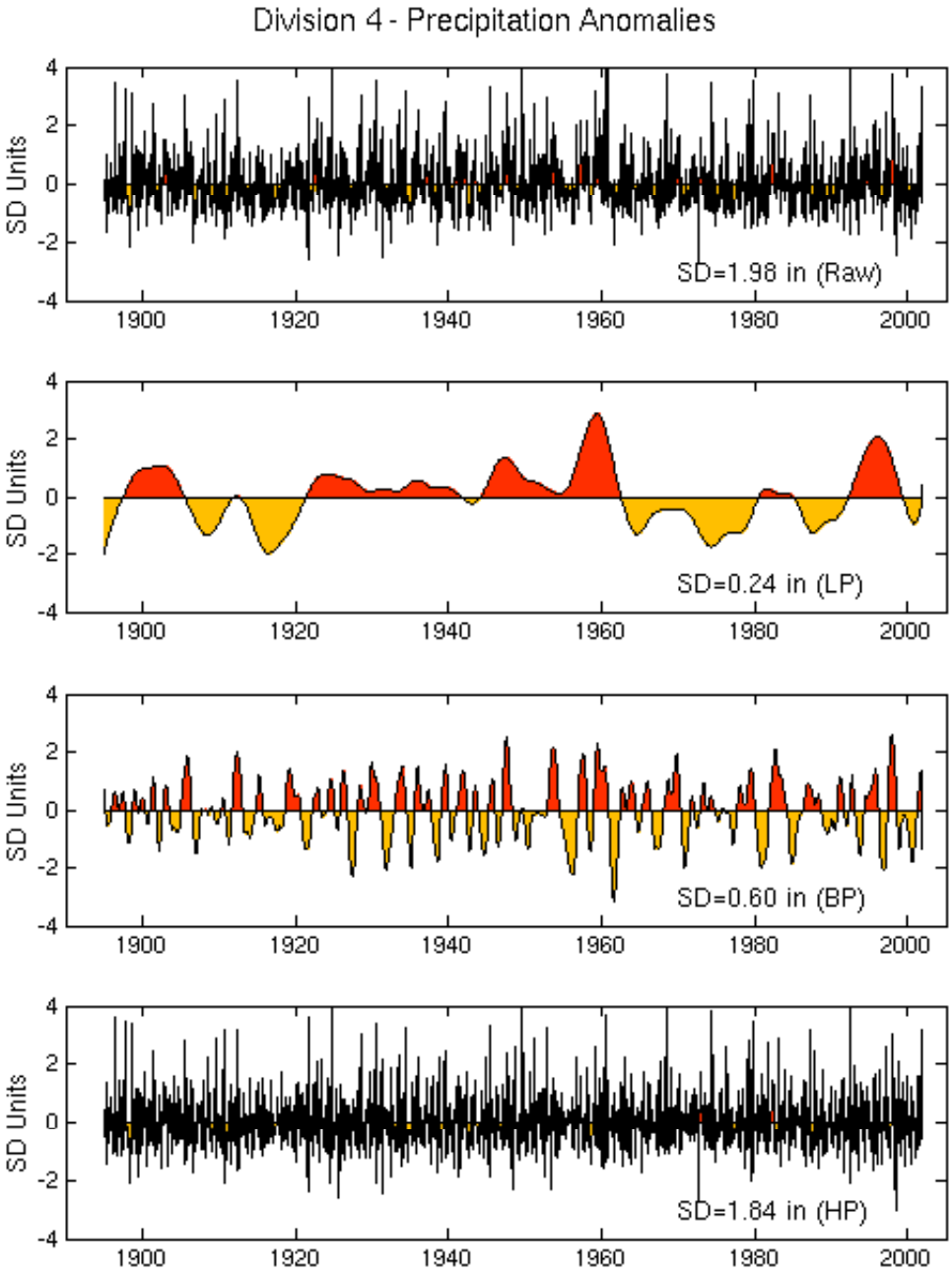

Fig. 3. Unfiltered time series of D4 monthly precipitation anomalies (Raw) and filtered to capture variability in three bands: scales greater than 8 yrs (LP), scales between 1.5 and 8 yrs (BP), and scales shorter than 1.5 yrs (HP). The time series have been standardized dividing them by their standard deviations: 1.98, 0.24, 0.60 and 1.84 inches, respectively.

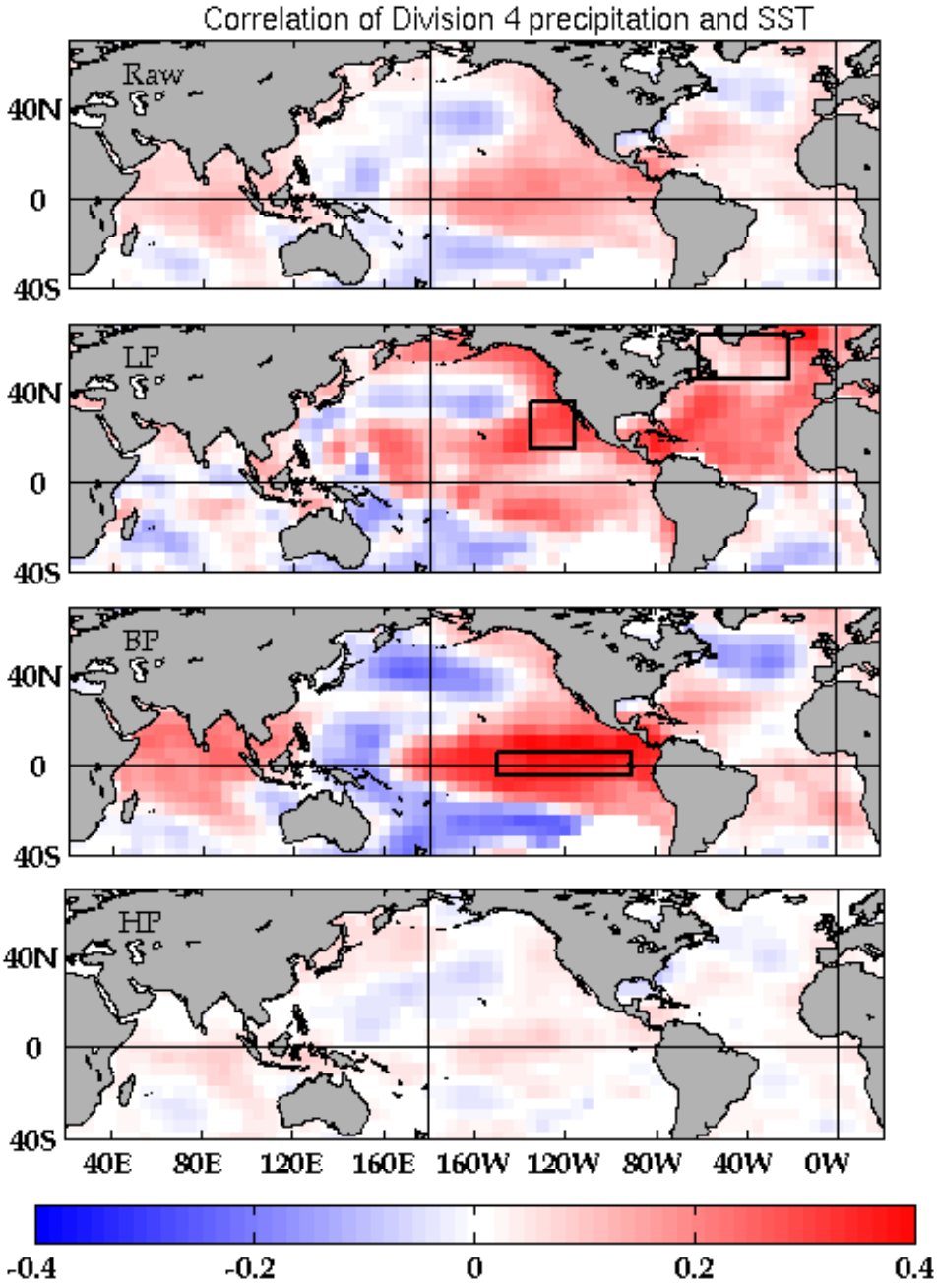

Fig. 4. Map of correlations between global monthly SST anomalies and the D4 monthly precipitation anomaly time series shown in Fig. 3. The boxes indicate the regions used to calculate the SST indices in the North Pacific, North Atlantic and tropical Pacific.

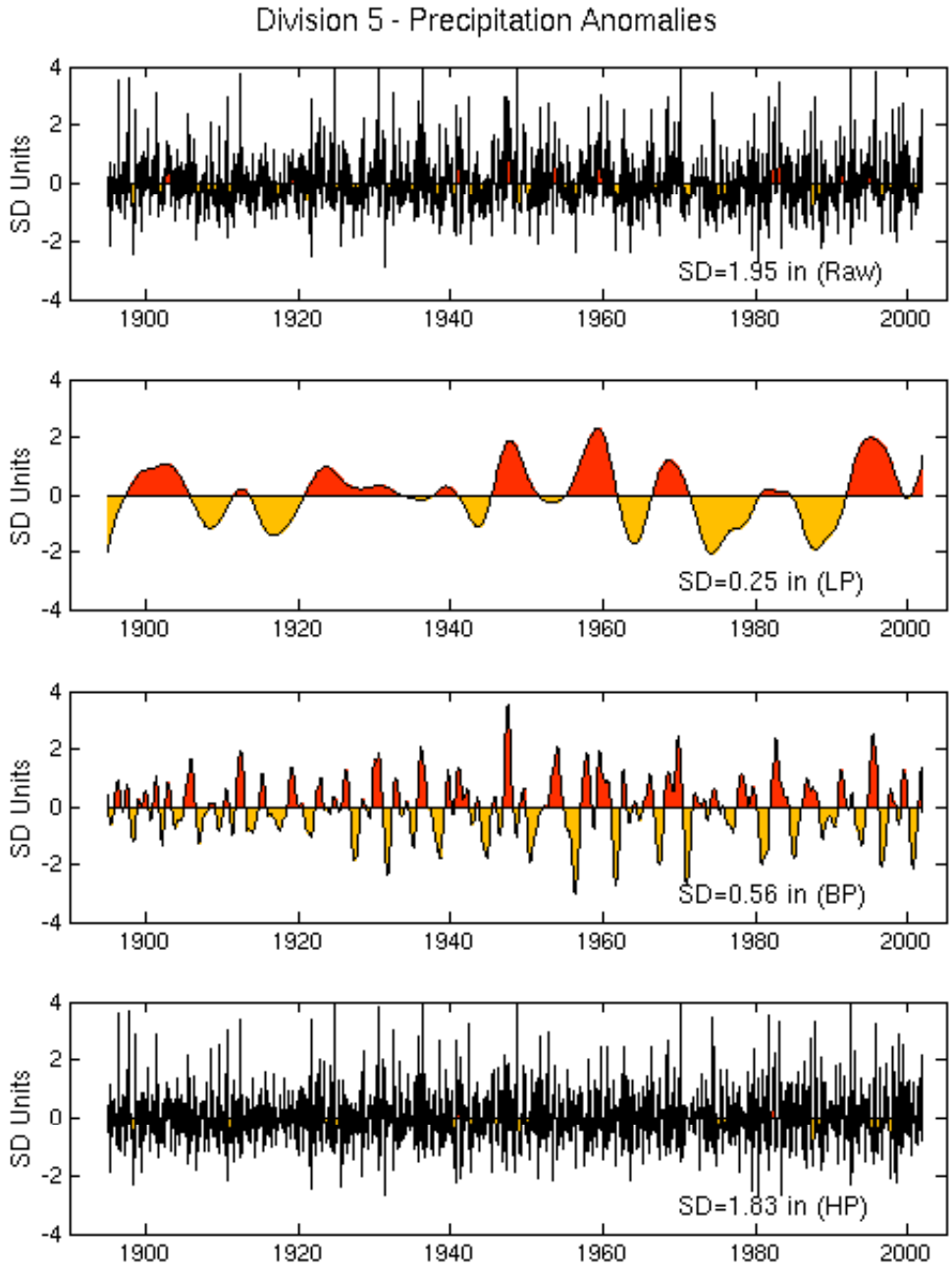

Fig. 5. Unfiltered time series of division 5 monthly precipitation anomalies (Raw) and filtered to capture variability in three bands: scales greater than 8 yrs (LP), scales between 1.5 and 8 yrs (BP), and scales shorter than 1.5 yrs (HP). The time series have been standardized dividing them by their standard deviations: 1.95, 0.25, 0.56 and 1.83 inches, respectively.

.

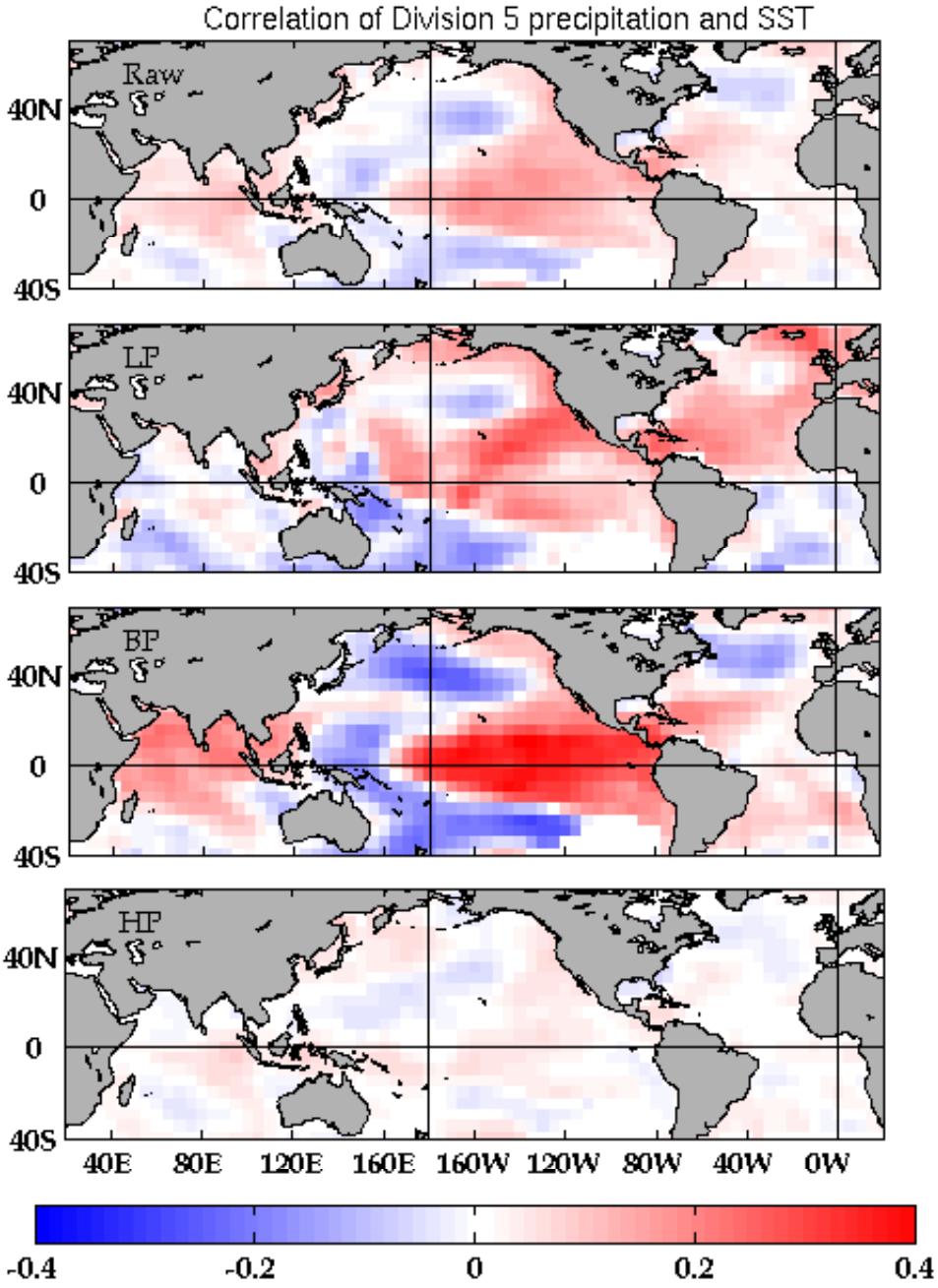

Fig. 6. Map of correlations between global monthly SST anomalies and the division 5 monthly precipitation anomaly time series shown in Fig. 5.

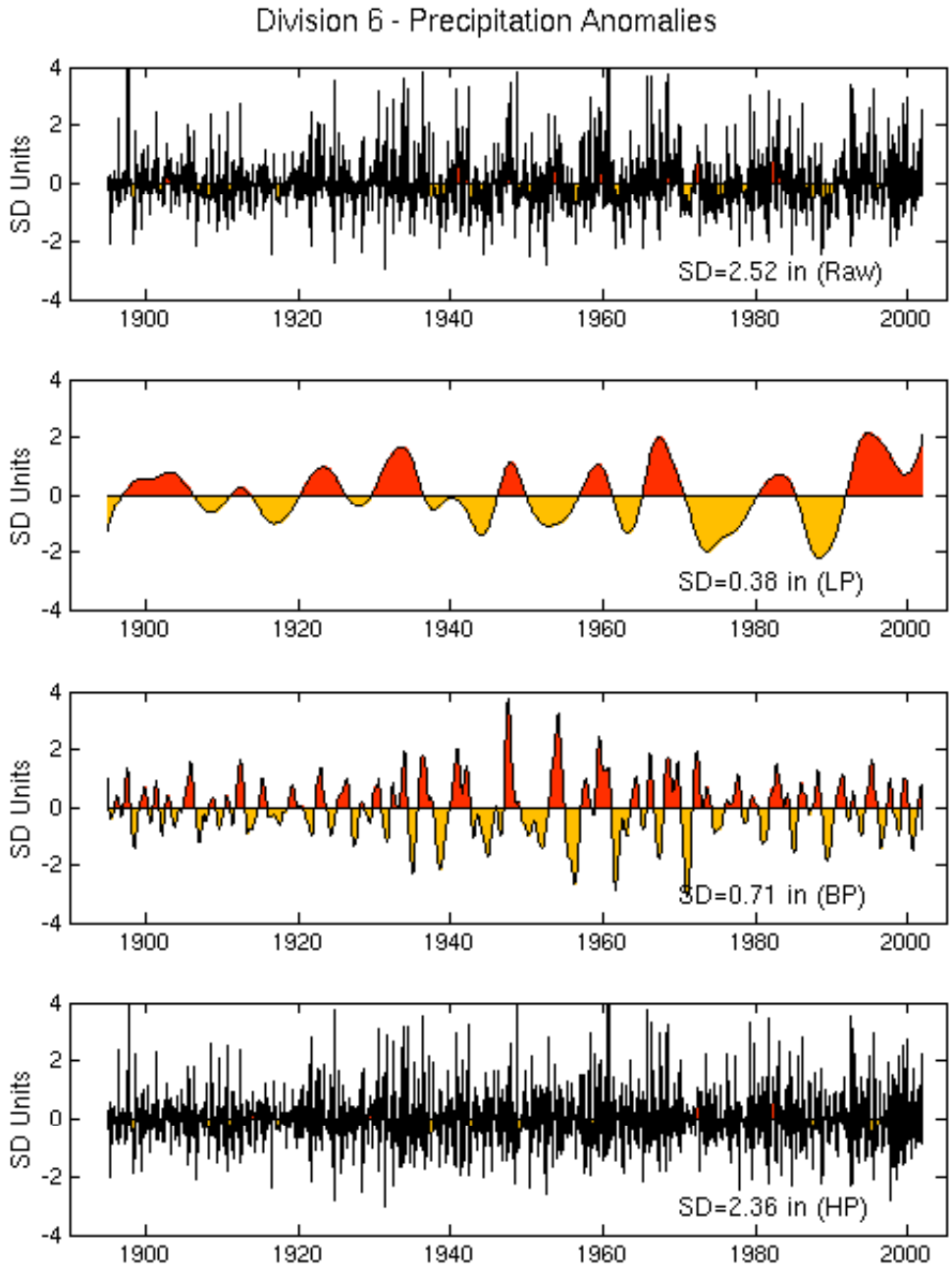

Fig. 7. Time series of division 6 monthly precipitation anomalies (Raw) and filtered to capture variability in three bands: scales greater than 8 yrs (LP), scales between 1.5 and 8 yrs (BP), and scales shorter than 1.5 yrs (HP). The time series have been standardized dividing them by their standard deviations: 2.52, 0.38, 0.71 and 2.36 inches, respectively.

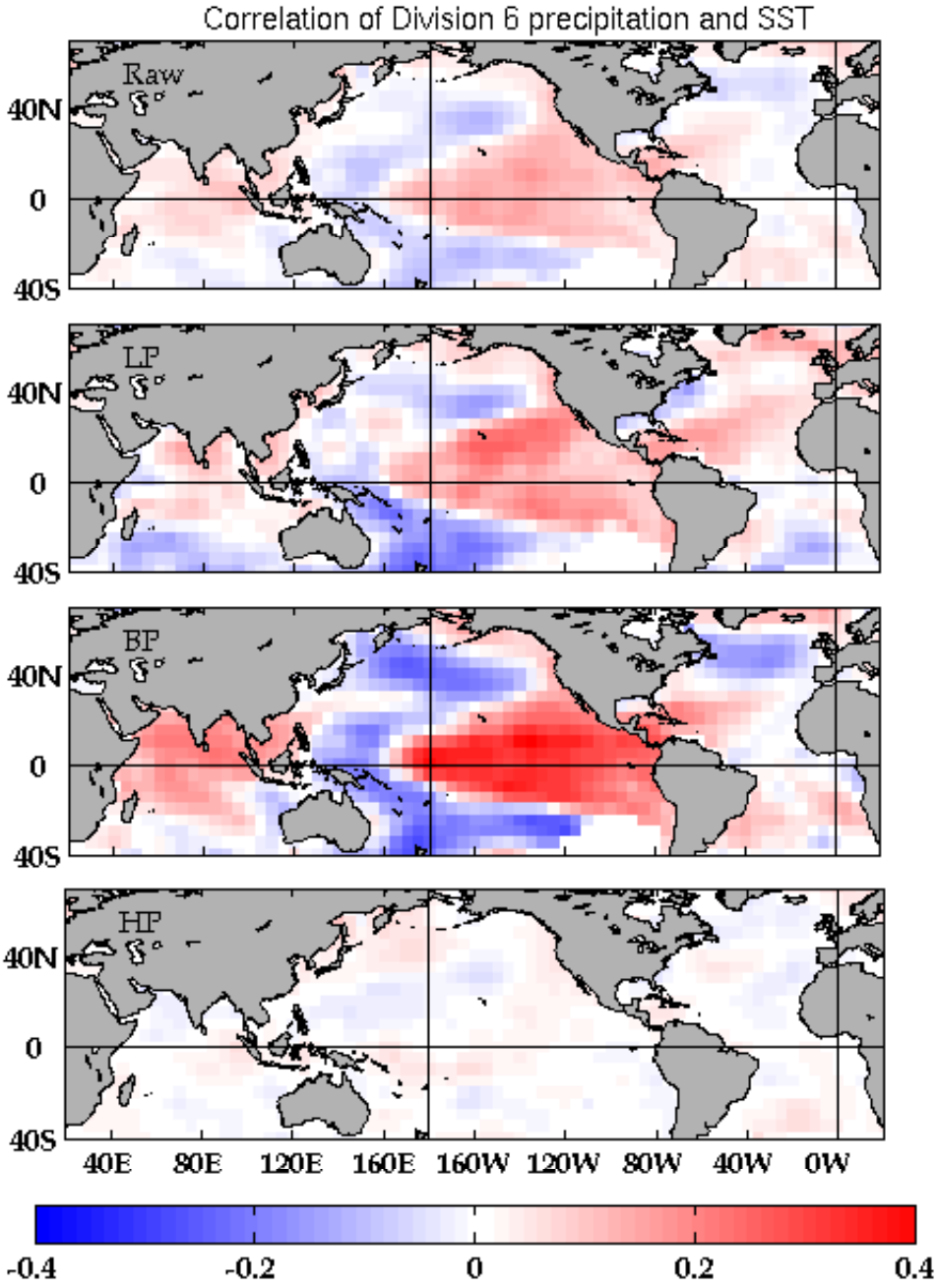

Fig. 8. . Map of correlations between global monthly SST anomalies and the division 6 monthly precipitation anomaly time series shown in Fig. 7.

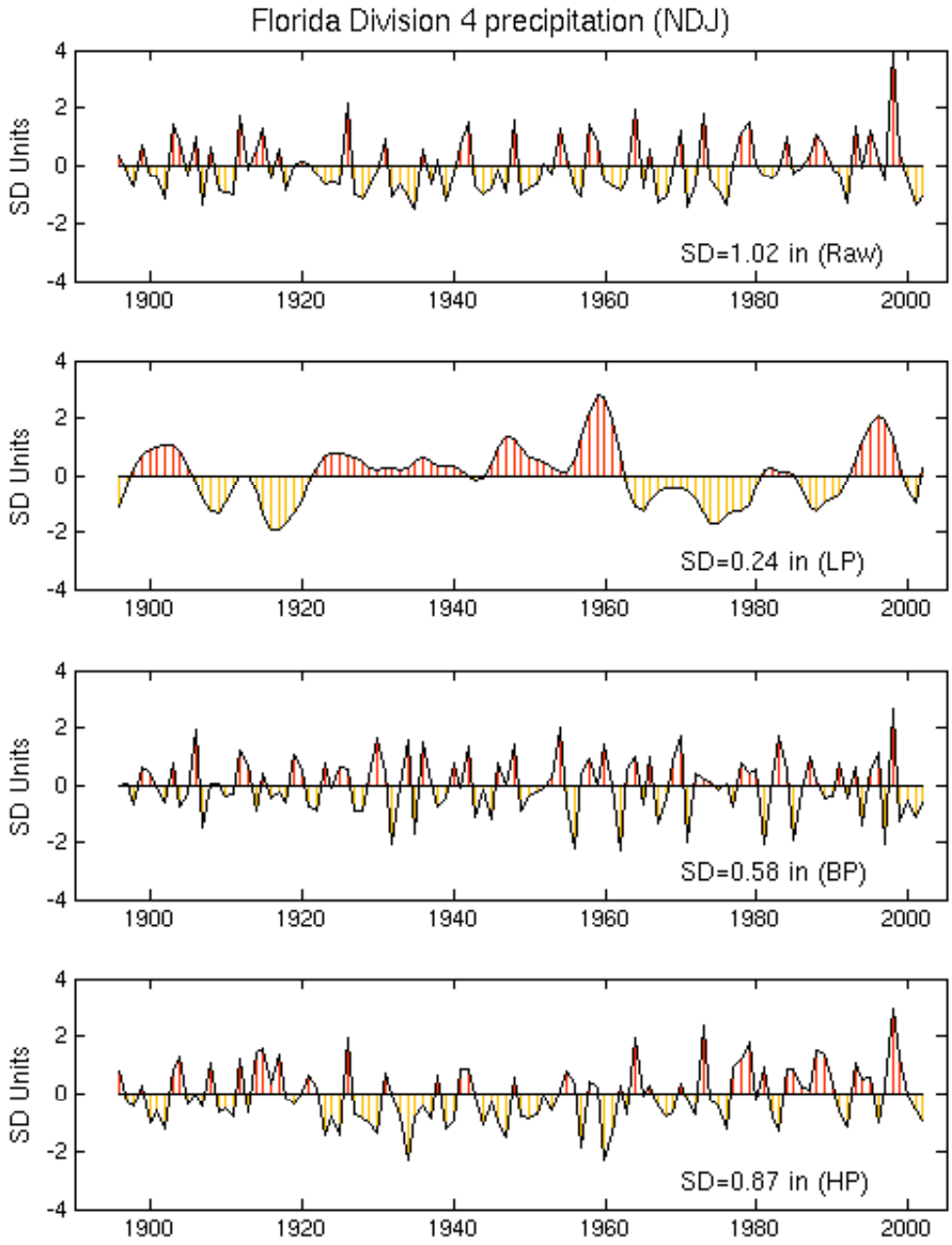

Fig. 9. As in Fig. 3 but for the November-December-January (NDJ) average.

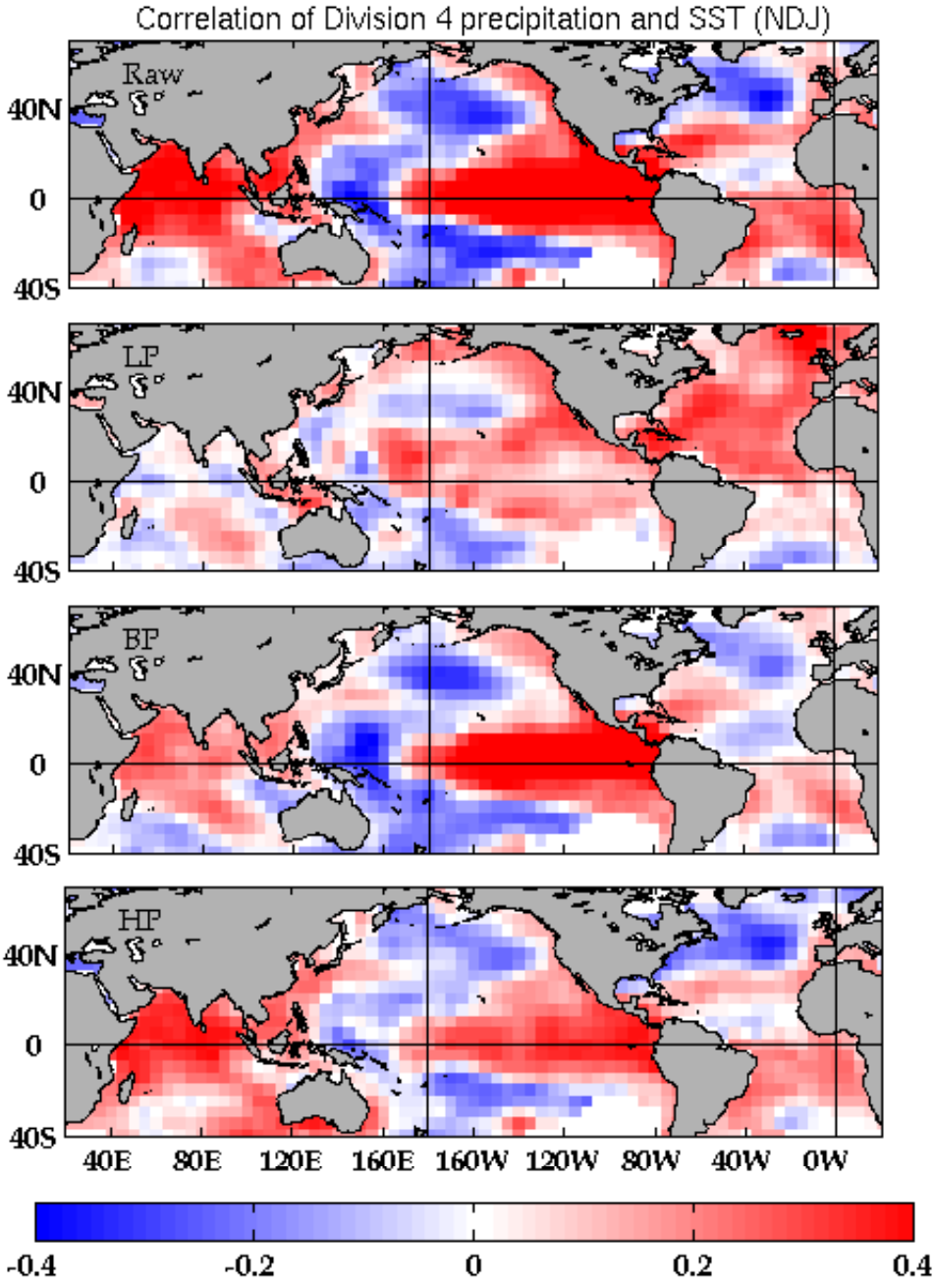

Fig. 10. Map of correlations between global November-December-January (NDJ) average SST anomalies and the NDJ precipitation anomaly time series shown in Fig. 9.

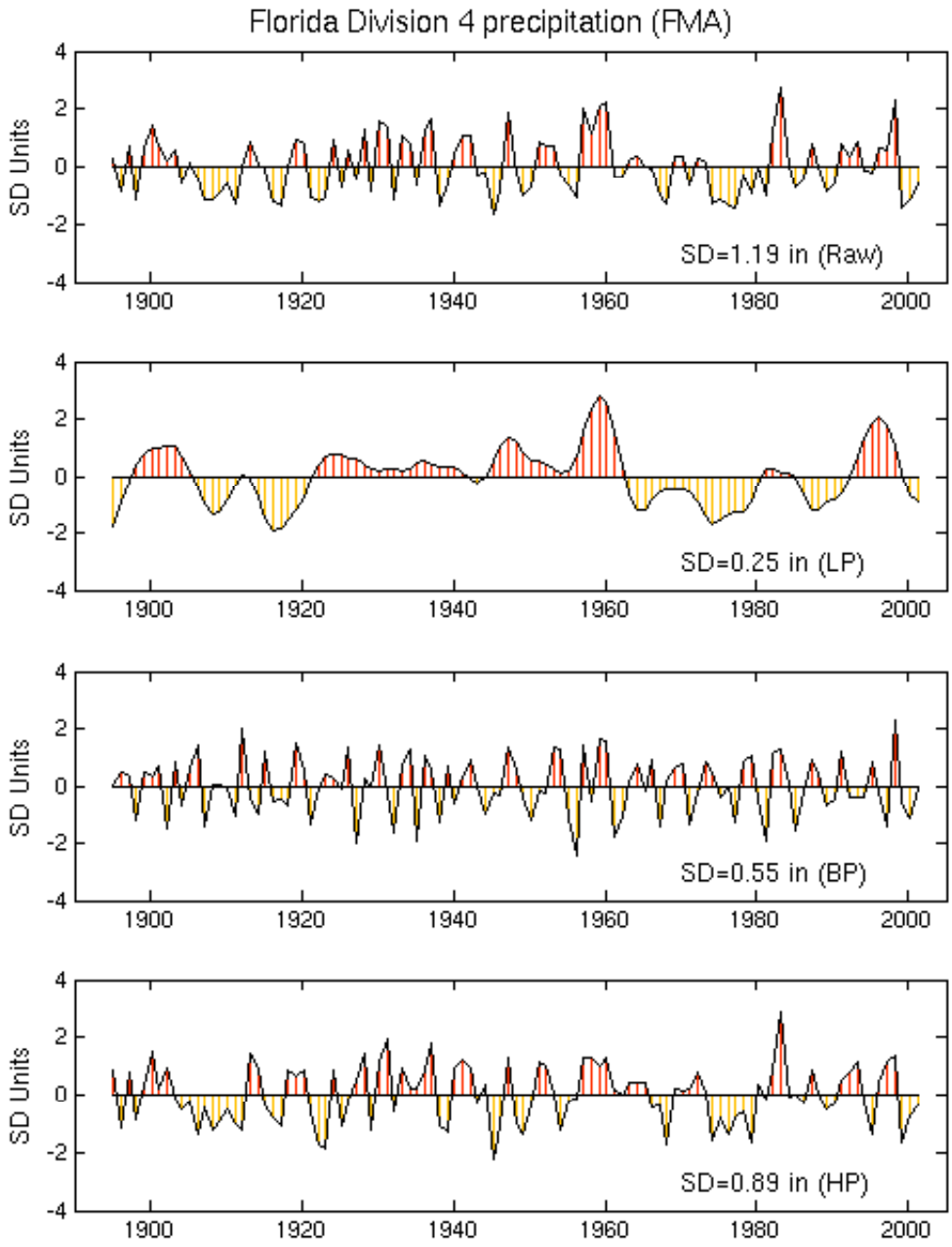

Fig. 11. Same as Fig. 3 but for the February-March-April (FMA) average.

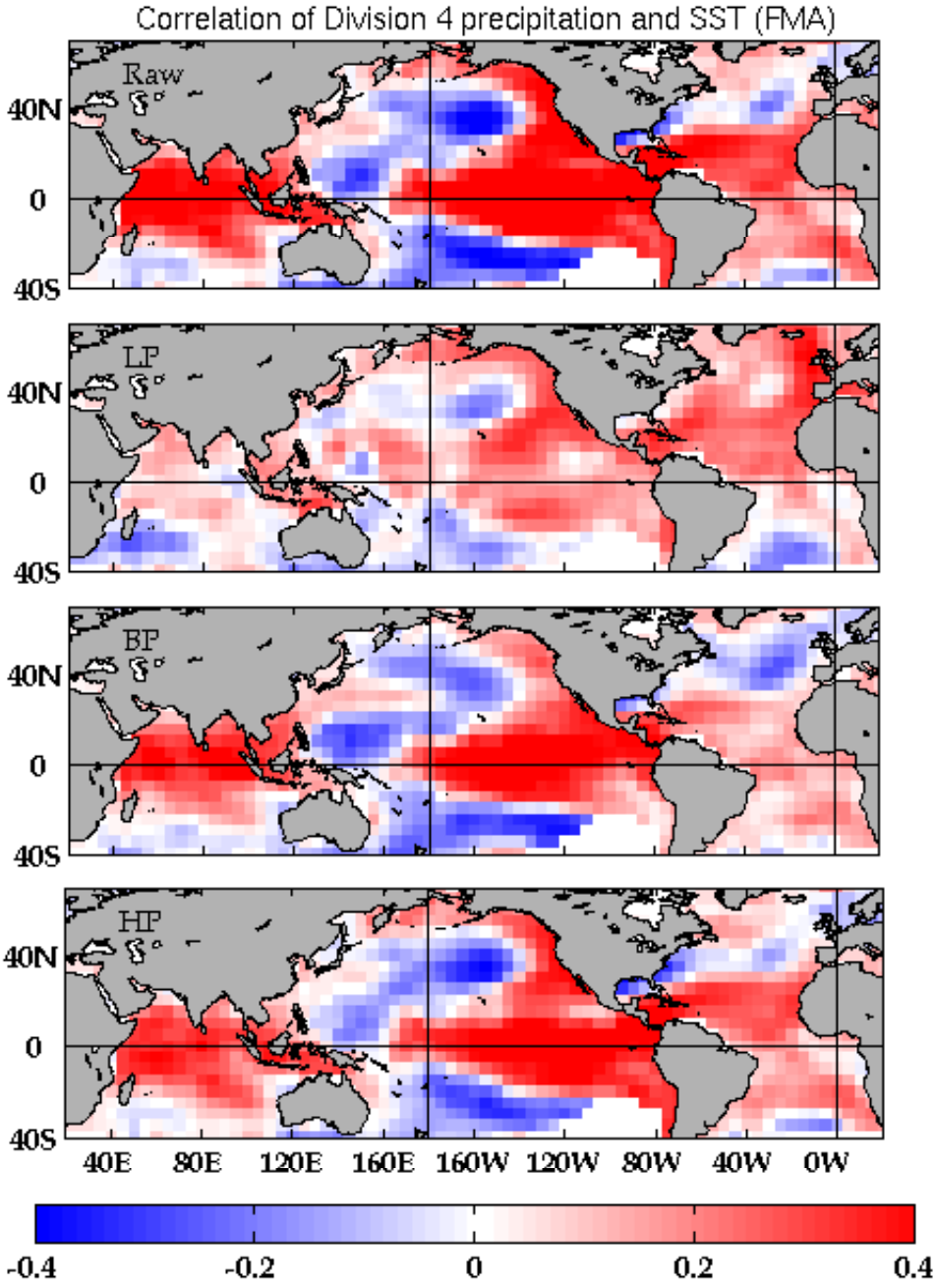

Fig. 12. Map of correlations between global February-March-April (FMA) average SST anomalies and the FMA precipitation anomaly time series shown in Fig. 11.

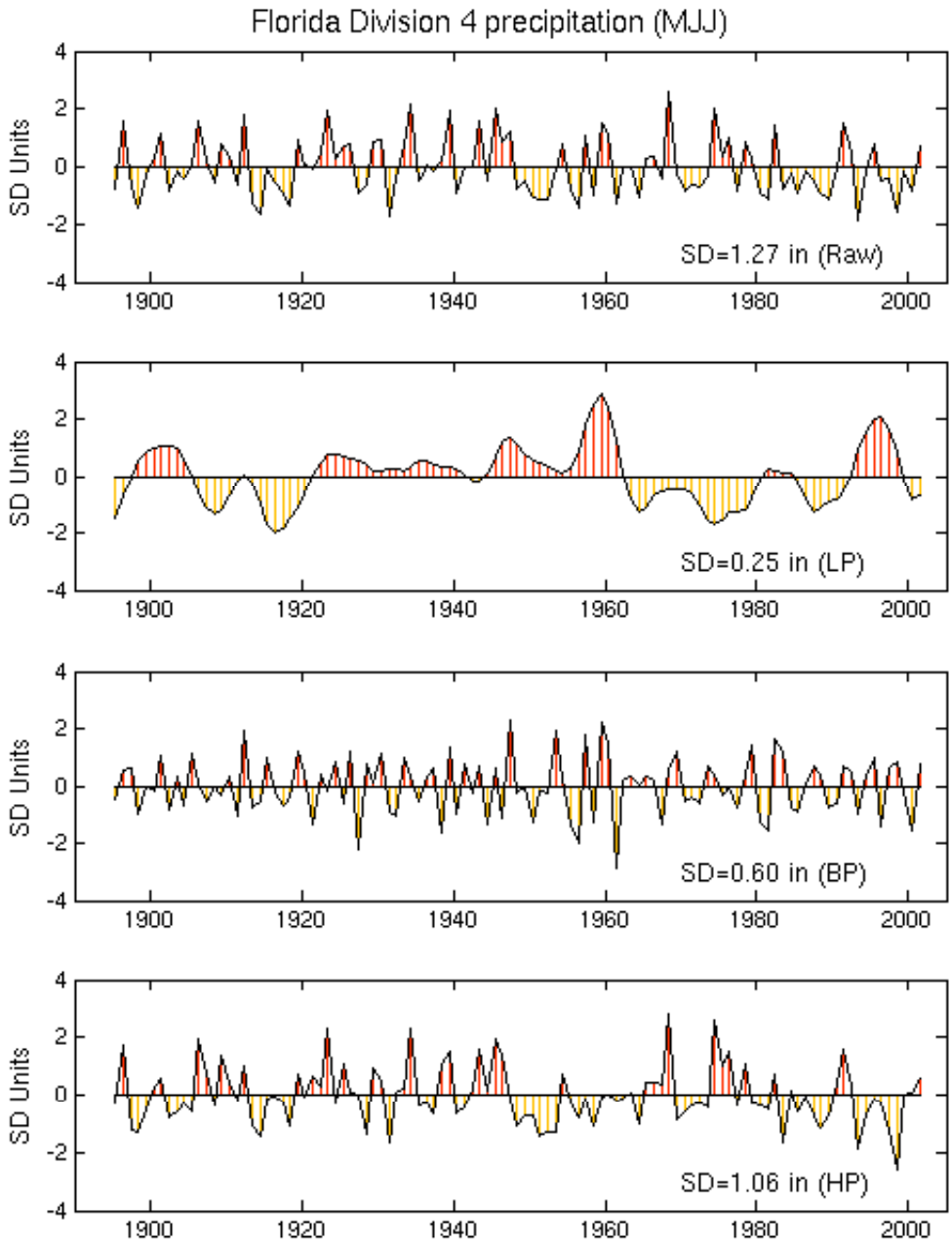

Fig. 13. Same as Fig. 3 but for the May-June-July (MJJ) average.

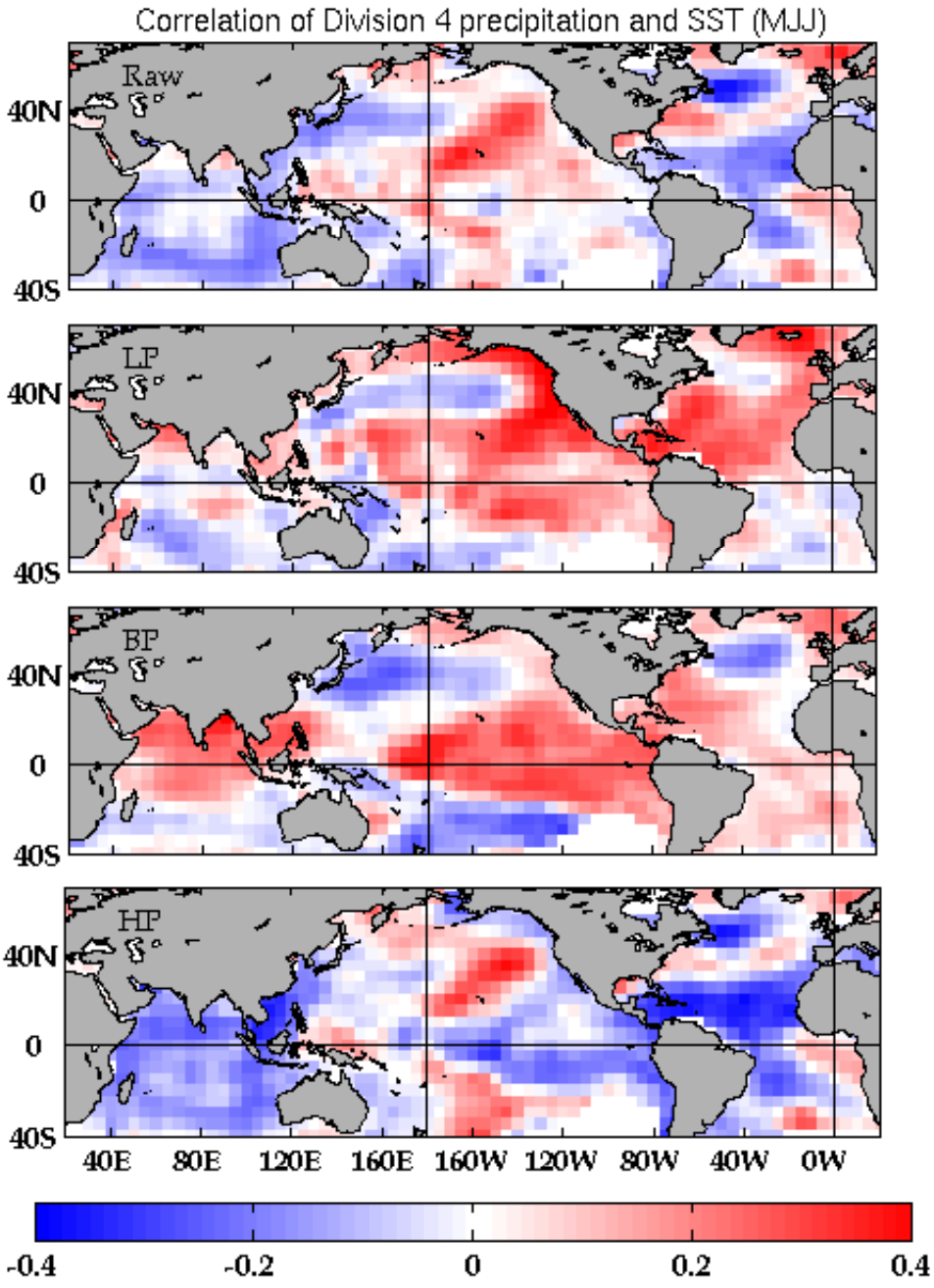

Fig. 14. Map of correlations between global May-June-July (MJJ) average SST anomalies and the MJJ precipitation anomaly time series shown in Fig. 13.

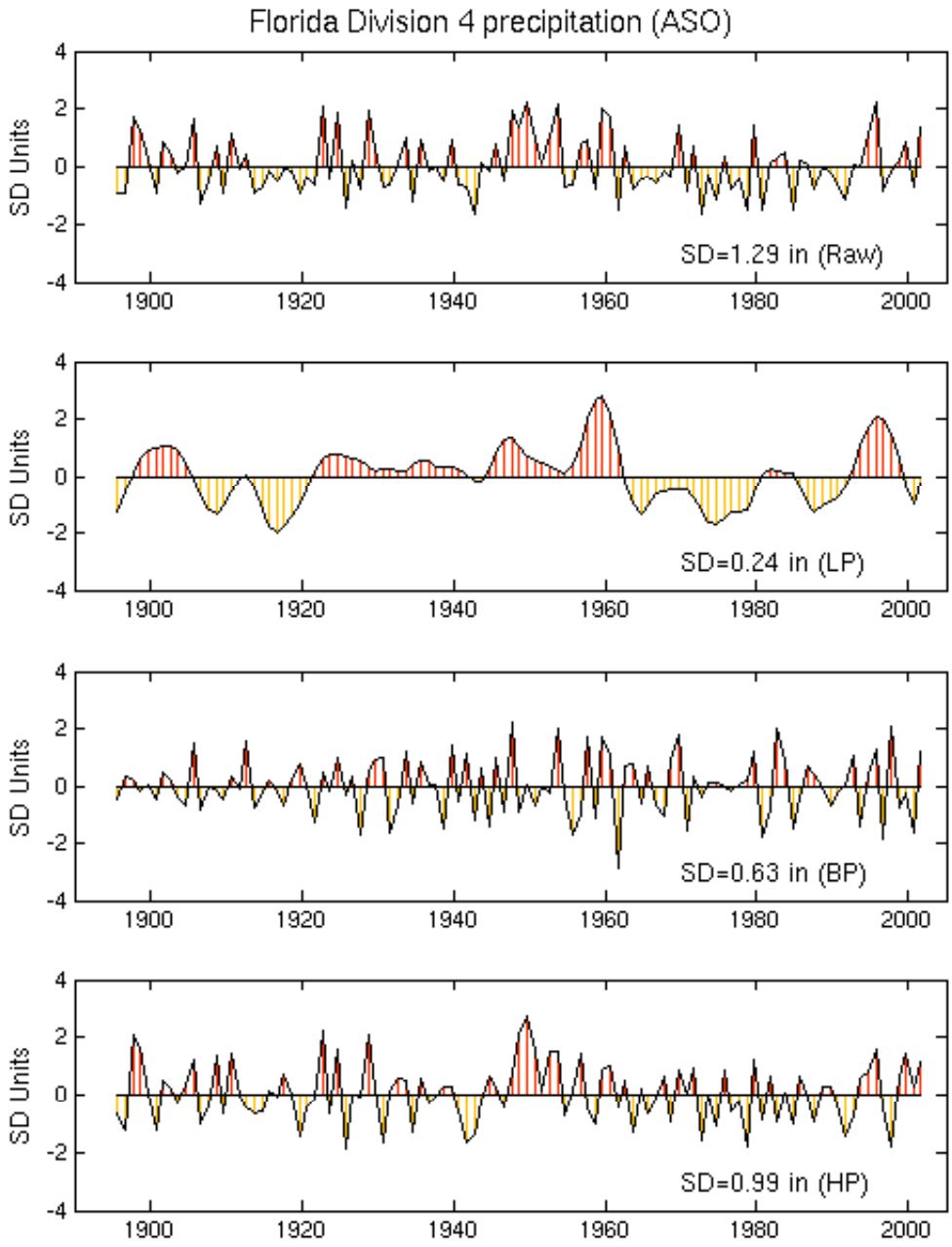

Fig. 15. Same as Fig. 3 but for the August-September-October (ASO) average.

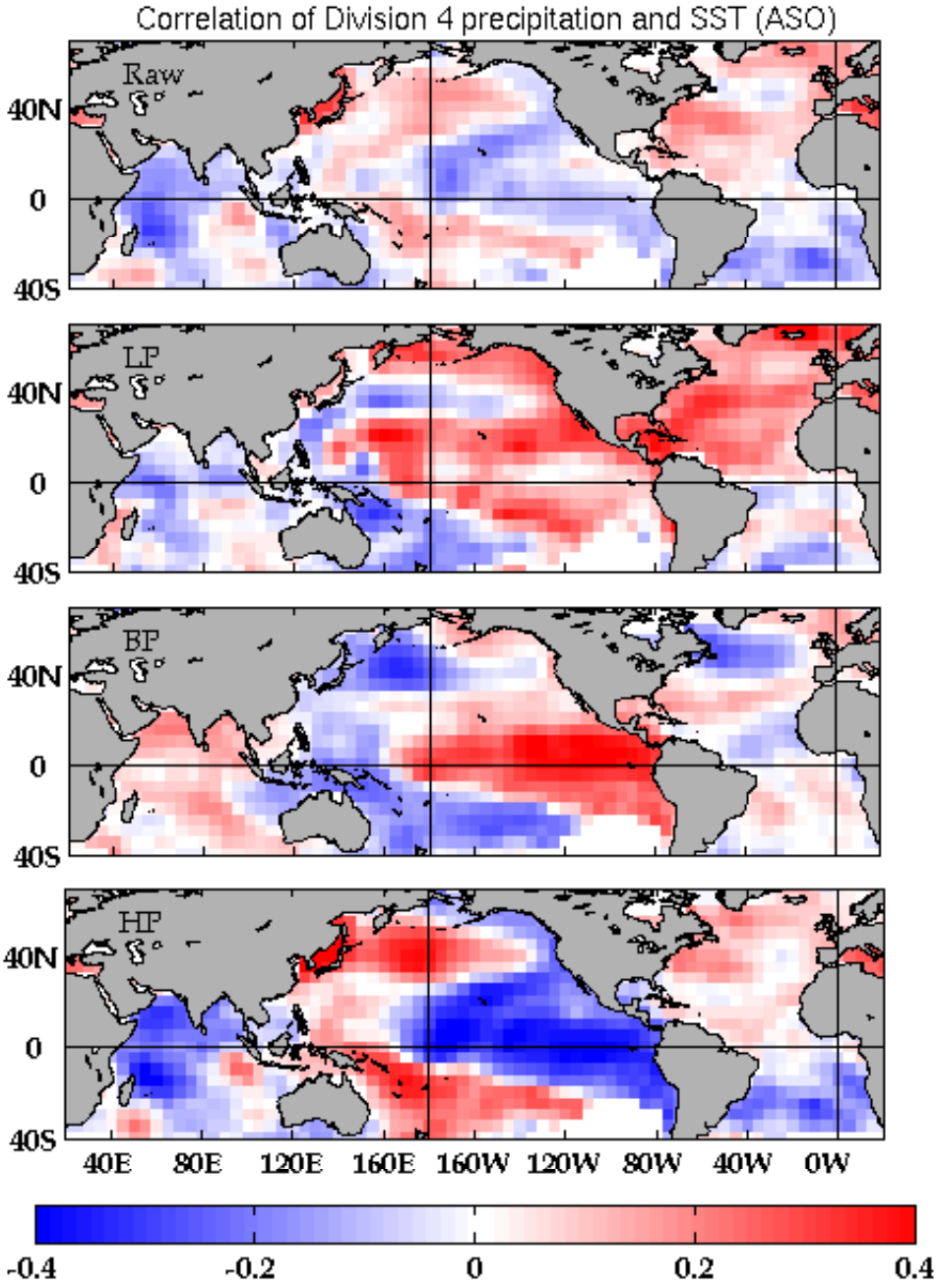

Fig. 16. Map of correlations between global August-September-October (ASO) average SST anomalies and the ASO precipitation anomaly time series shown in Fig. 15.

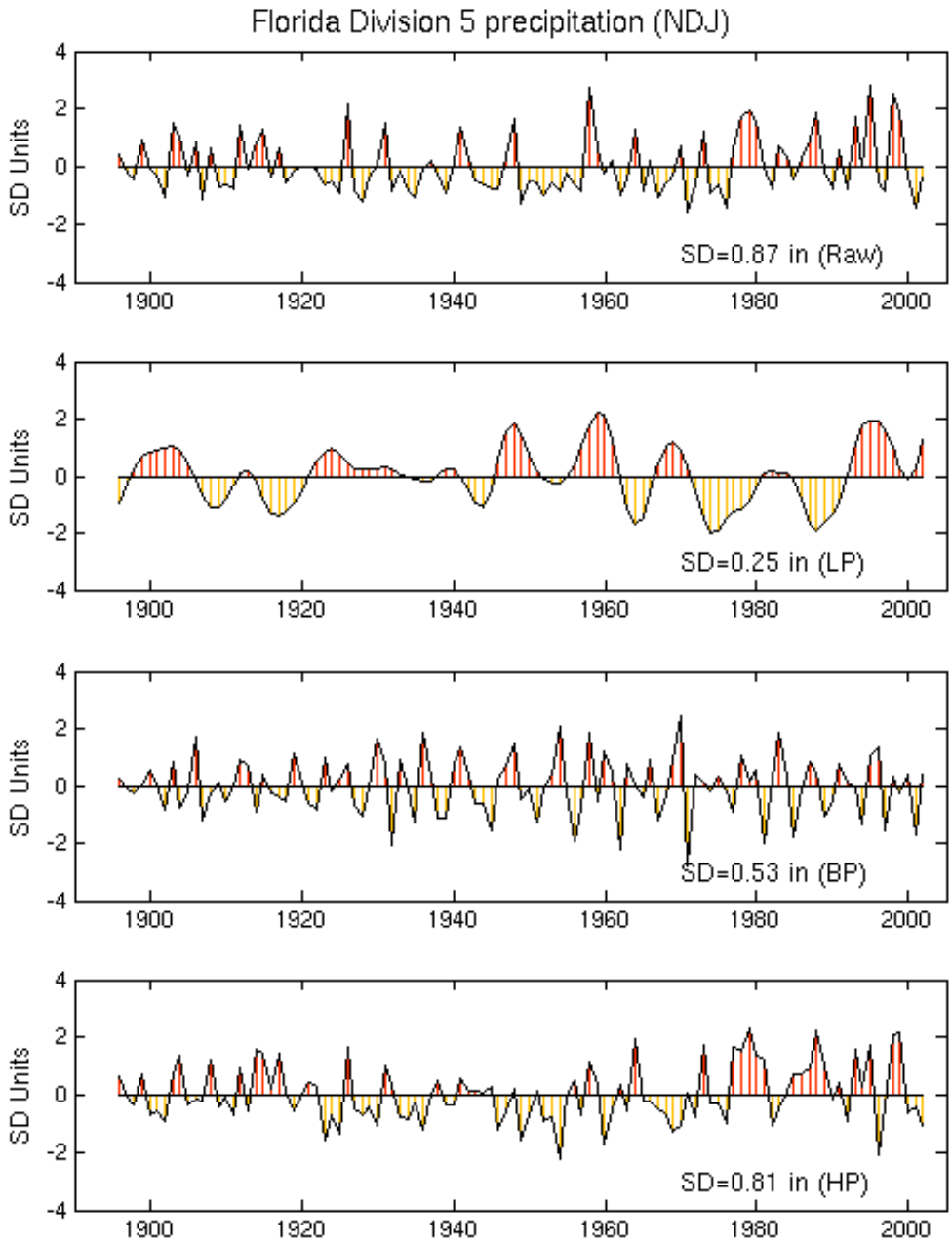

Fig. 17. Same as Fig. 5 but for the November-December-January (NDJ) average.

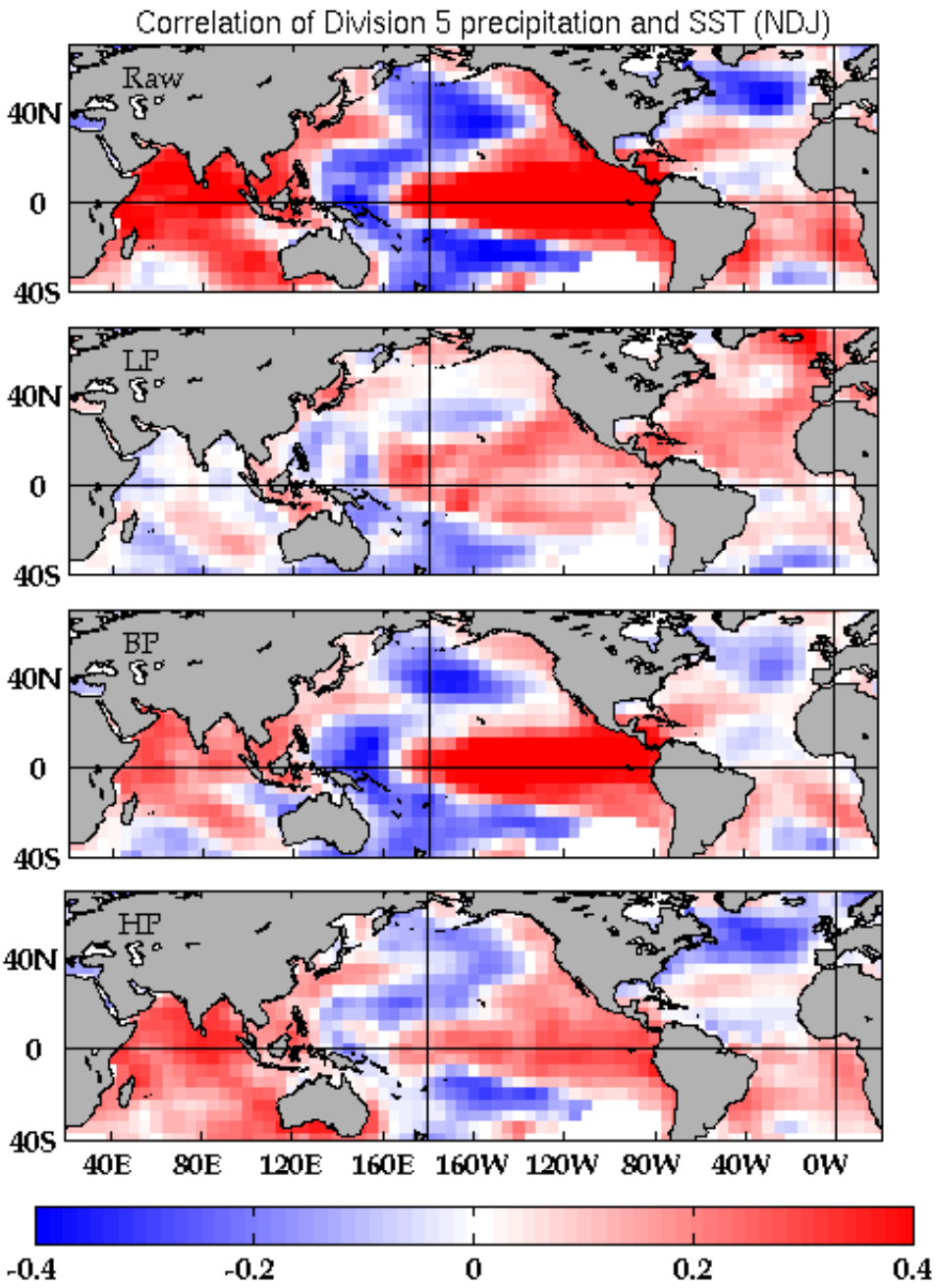

Fig. 18. Map of correlations between global November-December-January (NDJ) average SST anomalies and the NDJ precipitation anomaly time series shown in Fig. 17.

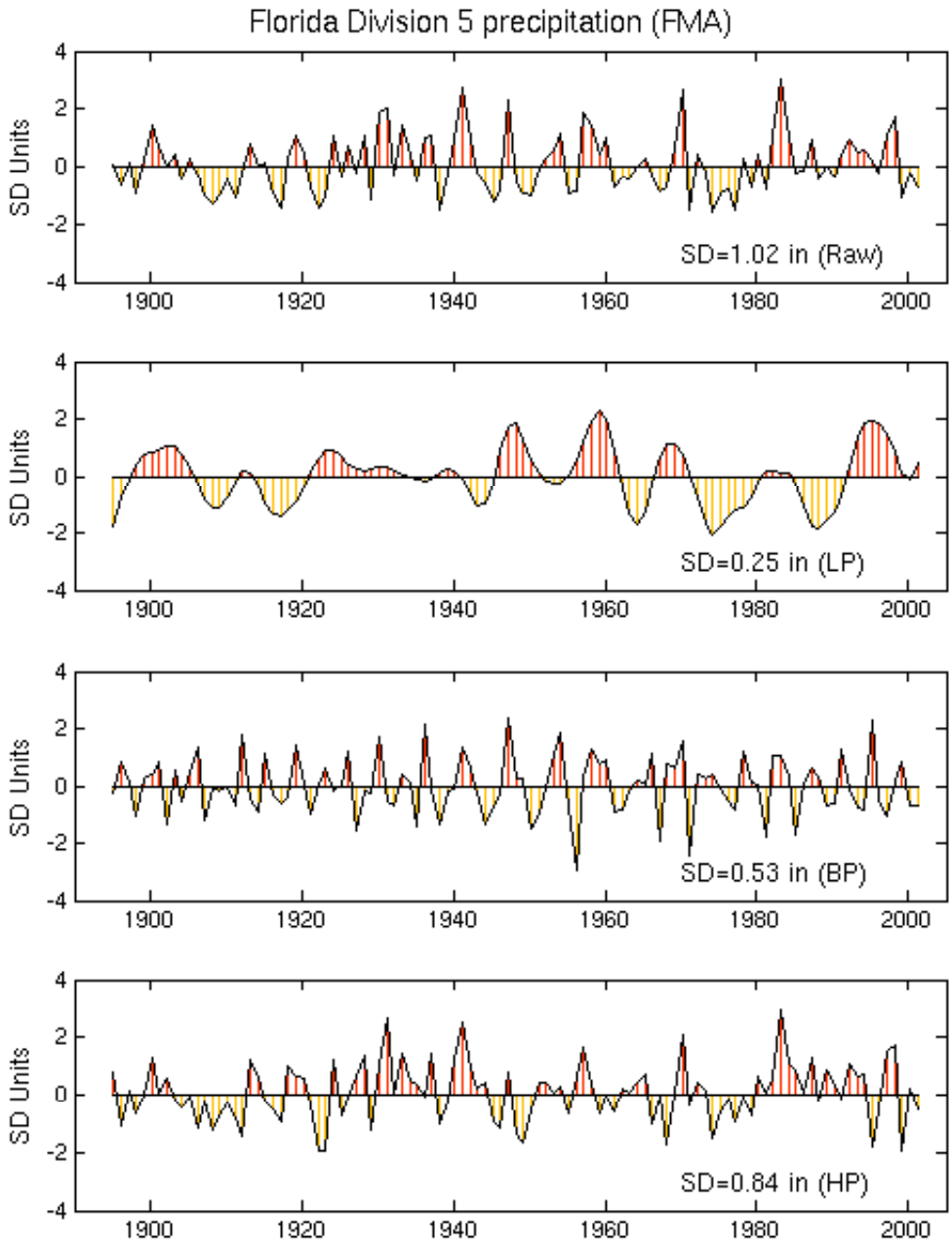

Fig. 19. Same as Fig. 5 but for the February-March-April (FMA) average.

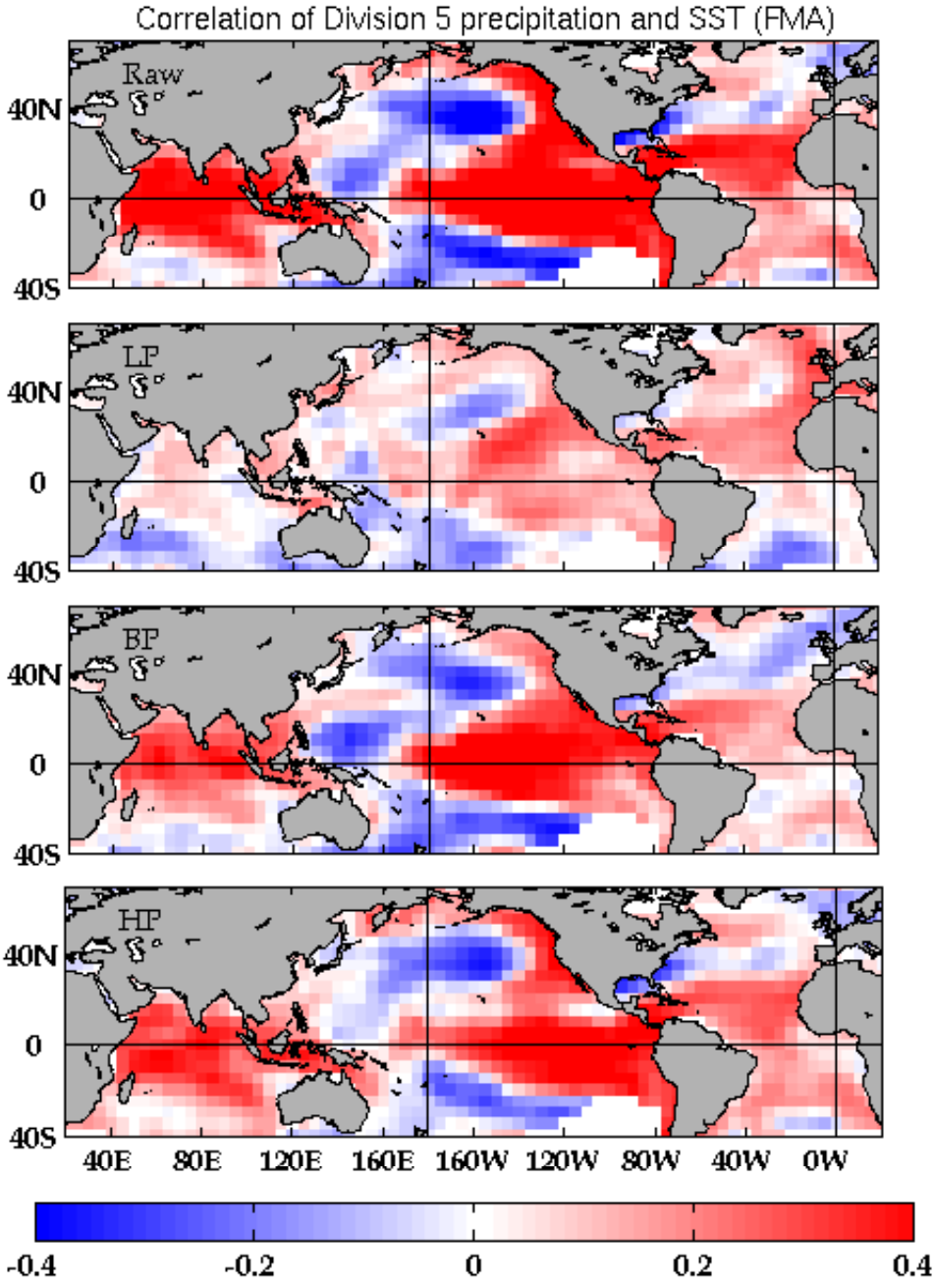

Fig.20. Map of correlations between global February-March-April (FMA) average SST anomalies and the FMA precipitation anomaly time series shown in Fig. 19.

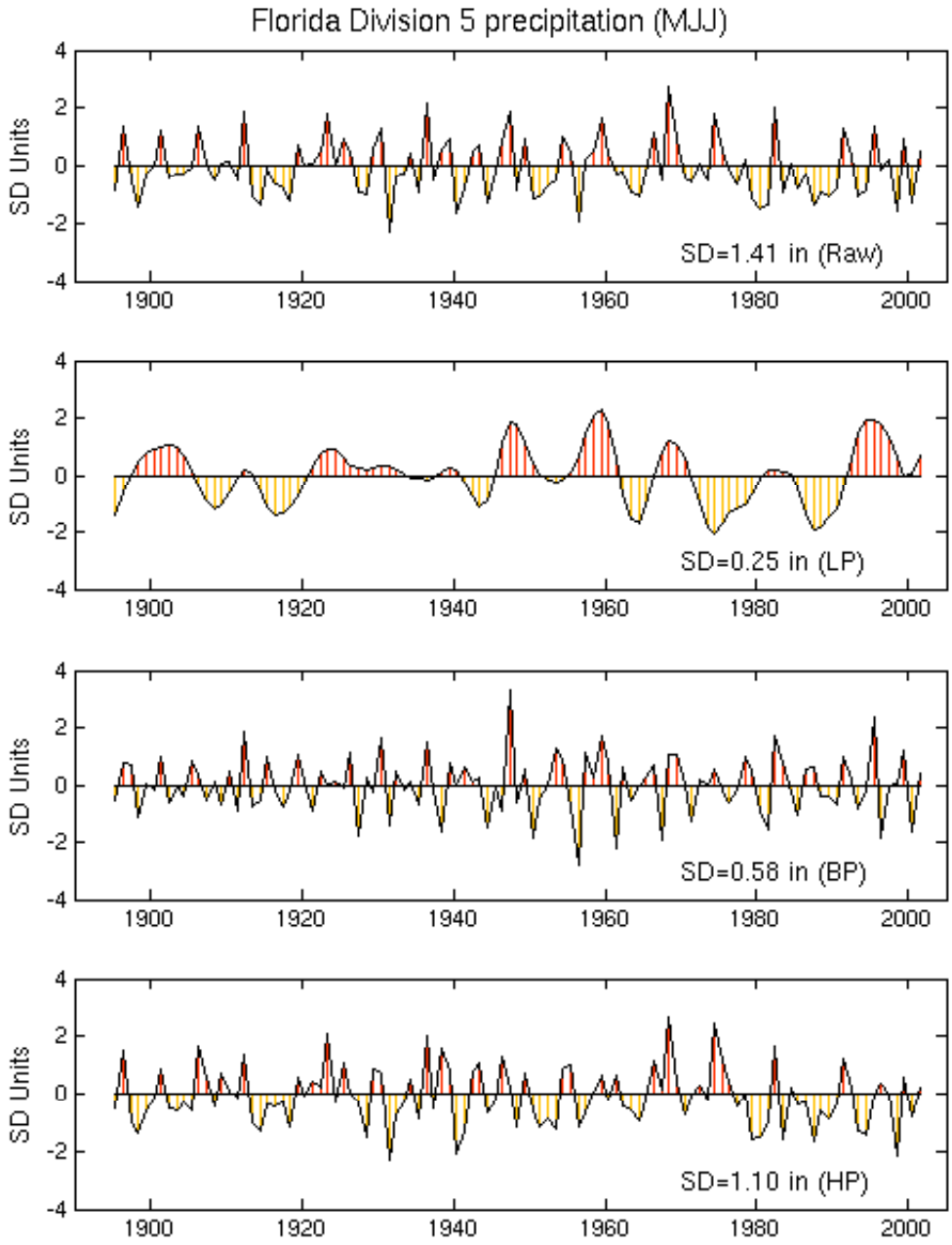

Fig. 21. Same as Fig. 5 but for the May-June-July (MJJ) average.

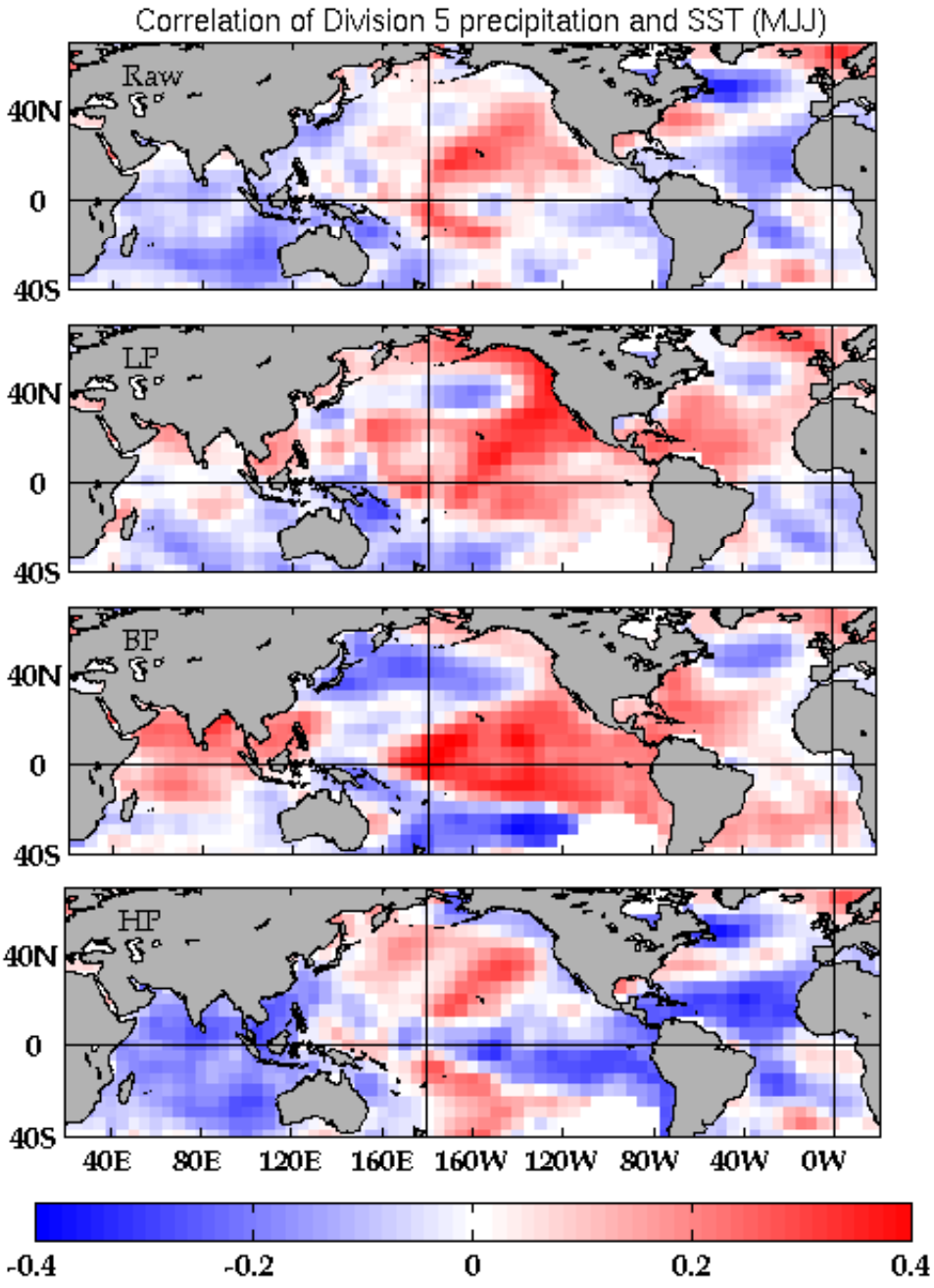

Fig. 22. Map of correlations between global May-June-July (MJJ) average SST anomalies and the MJJ precipitation anomaly time series shown in Fig. 21.

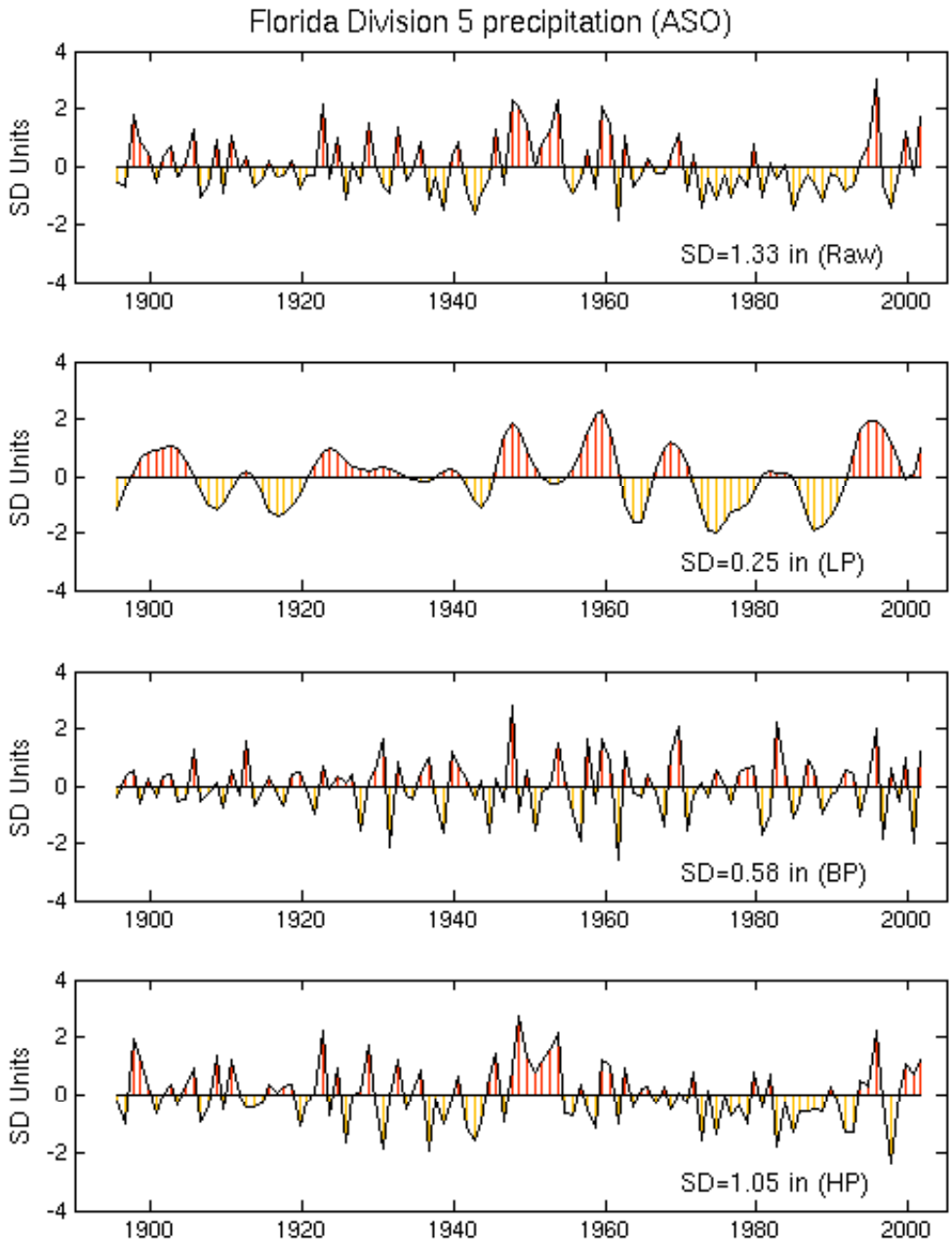

Fig. 23. Same as Fig. 5 but for the August-September-October (ASO) average.

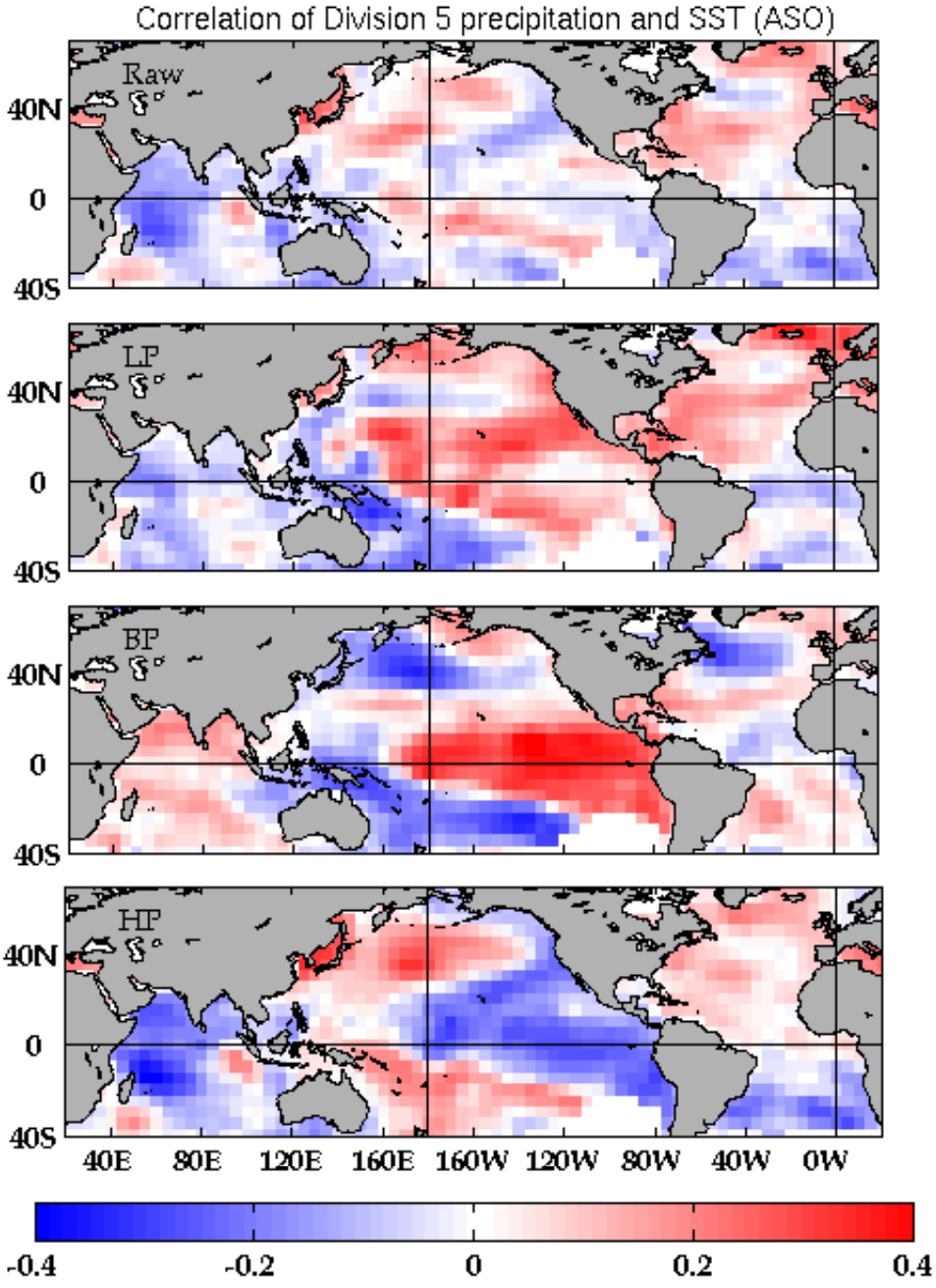

Fig. 24. Map of correlations between global August-September-October (ASO) average SST anomalies and the ASO precipitation anomaly time series shown in Fig. 23.

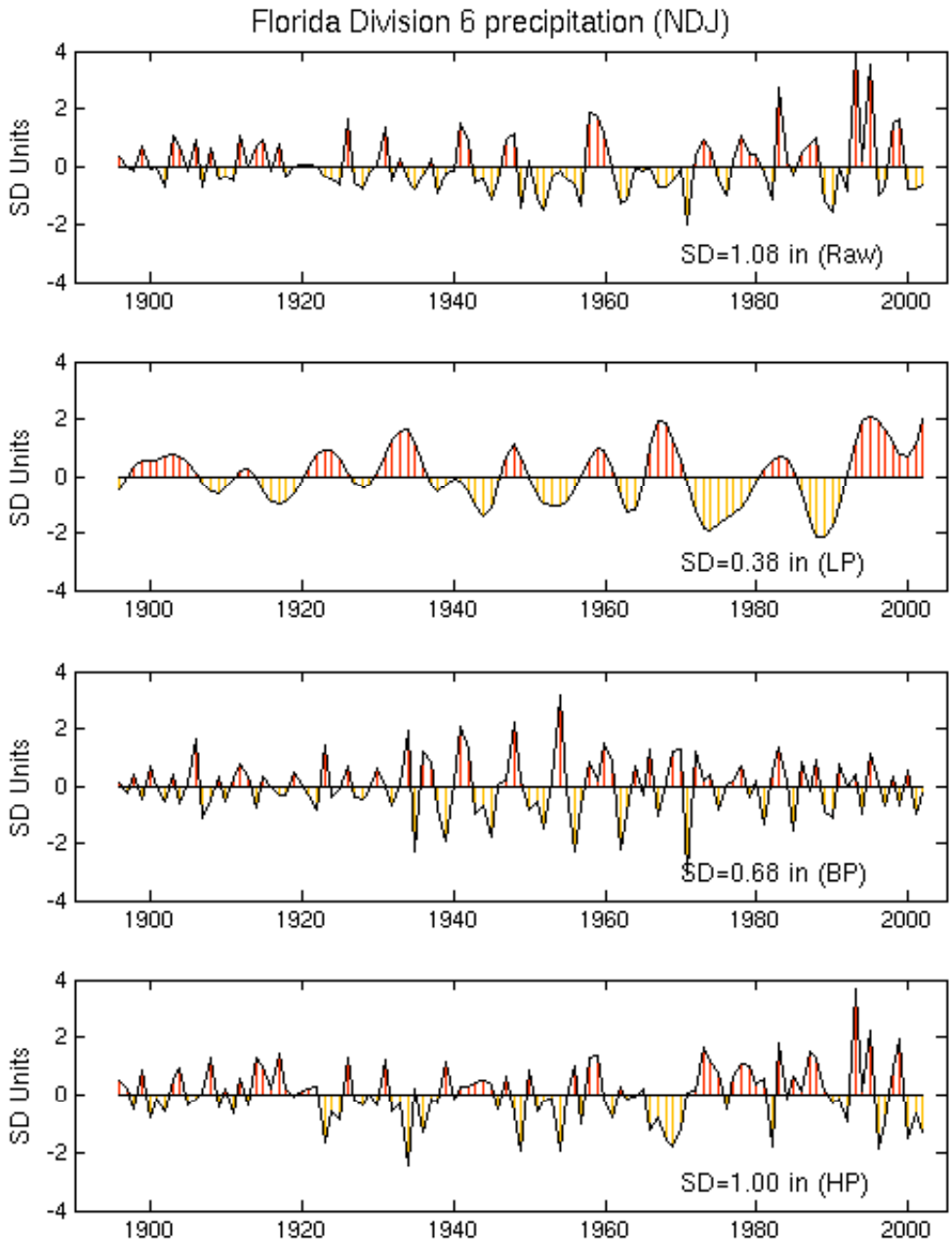

Fig. 25. Same as Fig. 7 but for the November-December-January (NDJ) average.

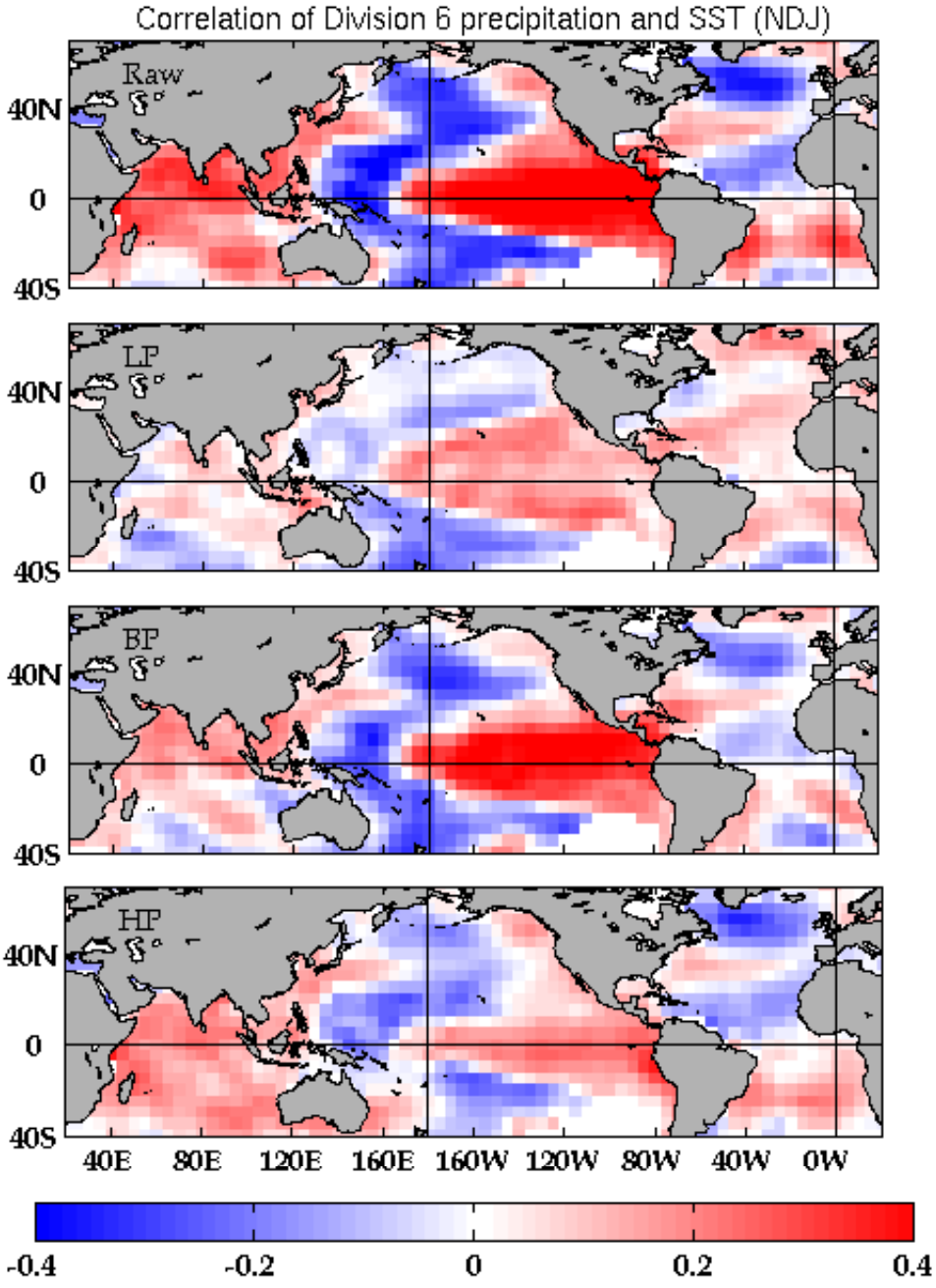

Fig. 26. Map of correlations between global November-December-January (NDJ) average SST anomalies and the NDJ precipitation anomaly time series shown in Fig. 25.

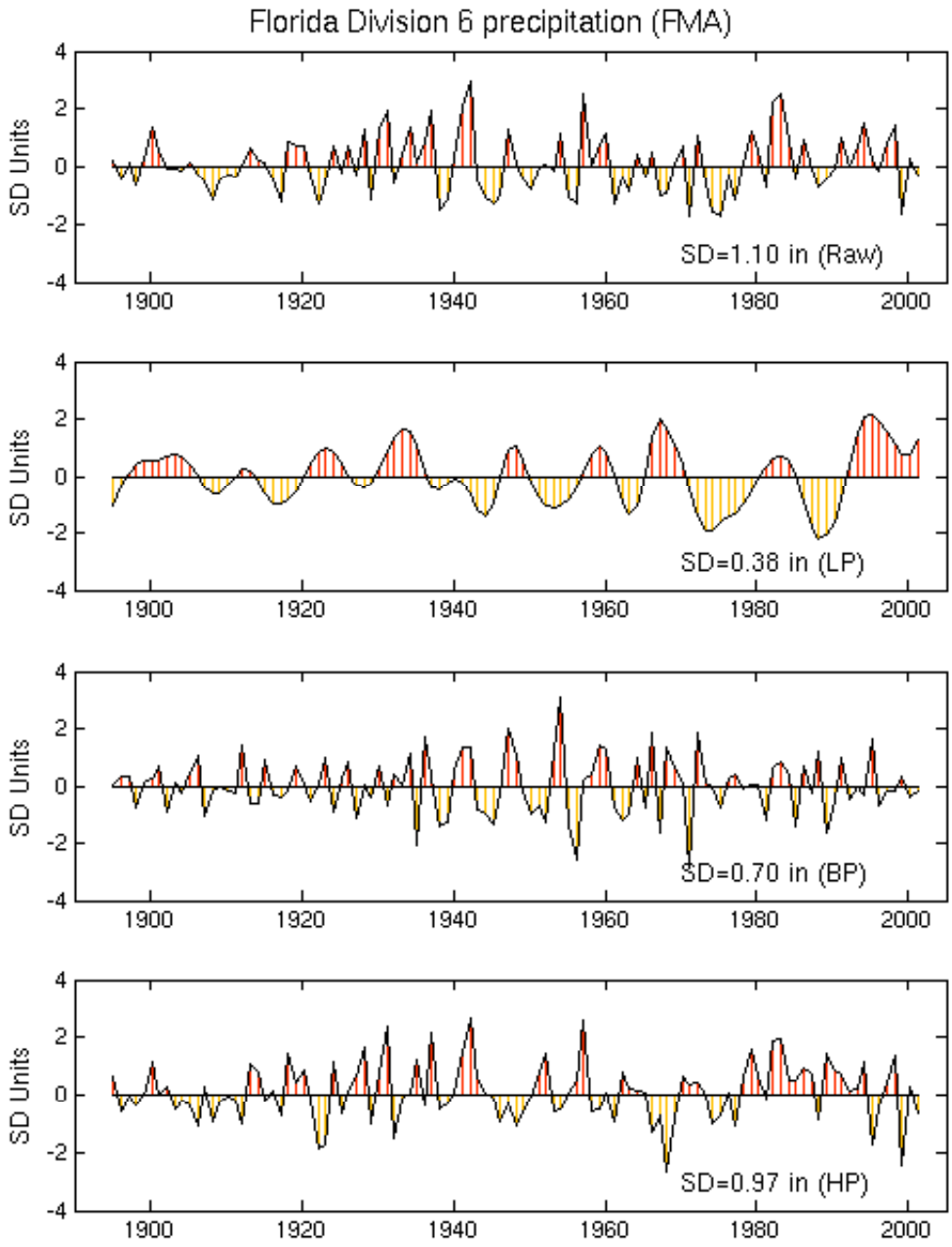

Fig. 27. Same as Fig. 7 but for the February-March-April (FMA) average.

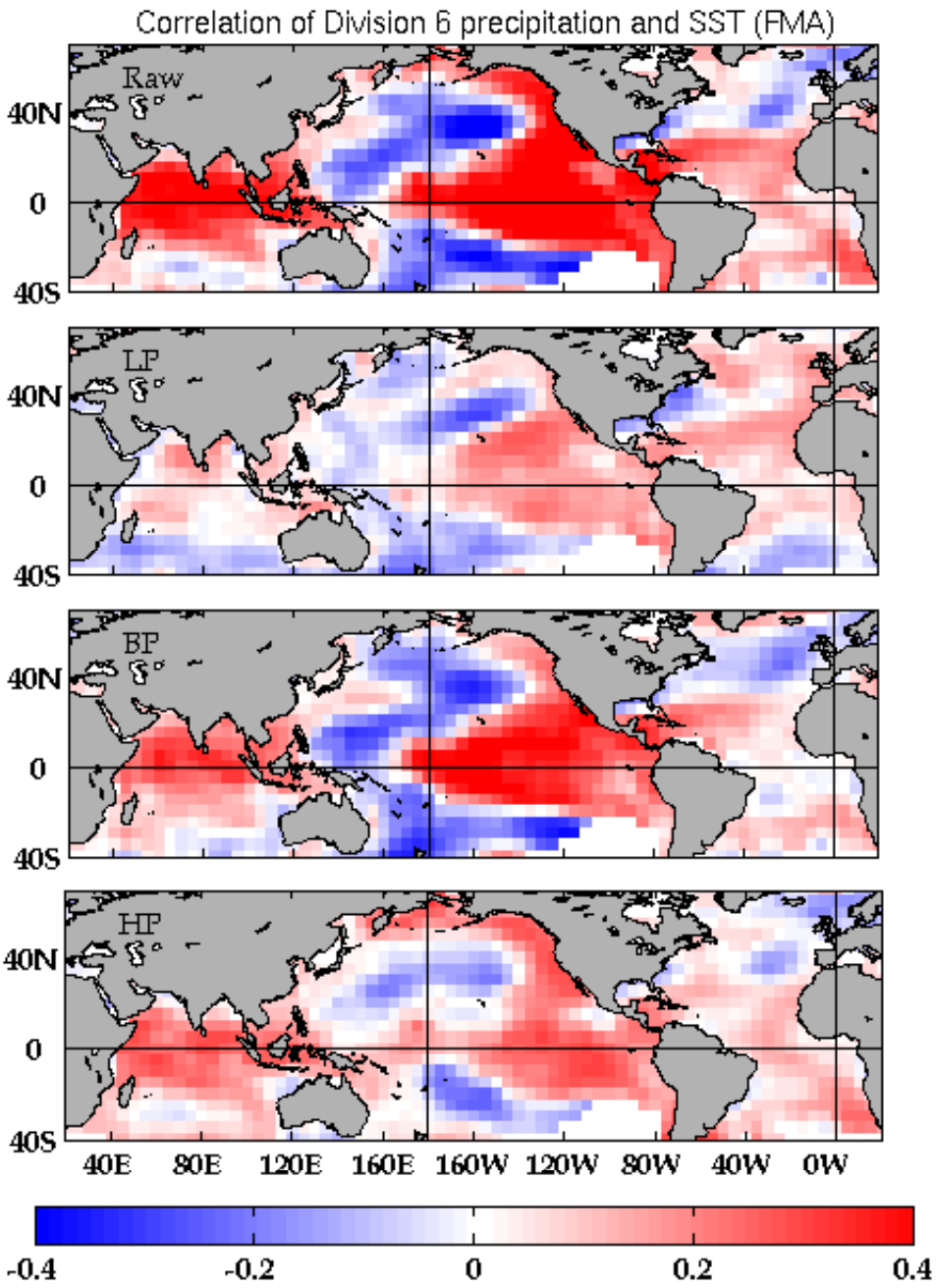

Fig. 28. Map of correlations between global February-March-April (FMA) average SST anomalies and the FMA precipitation anomaly time series shown in Fig. 27.

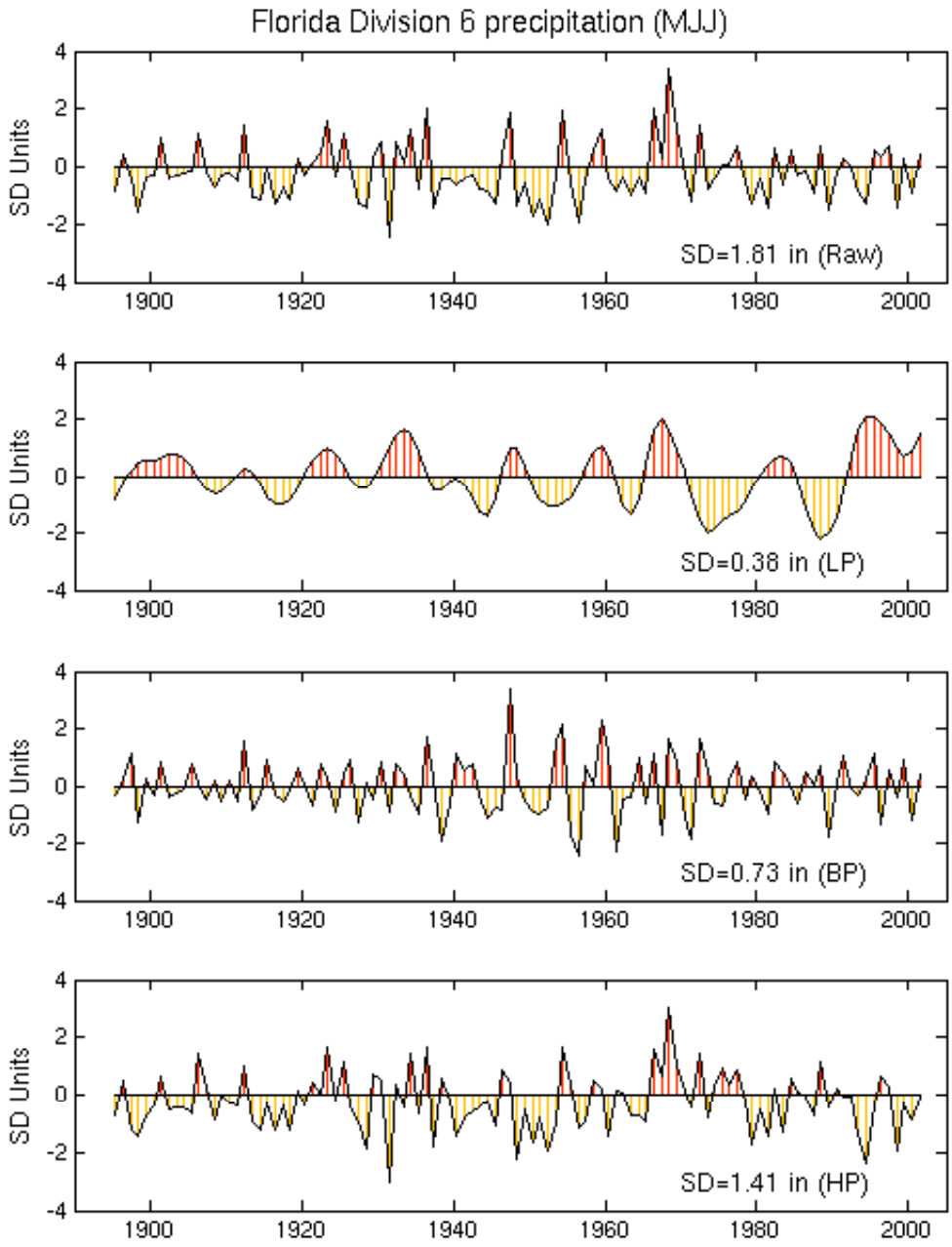

Fig. 29. Same as Fig. 7 but for the May-June-July (MJJ) average.

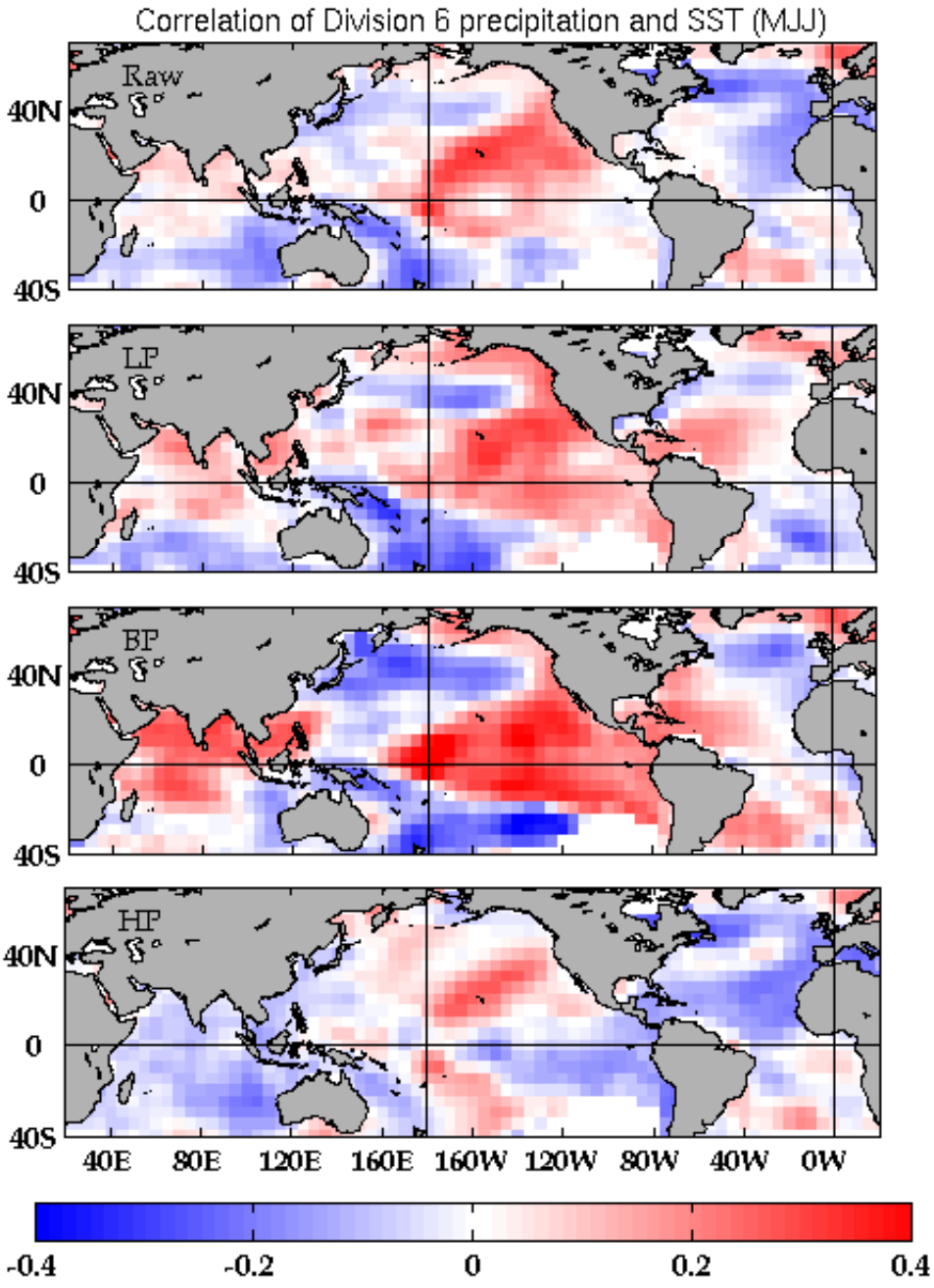

Fig. 30. Map of correlations between global May-June-July (MJJ) average SST anomalies and the MJJ precipitation anomaly time series shown in Fig. 29.

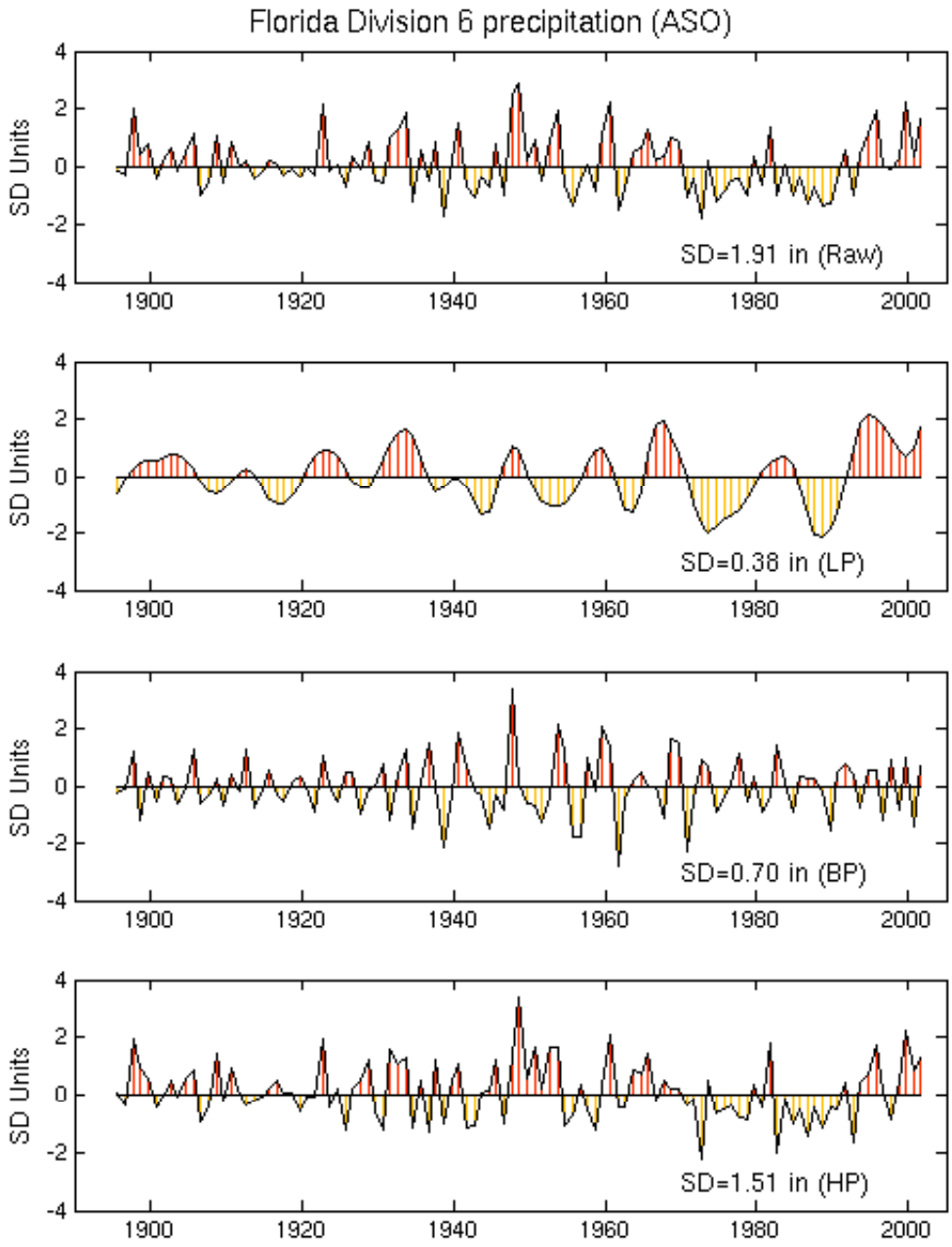

Fig. 31. Same as Fig. 7 but for the August-September-October (ASO) average.

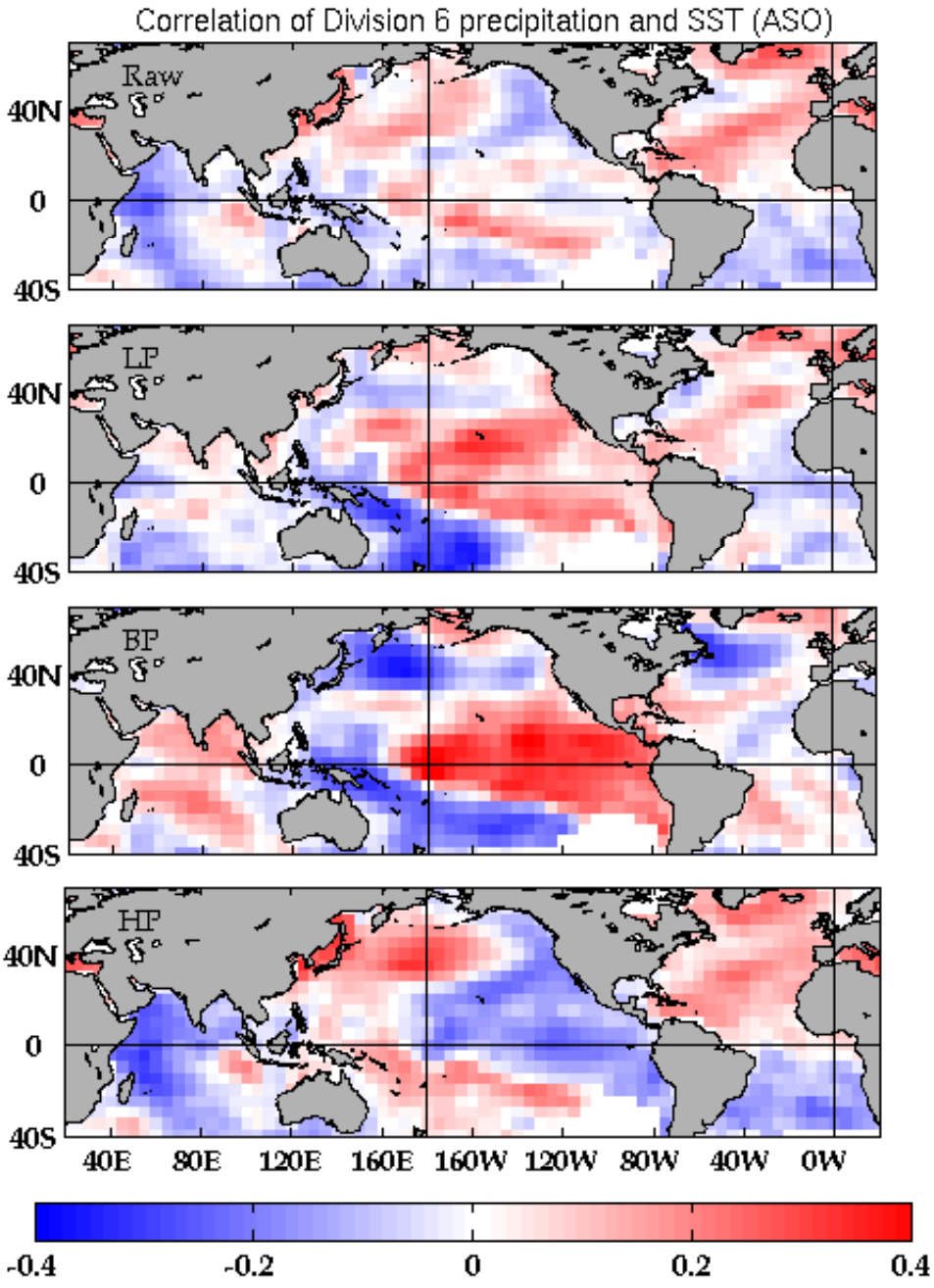

Fig. 32. Map of correlations between global August-September-October (ASO) average SST anomalies and the ASO precipitation anomaly time series shown in Fig. 31.

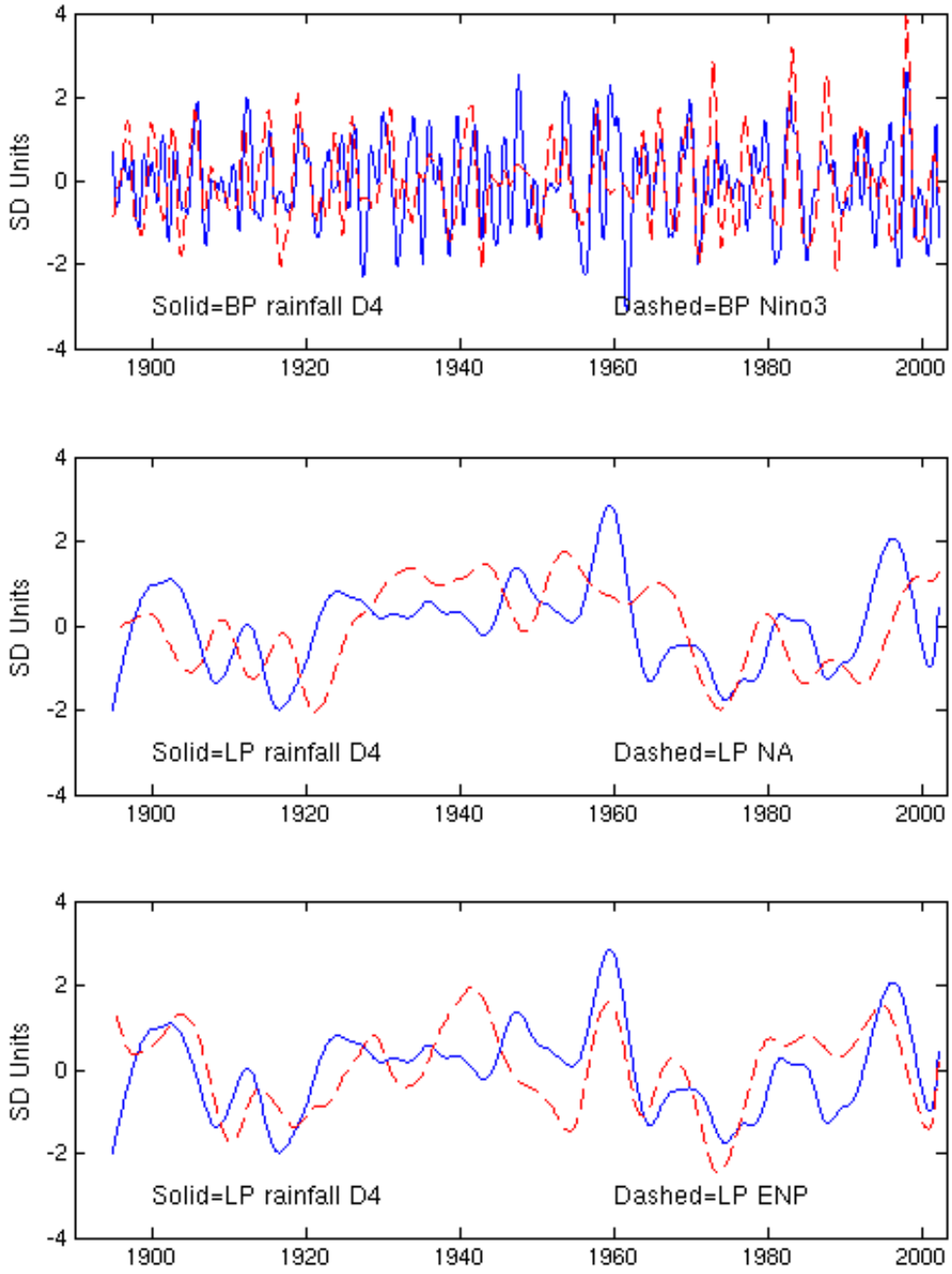

Fig. 33. Standardized comparison of: Band pass (BP) D4 rainfall anomalies and BP Niño3 SST anomalies (top), low pass (LP) D4 rainfall anomalies and LP North Atlantic (NA) SST anomalies (middle), and LP D4 rainfall anomalies and LP Eastern North Pacific (ENP) SST anomalies (bottom). The standard deviations of BP and LP D4 rainfall are 0.6 and 0.24 inches, respectively. The standard deviations of BP Niño3, LP NA, and LP ENP are 0.69, 0.26 and 0.29 ^{o}C, respectively.

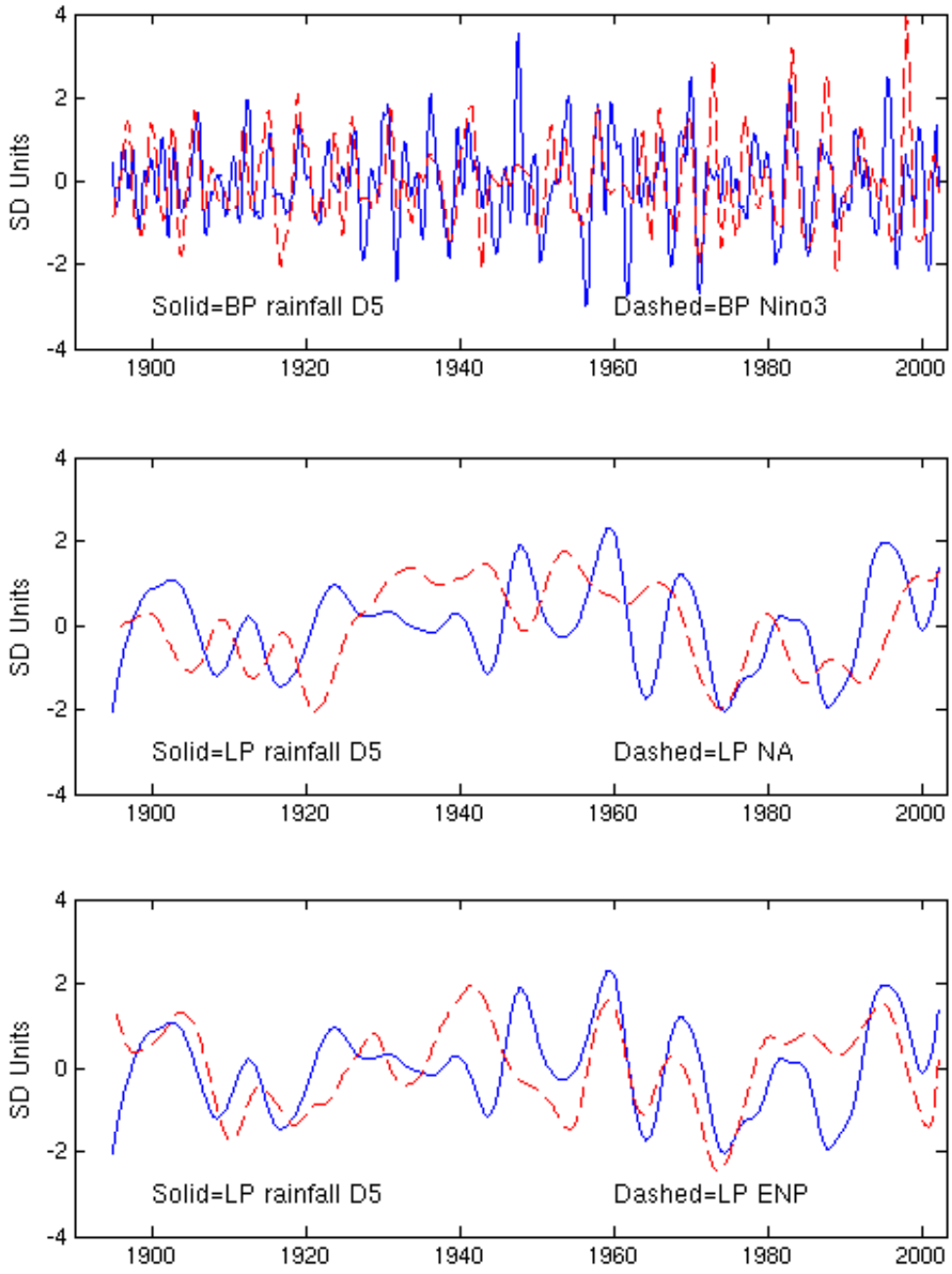

Fig. 34. Same as Fig. 33 but for Florida Division 5 (D5). The standard deviations of BP and LP D5 rainfall are 0.56 and 0.25 inches, respectively.

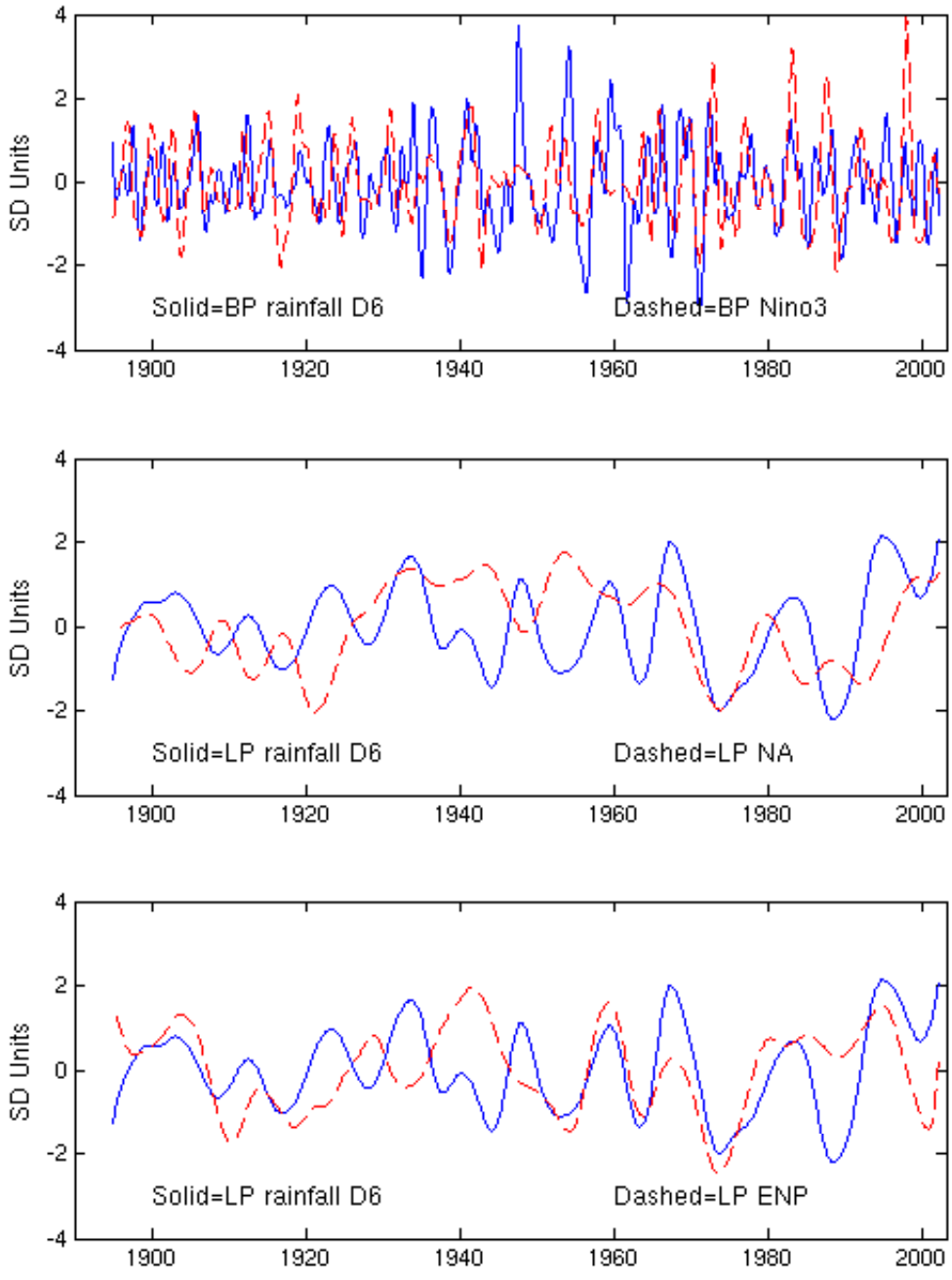

Fig. 35. Same as Fig. 33 but for Florida Division 6 (D6). The standard deviations of BP and LP D6 rainfall are 0.71 and 0.38 inches, respectively.

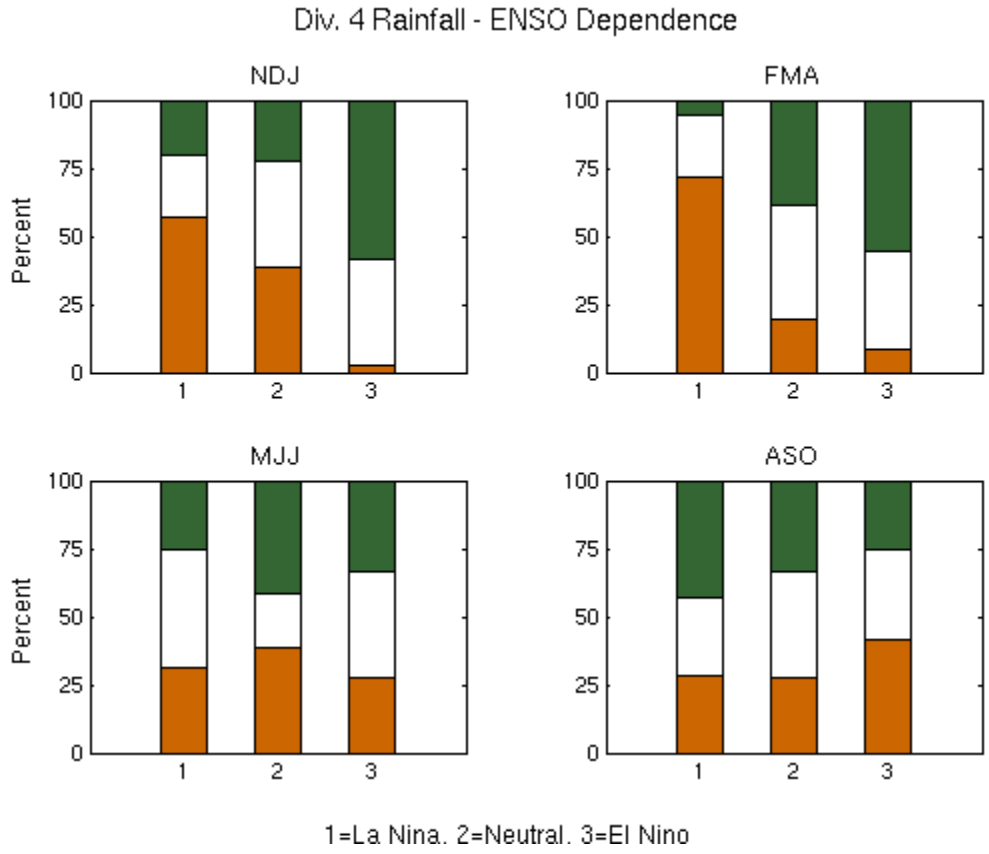

Fig. 36. Contingency plots (in percent) from terciles of Division 4 precipitation and Nino3 index for DJF, FMA, MJJ and ASO.

NDJ

Wet	20	22	58
Neutral	23	39	39
Dry	57	39	3
	La Nina	**Neutral**	**El Nino**

FMA

Wet	6	39	56
Neutral	23	42	36
Dry	71	19	8
	La Nina	**Neutral**	**El Nino**

MJJ

Wet	26	42	33
Neutral	43	19	39
Dry	31	39	28
	La Nina	**Neutral**	**El Nino**

ASO

Wet	43	33	25
Neutral	29	39	33
Dry	29	28	42
	La Nina	**Neutral**	**El Nino**

Table 1. Contingency tables corresponding to the contingency plots shown in Fig. 36. Numbers are in percent.

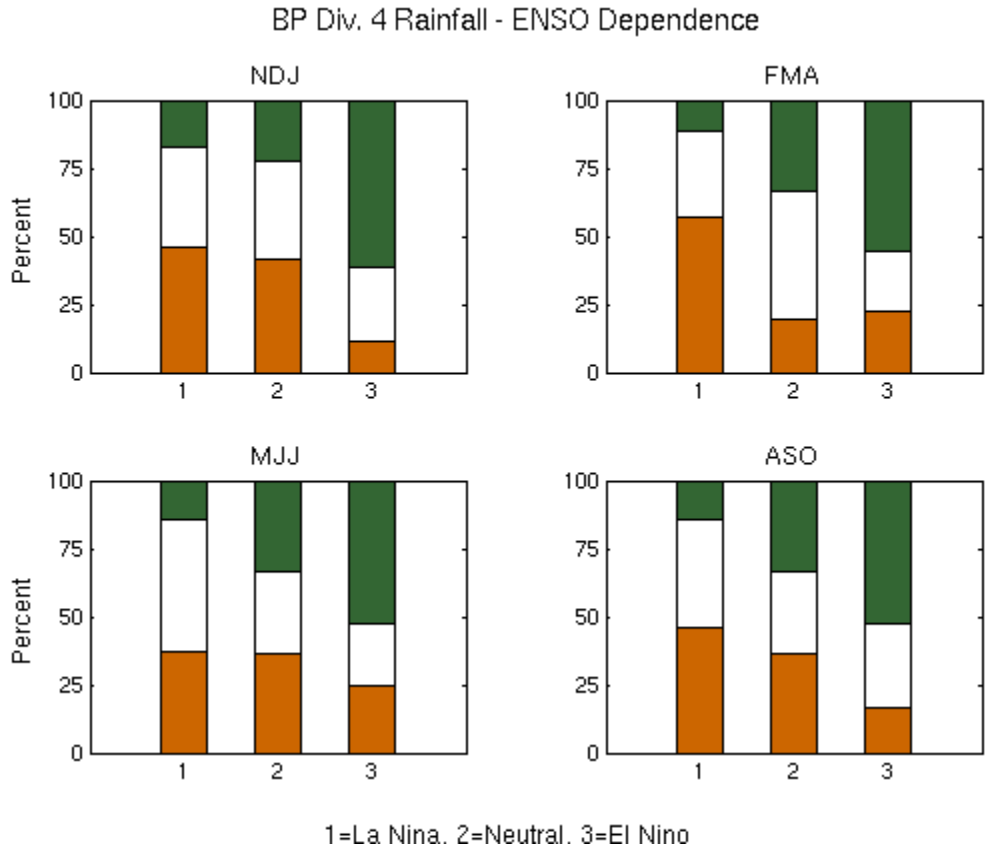

Fig. 37. Contingency plots (in percent) from terciles of band-passed (BP) Division 4 precipitation and Nino3 index for DJF, FMA, MJJ and ASO.

NDJ

Wet	17	22	61
Neutral	37	36	28
Dry	46	42	11
	La Nina	**Neutral**	**El Nino**

FMA

Wet	11	33	56
Neutral	31	47	22
Dry	57	19	22
	La Nina	**Neutral**	**El Nino**

MJJ

Wet	14	33	53
Neutral	49	31	22
Dry	37	36	25
	La Nina	**Neutral**	**El Nino**

ASO

Wet	14	33	53
Neutral	40	31	31
Dry	46	36	17
	La Nina	**Neutral**	**El Nino**

Table 2. Contingency tables corresponding to the contingency plots shown in Fig. 37. Numbers are in percent.

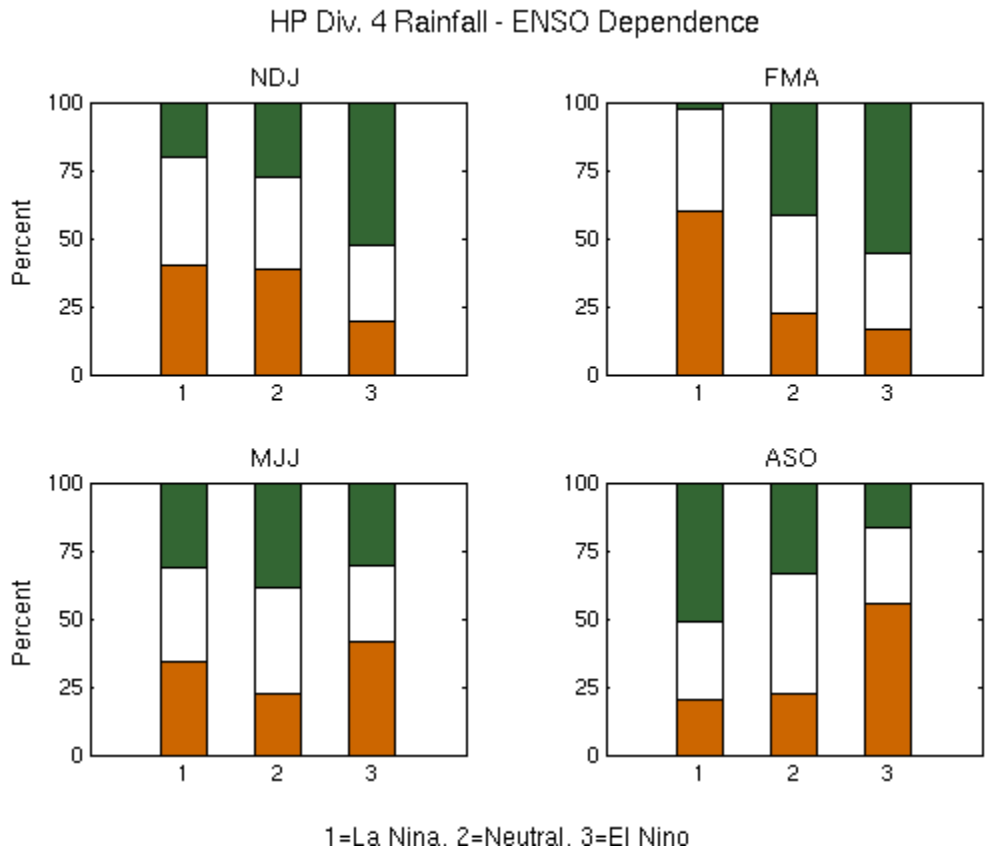

Fig. 38. Contingency plots (in percent) from terciles of high-passed (HP) Division 4 precipitation and Nino3 index for DJF, FMA, MJJ and ASO.

NDJ

Wet	20	28	53
Neutral	40	33	28
Dry	40	39	19
	La Nina	**Neutral**	**El Nino**

FMA

Wet	3	42	56
Neutral	37	36	28
Dry	60	22	17
	La Nina	**Neutral**	**El Nino**

MJJ

Wet	31	39	31
Neutral	34	39	28
Dry	34	22	42
	La Nina	**Neutral**	**El Nino**

ASO

Wet	51	33	17
Neutral	29	44	28
Dry	20	22	56
	La Nina	**Neutral**	**El Nino**

Table 3. Contingency tables corresponding to the contingency plots shown in Fig. 38. Numbers are in percent.

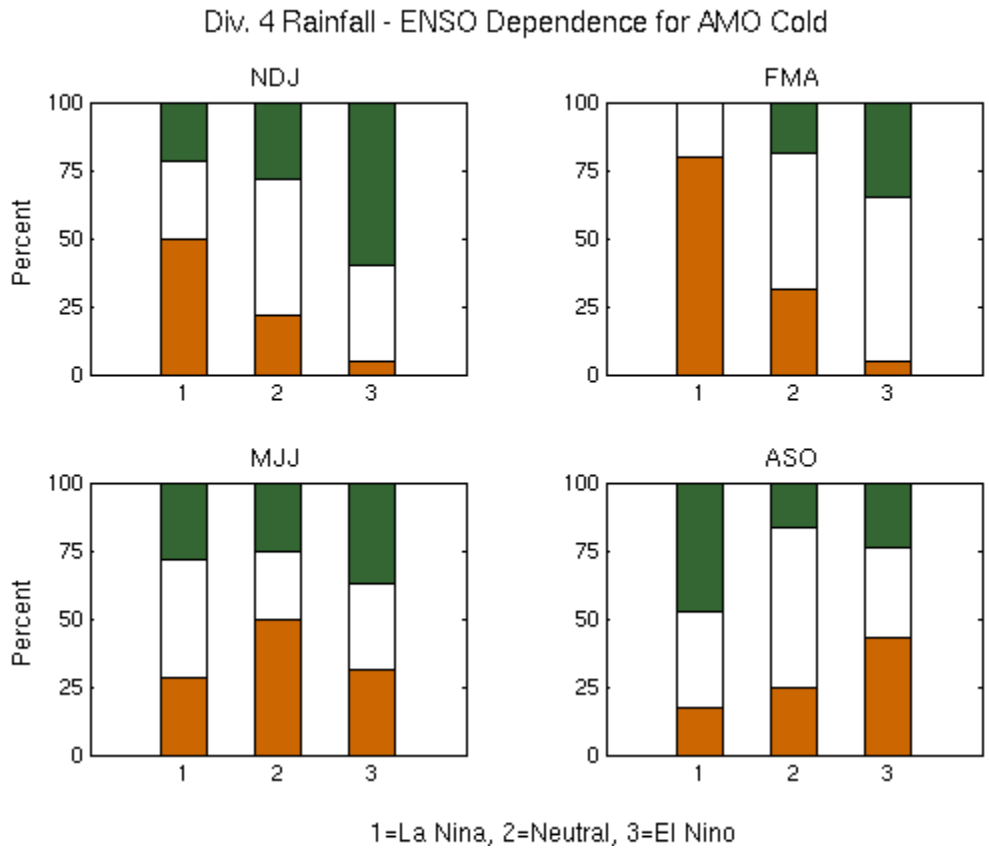

Fig. 39. Contingency plots (in percent) from terciles of Division 4 precipitation and Nino3 index when the AMO is in its cold phase for DJF, FMA, MJJ and ASO.

NDJ

Wet	21	29	60
Neutral	29	50	35
Dry	50	21	5
	La Nina	**Neutral**	**El Nino**

FMA

Wet	0	19	35
Neutral	20	50	60
Dry	80	31	5
	La Nina	**Neutral**	**El Nino**

MJJ

Wet	29	25	37
Neutral	43	25	32
Dry	29	50	32
	La Nina	**Neutral**	**El Nino**

ASO

Wet	47	17	24
Neutral	35	58	33
Dry	18	25	43
	La Nina	**Neutral**	**El Nino**

Table 4. Contingency tables corresponding to the contingency plots shown in Fig. 39. Numbers are in percent.

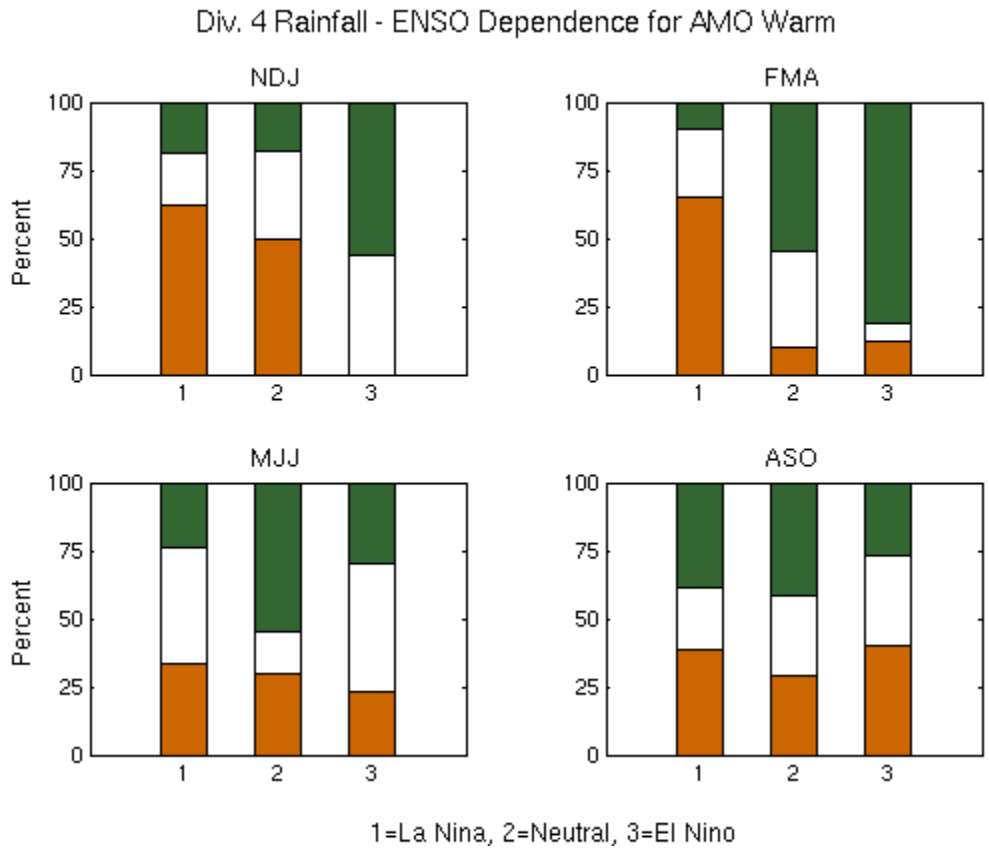

Fig. 40. Contingency plots (in percent) from terciles of Division 4 precipitation and Nino3 index when the AMO is in its warm phase for DJF, FMA, MJJ and ASO.

NDJ

Wet	19	18	56
Neutral	19	32	44
Dry	62	50	0
	La Nina	**Neutral**	**El Nino**

FMA

Wet	10	55	81
Neutral	25	35	6
Dry	65	10	13
	La Nina	**Neutral**	**El Nino**

MJJ

Wet	24	55	29
Neutral	43	15	47
Dry	33	30	24
	La Nina	**Neutral**	**El Nino**

ASO

Wet	39	42	27
Neutral	22	29	33
Dry	39	29	40
	La Nina	**Neutral**	**El Nino**

Table 5. Contingency tables corresponding to the contingency plots shown in Fig. 40. Numbers are in percent.

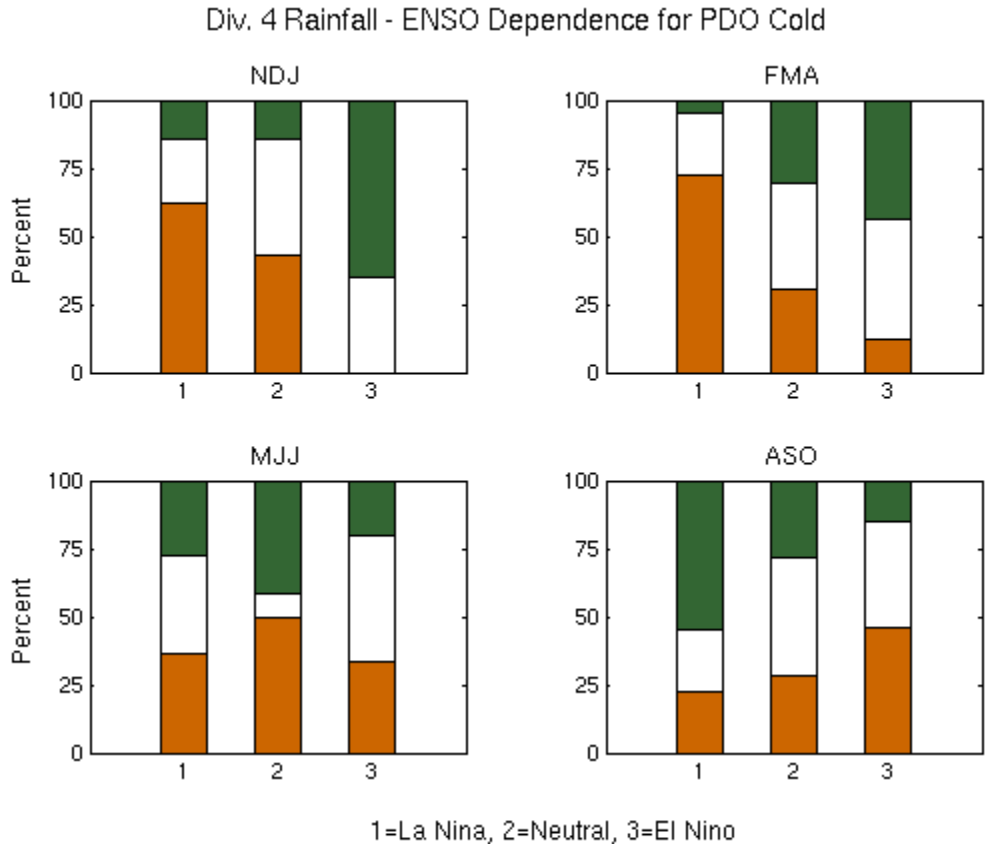

Fig. 41. Contingency plots (in percent) from terciles of Division 4 precipitation and Nino3 index when the PDO is in its cold phase for DJF, FMA, MJJ and ASO.

NDJ

Wet	14	14	65
Neutral	24	43	35
Dry	62	43	0
	La Nina	**Neutral**	**El Nino**

FMA

Wet	5	31	44
Neutral	23	38	44
Dry	73	31	13
	La Nina	**Neutral**	**El Nino**

MJJ

Wet	27	42	20
Neutral	36	8	47
Dry	36	50	33
	La Nina	**Neutral**	**El Nino**

ASO

Wet	55	29	15
Neutral	23	43	38
Dry	23	29	46
	La Nina	**Neutral**	**El Nino**

Table 6. Contingency tables corresponding to the contingency plots shown in Fig. 41. Numbers are in percent.

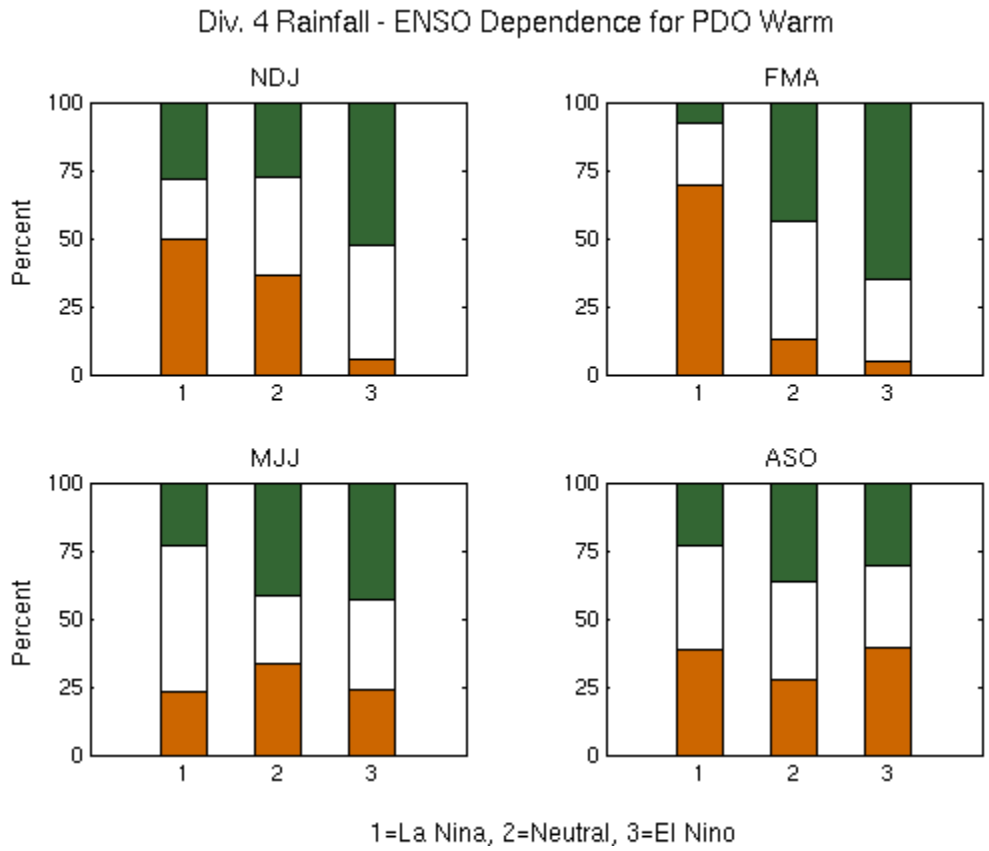

Fig. 42. Contingency plots (in percent) from terciles of Division 4 precipitation and Nino3 index when the PDO is in its warm phase for DJF, FMA, MJJ and ASO.

NDJ

Wet	29	27	53
Neutral	21	36	42
Dry	50	36	5
	La Nina	**Neutral**	**El Nino**

FMA

Wet	8	43	65
Neutral	23	43	30
Dry	69	13	5
	La Nina	**Neutral**	**El Nino**

MJJ

Wet	23	42	43
Neutral	54	25	33
Dry	23	33	24
	La Nina	**Neutral**	**El Nino**

ASO

Wet	23	36	30
Neutral	38	36	30
Dry	38	27	39
	La Nina	**Neutral**	**El Nino**

Table 7. Contingency tables corresponding to the contingency plots shown in Fig. 42. Numbers are in percent.

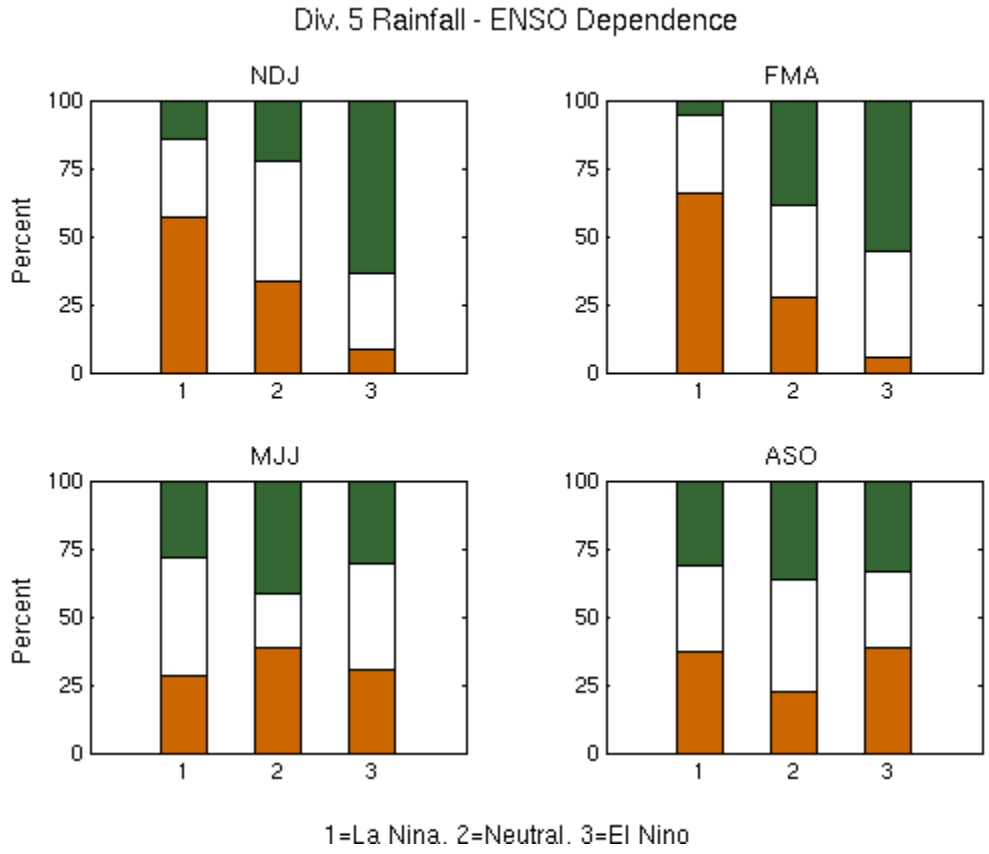

Fig. 43. Contingency plots (in percent) from terciles of Division 5 precipitation and Nino3 index for DJF, FMA, MJJ and ASO.

NDJ

Wet	14	22	64
Neutral	29	44	28
Dry	57	33	8
	La Nina	**Neutral**	**El Nino**

FMA

Wet	6	39	56
Neutral	29	33	39
Dry	66	28	6
	La Nina	**Neutral**	**El Nino**

MJJ

Wet	29	42	31
Neutral	43	19	39
Dry	29	39	31
	La Nina	**Neutral**	**El Nino**

ASO

Wet	31	36	33
Neutral	31	42	28
Dry	37	22	39
	La Nina	**Neutral**	**El Nino**

Table 8. Contingency tables corresponding to the contingency plots shown in Fig. 43. Numbers are in percent.

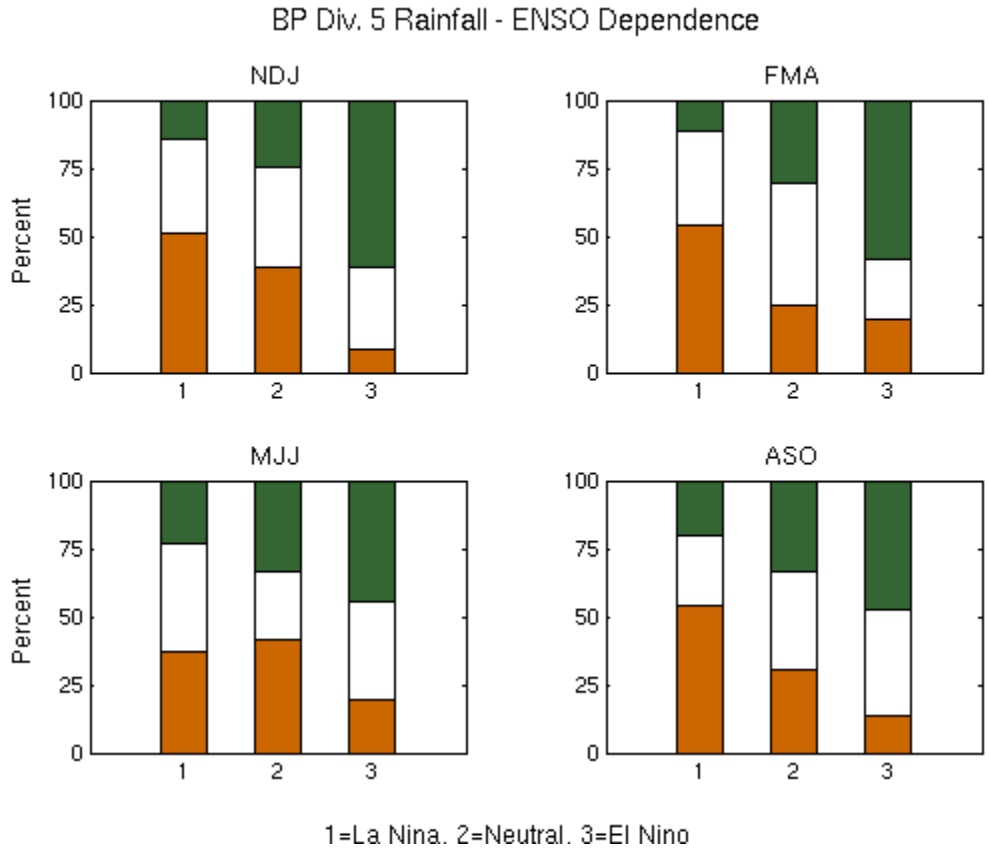

Fig. 44. Contingency plots (in percent) from terciles of band-passed (BP) Division 5 precipitation and Nino3 index for DJF, FMA, MJJ and ASO.

NDJ

Wet	14	25	61
Neutral	34	36	31
Dry	51	39	8
	La Nina	**Neutral**	**El Nino**

FMA

Wet	11	31	58
Neutral	34	44	22
Dry	54	25	19
	La Nina	**Neutral**	**El Nino**

MJJ

Wet	23	33	44
Neutral	40	25	36
Dry	37	42	19
	La Nina	**Neutral**	**El Nino**

ASO

Wet	20	33	47
Neutral	26	36	39
Dry	54	31	14
	La Nina	**Neutral**	**El Nino**

Table 9. Contingency tables corresponding to the contingency plots shown in Fig. 44. Numbers are in percent.

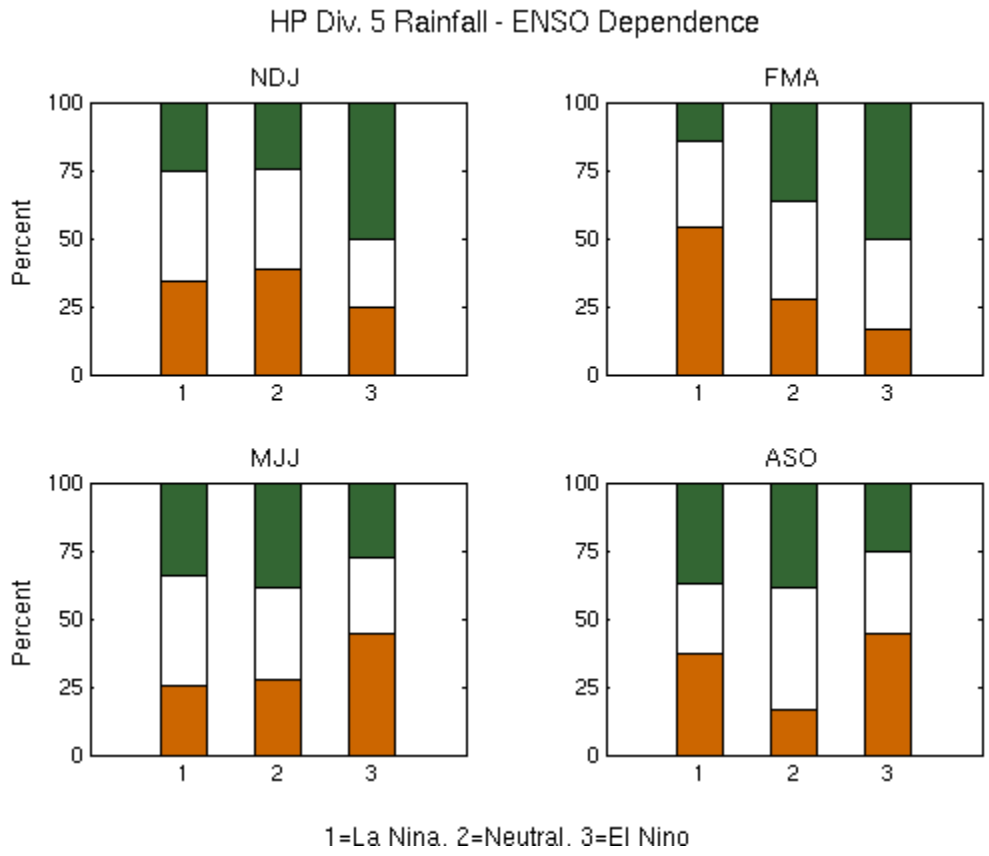

Fig. 45. Contingency plots (in percent) from terciles of high-passed (HP) Division 5 precipitation and Nino3 index for DJF, FMA, MJJ and ASO.

NDJ

Wet	26	25	50
Neutral	40	36	25
Dry	34	39	25
	La Nina	**Neutral**	**El Nino**

FMA

Wet	14	36	50
Neutral	31	36	33
Dry	54	27	17
	La Nina	**Neutral**	**El Nino**

MJJ

Wet	34	39	28
Neutral	40	33	28
Dry	26	28	44
	La Nina	**Neutral**	**El Nino**

ASO

Wet	37	39	25
Neutral	26	44	31
Dry	37	17	44
	La Nina	**Neutral**	**El Nino**

Table 10. Contingency tables corresponding to the contingency plots shown in Fig. 45. Numbers are in percent.

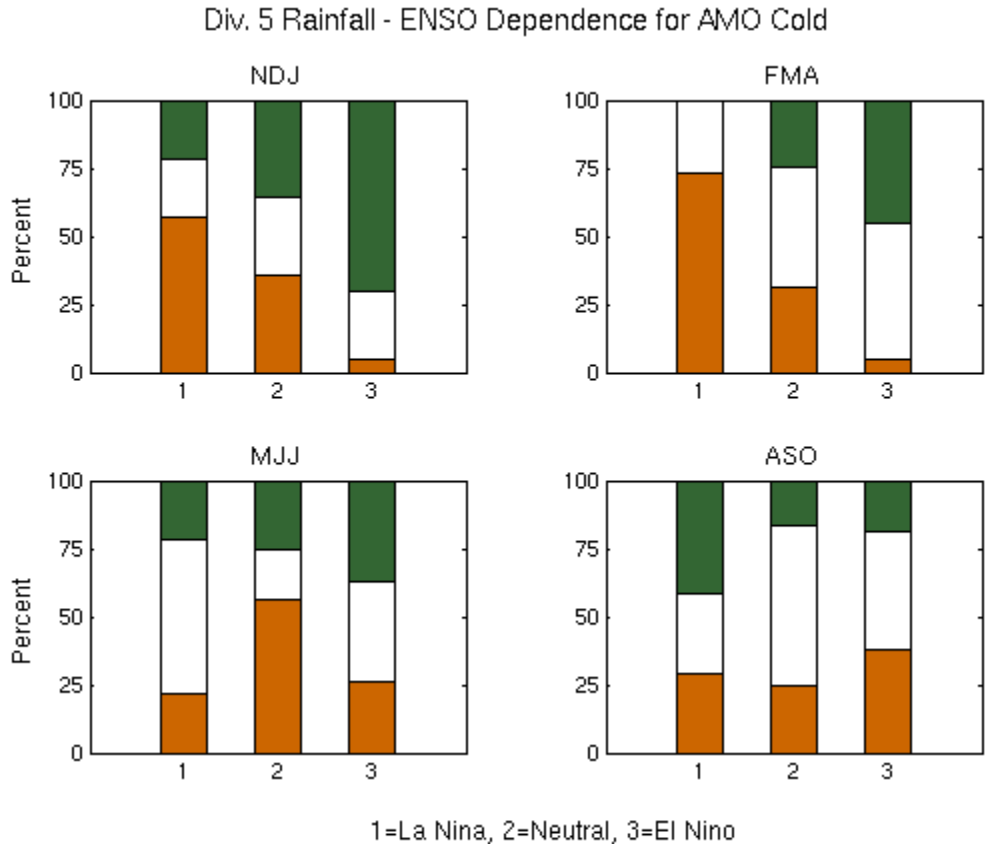

Fig. 46. Contingency plots (in percent) from terciles of Division 5 precipitation and Nino3 index when the AMO is in its cold phase for DJF, FMA, MJJ and ASO.

NDJ

Wet	21	36	70
Neutral	21	29	25
Dry	57	36	5
	La Nina	**Neutral**	**El Nino**

FMA

Wet	0	25	45
Neutral	27	44	50
Dry	73	31	5
	La Nina	**Neutral**	**El Nino**

MJJ

Wet	21	25	37
Neutral	57	19	37
Dry	21	56	26
	La Nina	**Neutral**	**El Nino**

ASO

Wet	39	42	27
Neutral	22	29	33
Dry	39	29	40
	La Nina	**Neutral**	**El Nino**

Table 11. Contingency tables corresponding to the contingency plots shown in Fig. 46. Numbers are in percent.

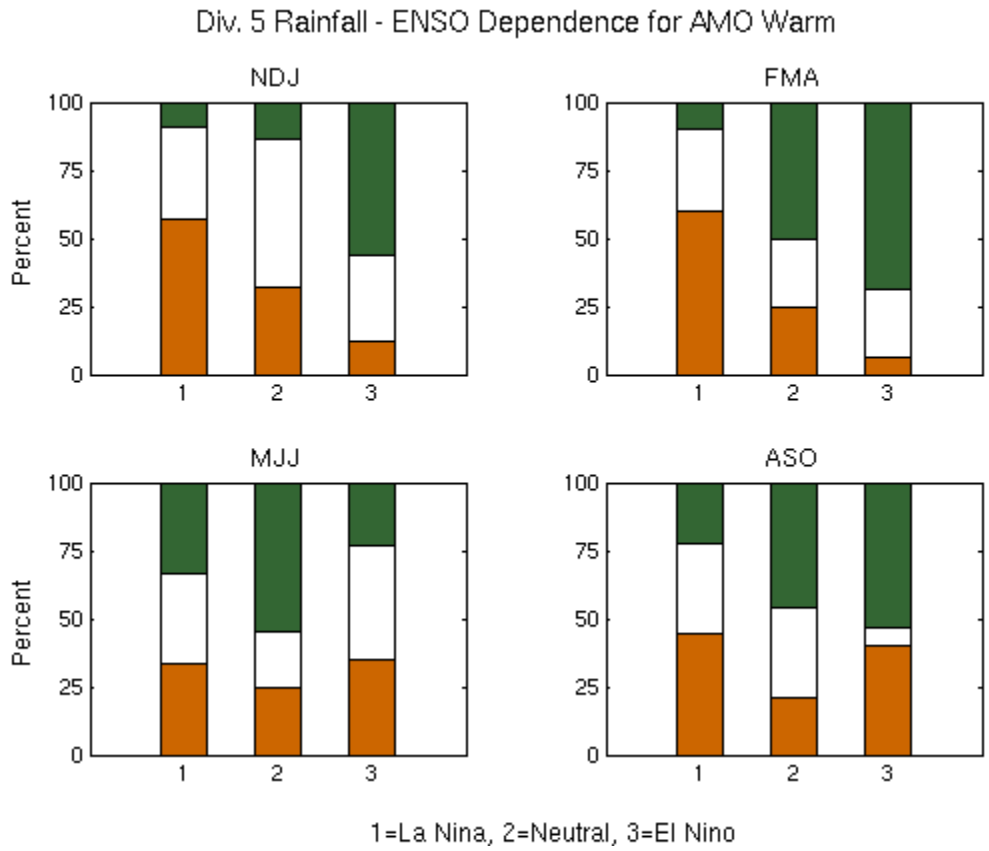

Fig. 47. Contingency plots (in percent) from terciles of Division 5 precipitation and Nino3 index when the AMO is in its warm phase for DJF, FMA, MJJ and ASO.

NDJ

Wet	10	14	56
Neutral	33	55	31
Dry	57	32	13
	La Nina	**Neutral**	**El Nino**

FMA

Wet	10	50	69
Neutral	30	25	25
Dry	60	25	6
	La Nina	**Neutral**	**El Nino**

MJJ

Wet	33	55	24
Neutral	33	20	41
Dry	33	25	35
	La Nina	**Neutral**	**El Nino**

ASO

Wet	22	46	53
Neutral	33	33	7
Dry	44	21	40
	La Nina	**Neutral**	**El Nino**

Table 12. Contingency tables corresponding to the contingency plots shown in Fig. 47. Numbers are in percent.

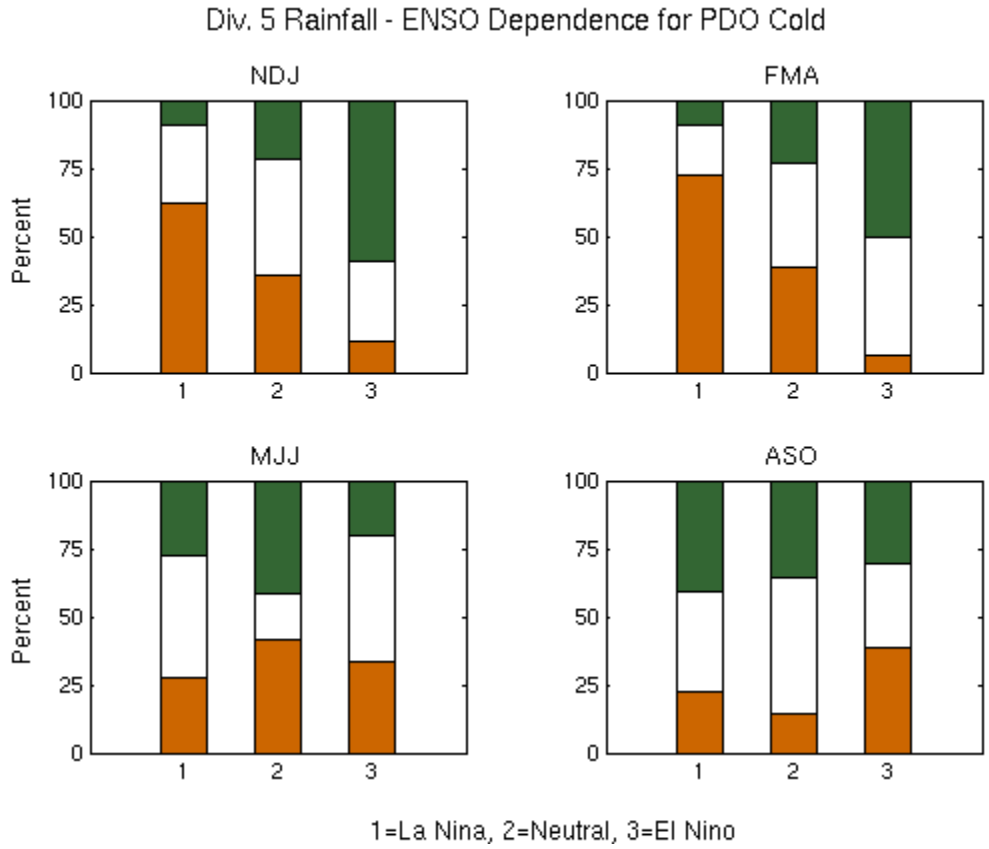

Fig. 48. Contingency plots (in percent) from terciles of Division 5 precipitation and Nino3 index when the PDO is in its cold phase for DJF, FMA, MJJ and ASO.

NDJ

Wet	10	21	59
Neutral	29	43	29
Dry	62	36	12
	La Nina	**Neutral**	**El Nino**

FMA

Wet	9	23	50
Neutral	18	38	44
Dry	73	38	6
	La Nina	**Neutral**	**El Nino**

MJJ

Wet	27	42	20
Neutral	45	17	47
Dry	27	42	33
	La Nina	**Neutral**	**El Nino**

ASO

Wet	41	36	31
Neutral	36	50	31
Dry	23	14	38
	La Nina	**Neutral**	**El Nino**

Table 13. Contingency tables corresponding to the contingency plots shown in Fig. 48. Numbers are in percent.

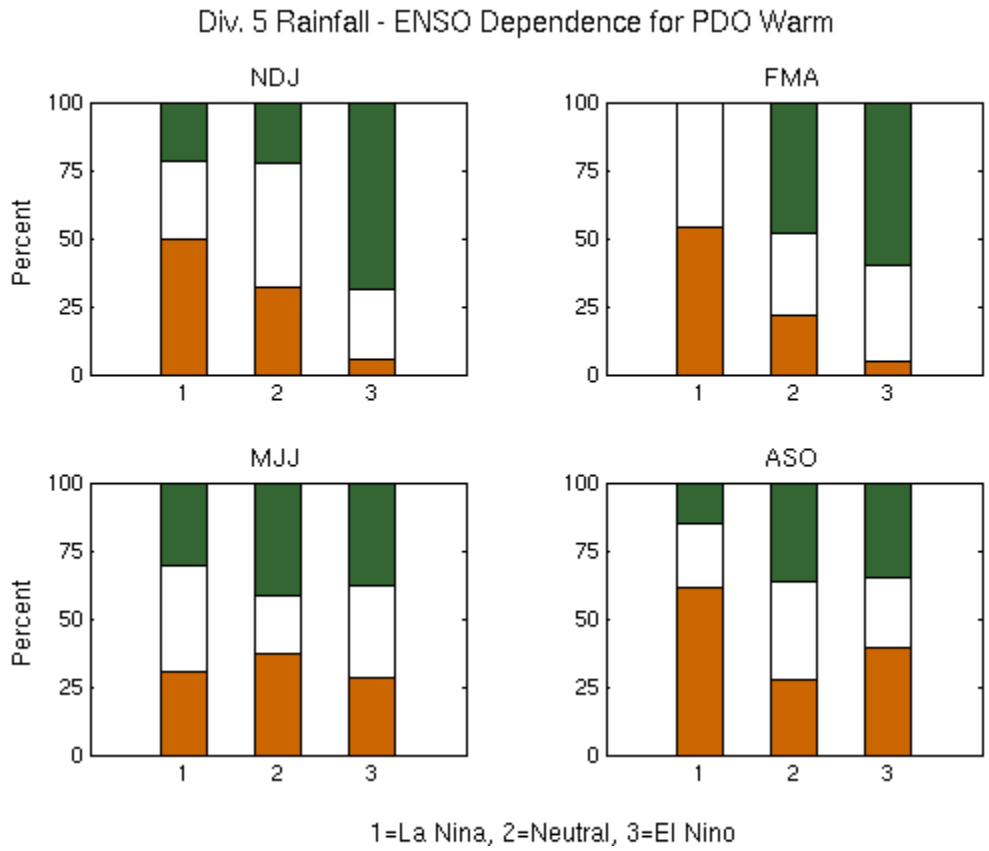

Fig. 49. Contingency plots (in percent) from terciles of Division 5 precipitation and Nino3 index when the PDO is in its warm phase for DJF, FMA, MJJ and ASO.

NDJ

Wet	21	23	68
Neutral	29	45	26
Dry	50	32	5
	La Nina	**Neutral**	**El Nino**

FMA

Wet	0	48	60
Neutral	46	30	35
Dry	54	22	5
	La Nina	**Neutral**	**El Nino**

MJJ

Wet	31	42	38
Neutral	38	21	33
Dry	31	38	29
	La Nina	**Neutral**	**El Nino**

ASO

Wet	15	36	35
Neutral	23	36	26
Dry	62	27	39
	La Nina	**Neutral**	**El Nino**

Table 14. Contingency tables corresponding to the contingency plots shown in Fig. 49. Numbers are in percent.

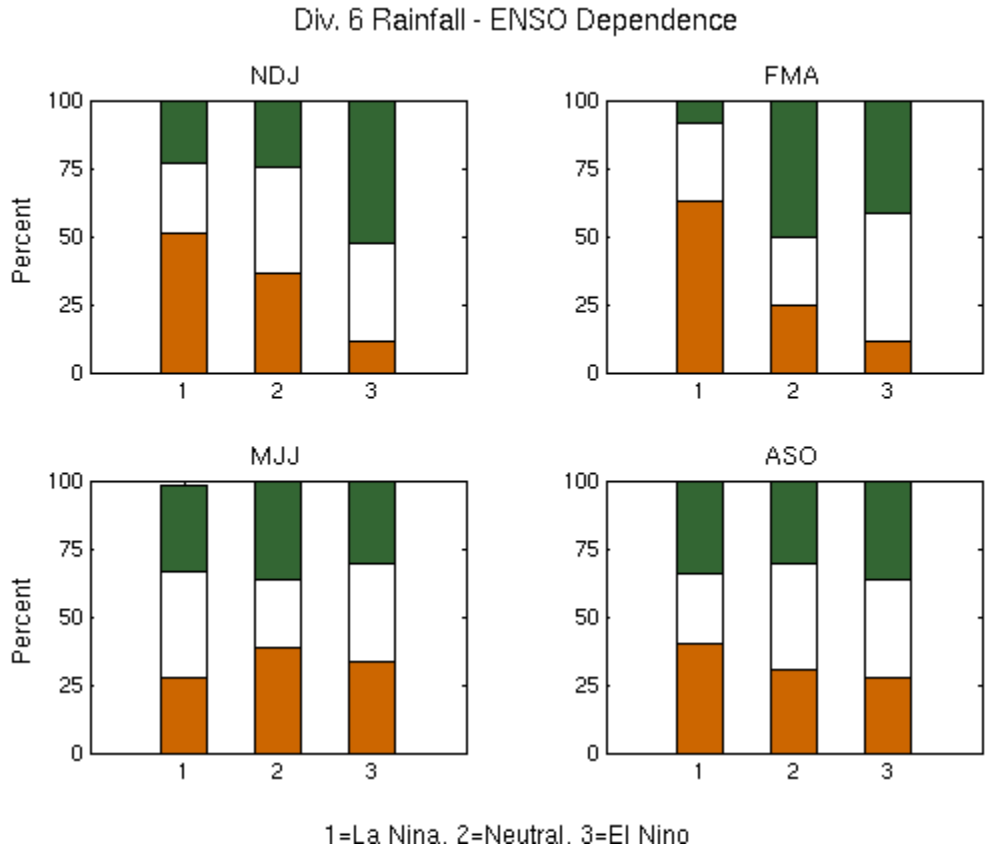

Fig. 50. Contingency plots (in percent) from terciles of Division 6 precipitation and Nino3 index for DJF, FMA, MJJ and ASO.

NDJ

Wet	23	25	53
Neutral	26	39	36
Dry	51	36	11
	La Nina	**Neutral**	**El Nino**

FMA

Wet	9	50	42
Neutral	29	25	47
Dry	63	25	11
	La Nina	**Neutral**	**El Nino**

MJJ

Wet	31	37	31
Neutral	39	25	36
Dry	28	39	33
	La Nina	**Neutral**	**El Nino**

ASO

Wet	34	31	36
Neutral	26	39	36
Dry	40	31	28
	La Nina	**Neutral**	**El Nino**

Table 15. Contingency tables corresponding to the contingency plots shown in Fig. 50. Numbers are in percent.

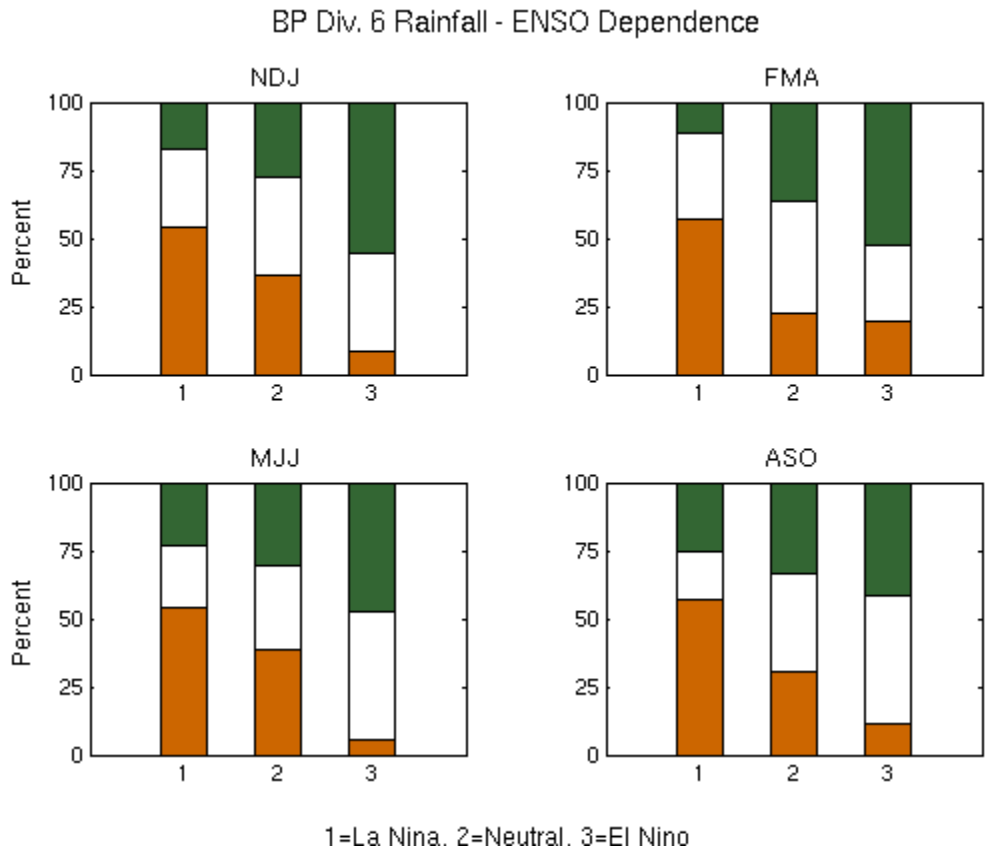

Fig. 51. Contingency plots (in percent) from terciles of band-passed (BP) Division 6 precipitation and Nino3 index for DJF, FMA, MJJ and ASO.

NDJ

Wet	17	28	56
Neutral	29	36	36
Dry	54	36	8
	La Nina	**Neutral**	**El Nino**

FMA

Wet	11	36	53
Neutral	31	42	28
Dry	57	22	19
	La Nina	**Neutral**	**El Nino**

MJJ

Wet	23	31	47
Neutral	23	31	47
Dry	54	39	6
	La Nina	**Neutral**	**El Nino**

ASO

Wet	26	33	42
Neutral	17	36	47
Dry	57	31	11
	La Nina	**Neutral**	**El Nino**

Table 16. Contingency tables corresponding to the contingency plots shown in Fig. 51. Numbers are in percent.

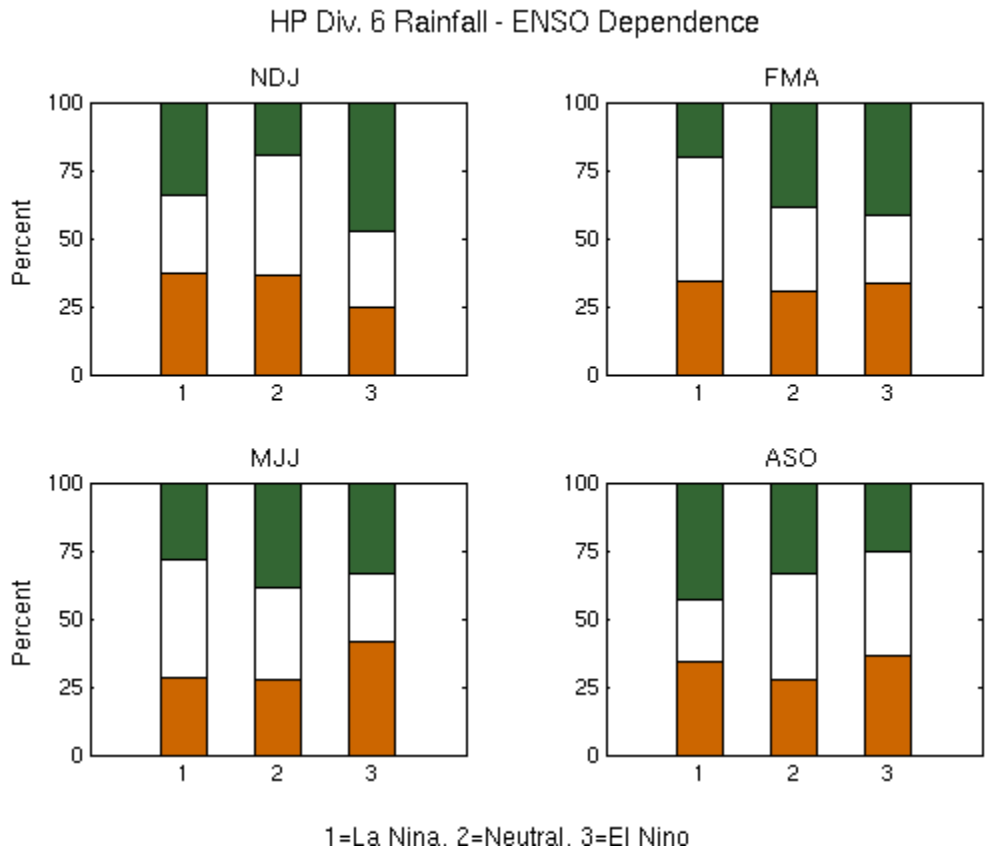

Fig. 52. Contingency plots (in percent) from terciles of high-passed (HP) Division 6 precipitation and Nino3 index for DJF, FMA, MJJ and ASO.

NDJ

Wet	34	19	47
Neutral	29	44	28
Dry	37	36	25
	La Nina	**Neutral**	**El Nino**

FMA

Wet	20	39	42
Neutral	46	31	25
Dry	34	31	33
	La Nina	**Neutral**	**El Nino**

MJJ

Wet	29	39	33
Neutral	43	33	25
Dry	29	28	42
	La Nina	**Neutral**	**El Nino**

ASO

Wet	43	33	25
Neutral	23	39	39
Dry	34	28	36
	La Nina	**Neutral**	**El Nino**

Table 17. Contingency tables corresponding to the contingency plots shown in Fig. 52. Numbers are in percent.

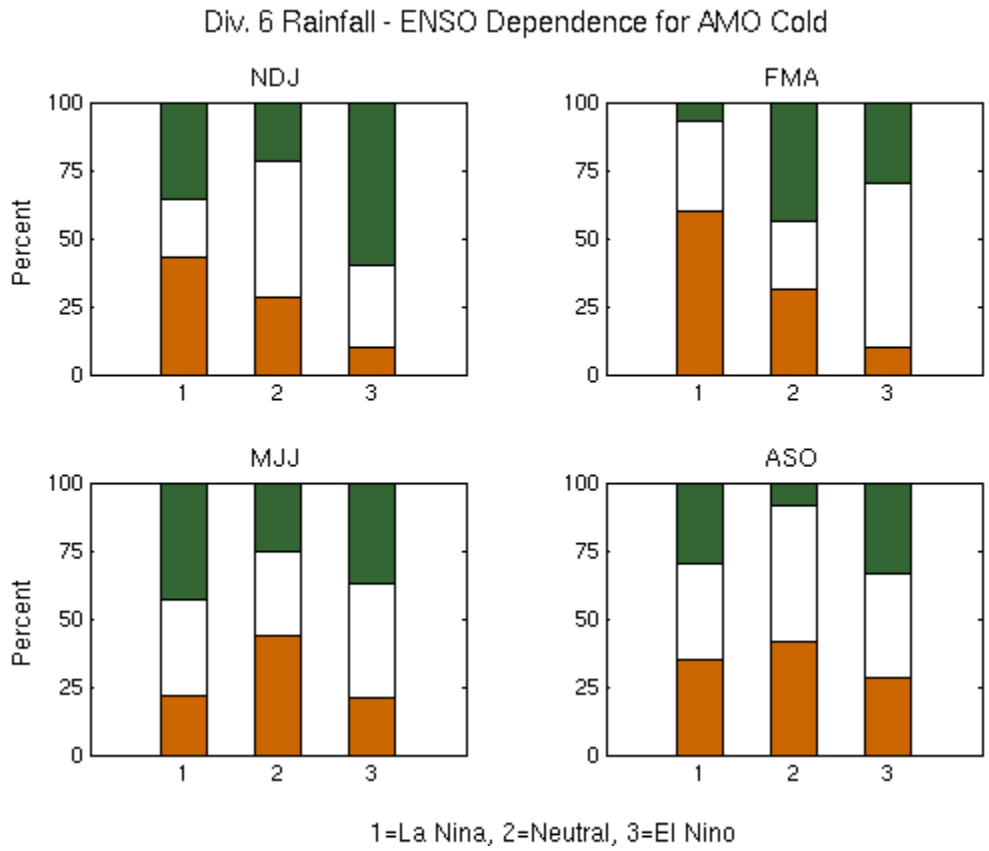

Fig. 53. Contingency plots (in percent) from terciles of Division 6 precipitation and Nino3 index when the AMO is in its cold phase for DJF, FMA, MJJ and ASO.

NDJ

Wet	36	21	60
Neutral	21	50	30
Dry	43	29	10
	La Nina	**Neutral**	**El Nino**

FMA

Wet	7	44	30
Neutral	33	25	60
Dry	60	31	10
	La Nina	**Neutral**	**El Nino**

MJJ

Wet	43	25	37
Neutral	36	31	42
Dry	21	44	21
	La Nina	**Neutral**	**El Nino**

ASO

Wet	29	8	33
Neutral	35	50	38
Dry	35	42	29
	La Nina	**Neutral**	**El Nino**

Table 18. Contingency tables corresponding to the contingency plots shown in Fig. 53 . Numbers are in percent.

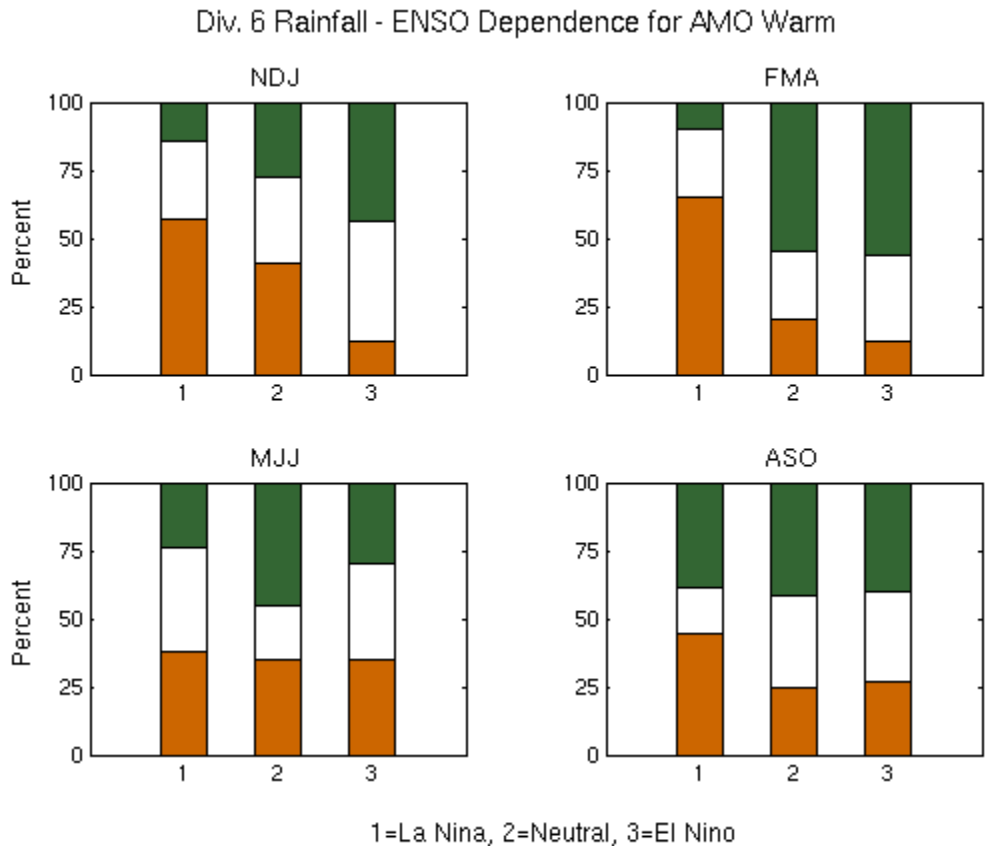

Fig. 54. Contingency plots (in percent) from terciles of Division 6 precipitation and Nino3 index when the AMO is in its warm phase for DJF, FMA, MJJ and ASO.

NDJ

Wet	14	27	44
Neutral	29	32	44
Dry	57	41	13
	La Nina	**Neutral**	**El Nino**

FMA

Wet	10	55	56
Neutral	25	25	31
Dry	65	20	13
	La Nina	**Neutral**	**El Nino**

MJJ

Wet	24	45	29
Neutral	38	20	35
Dry	38	35	35
	La Nina	**Neutral**	**El Nino**

ASO

Wet	39	42	40
Neutral	17	33	33
Dry	44	25	27
	La Nina	**Neutral**	**El Nino**

Table 19. Contingency tables corresponding to the contingency plots shown in Fig. 54. Numbers are in percent.

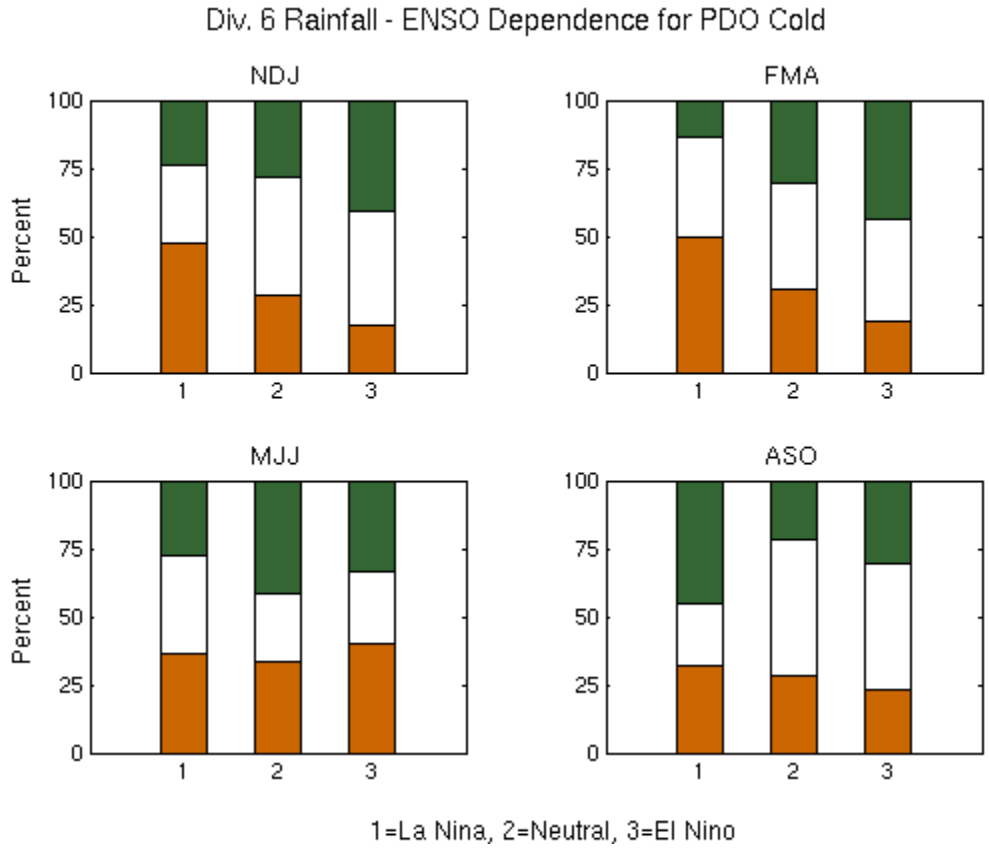

Fig. 55. Contingency plots (in percent) from terciles of Division 6 precipitation and Nino3 index when the PDO is in its cold phase for DJF, FMA, MJJ and ASO.

NDJ

Wet	24	29	41
Neutral	29	43	41
Dry	48	29	18
	La Nina	**Neutral**	**El Nino**

FMA

Wet	14	31	44
Neutral	36	38	38
Dry	50	31	19
	La Nina	**Neutral**	**El Nino**

MJJ

Wet	27	42	33
Neutral	36	25	27
Dry	36	33	40
	La Nina	**Neutral**	**El Nino**

ASO

Wet	45	21	31
Neutral	23	50	46
Dry	32	29	23
	La Nina	**Neutral**	**El Nino**

Fig. 20. Contingency tables corresponding to the contingency plots shown in Fig. 55. Numbers are in percent.

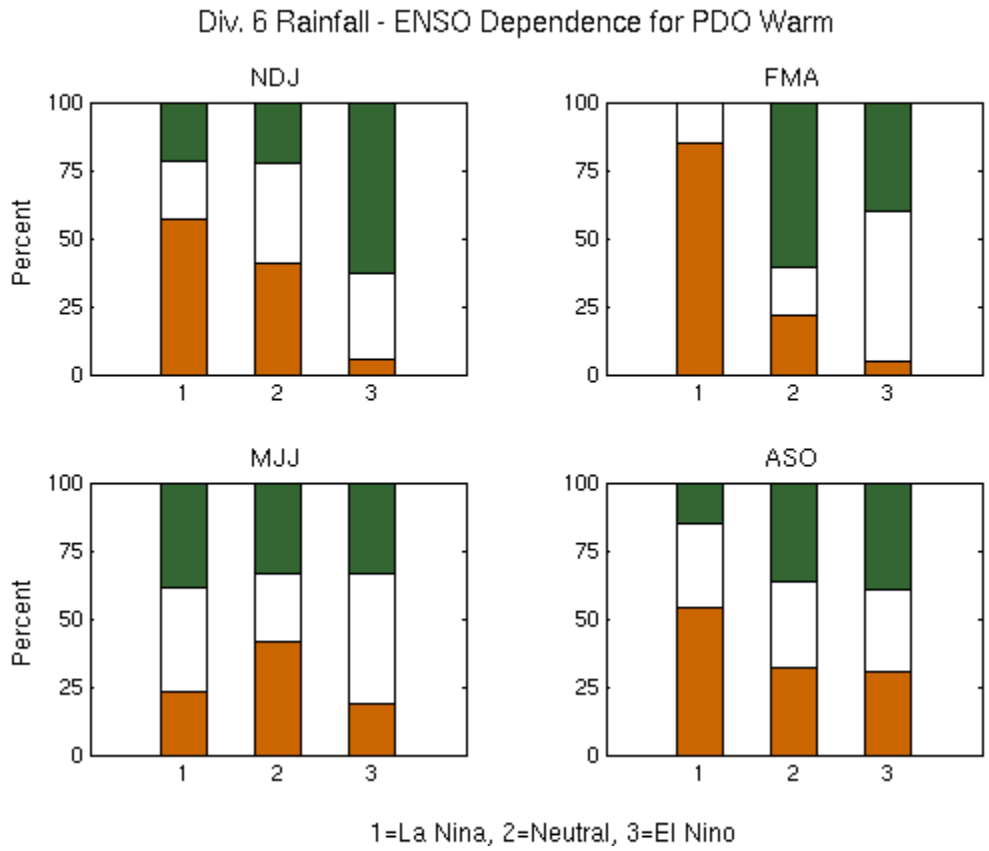

Fig. 56. Contingency plots (in percent) from terciles of Division 6 precipitation and Nino3 index when the PDO is in its warm phase for DJF, FMA, MJJ and ASO.

NDJ

Wet	21	23	63
Neutral	21	36	32
Dry	57	41	5
	La Nina	**Neutral**	**El Nino**

FMA

Wet	0	61	40
Neutral	15	17	55
Dry	85	22	5
	La Nina	**Neutral**	**El Nino**

MJJ

Wet	38	33	33
Neutral	38	25	48
Dry	23	42	19
	La Nina	**Neutral**	**El Nino**

ASO

Wet	15	36	39
Neutral	31	32	30
Dry	54	32	30
	La Nina	**Neutral**	**El Nino**

Table 21. Contingency tables corresponding to the contingency plots shown in Fig. 56. Numbers are in percent.

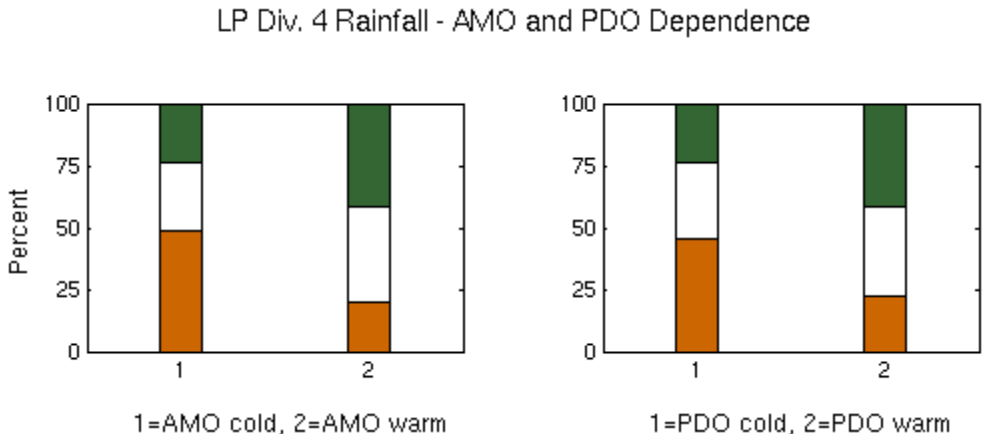

Fig. 57. Contingency plots (in percent) showing terciles of low-passed Division 4 precipitation versus the two phases (warm and cold) of the AMO (left) and PDO (right).

Wet	24	41
Neutral	27	39
Dry	49	20
	AMO-	**AMO+**

Wet	24	42
Neutral	31	36
Dry	46	23
	PDO-	**PDO+**

Table 22. Contingency tables corresponding to the contingency plots in Fig. 57. Numbers are in percent.

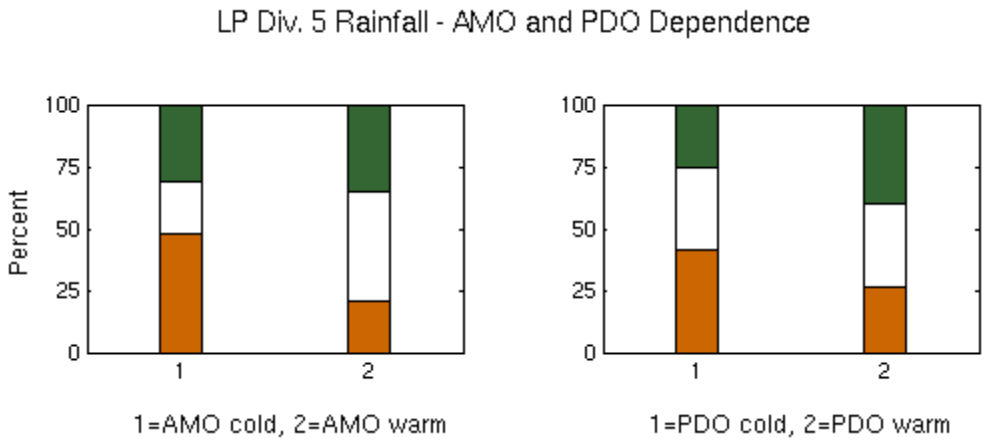

Fig. 58. Contingency plots (in percent) showing terciles of low-passed Division 5 precipitation versus the two phases (warm and cold) of the AMO (left) and PDO (right).

Wet	31	35
Neutral	21	44
Dry	48	21
	AMO-	**AMO+**

Wet	25	40
Neutral	33	33
Dry	41	26
	PDO-	**PDO+**

Table 23. Contingency tables corresponding to the contingency plots in Fig. 58. Numbers are in percent.

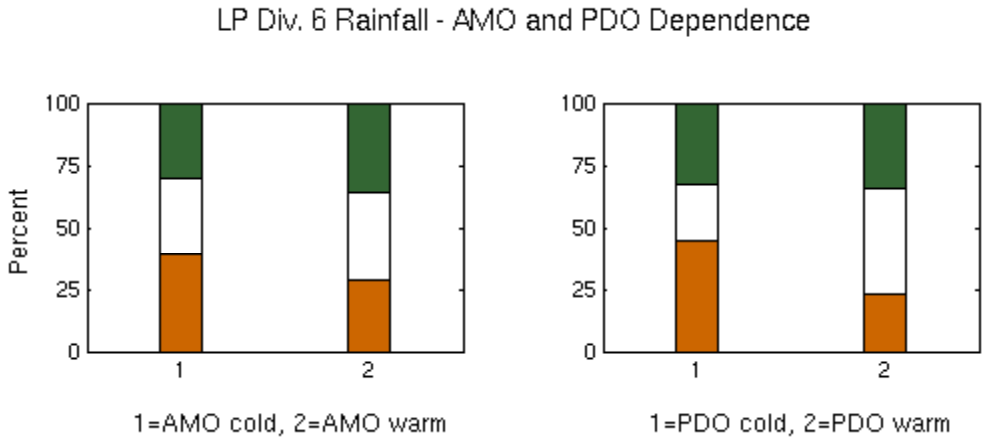

Fig. 59. Contingency plots (in percent) showing terciles of low-passed Division 6 precipitation versus the two phases (warm and cold) of the AMO (left) and PDO (right).

Wet	31	36
Neutral	30	36
Dry	39	28
	AMO-	**AMO+**

Wet	32	34
Neutral	23	43
Dry	45	23
	PDO-	**PDO+**

Table 24. Contingency tables corresponding to the contingency plots in Fig. 59. Numbers are in percent.

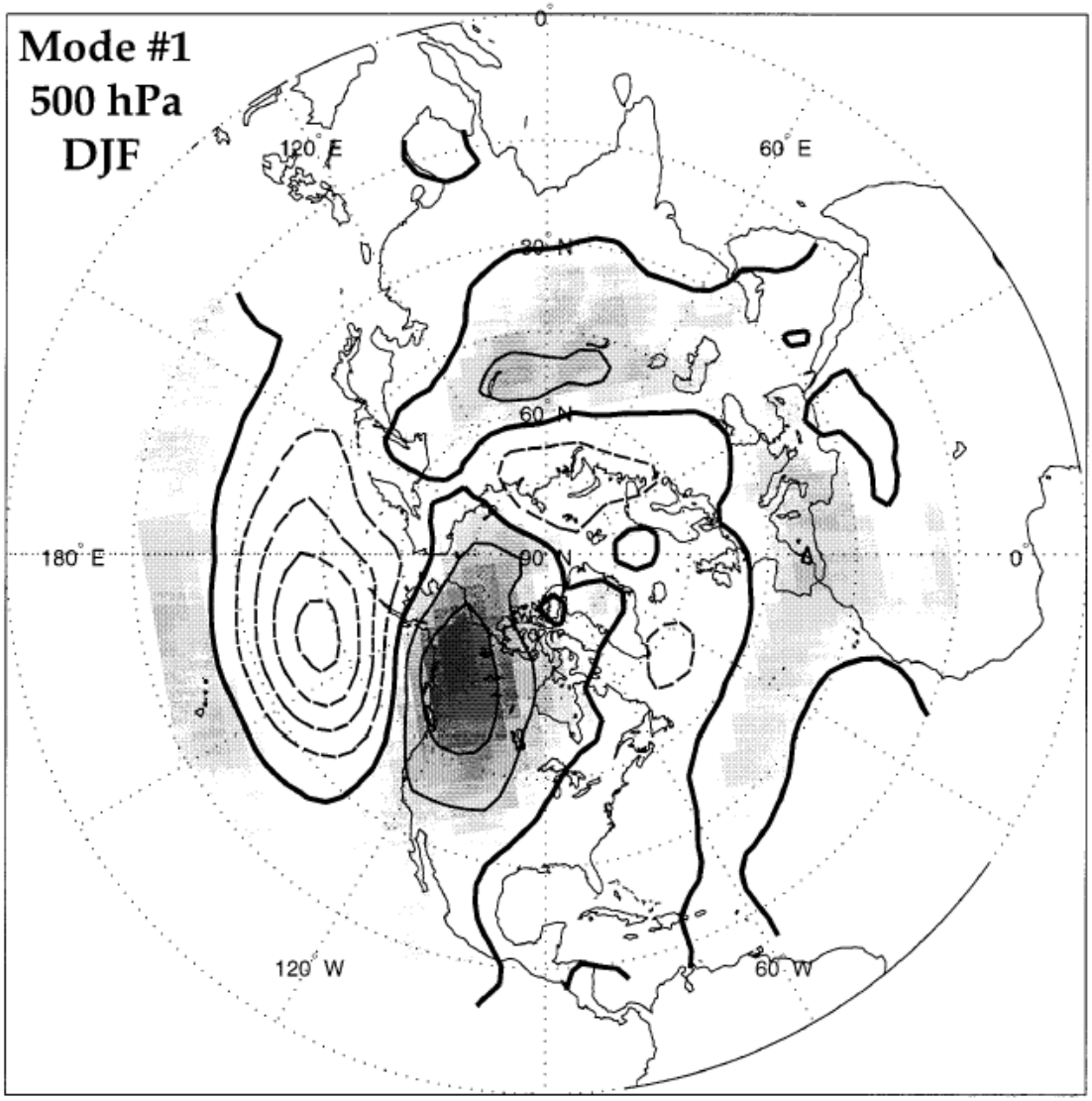

Fig. 60. Half the difference between composite averages of 500-hPa pressure heights with respect to positive and negative values of the Pacific decadal mode of SST anomaly variability. Contour interval is 20 geopotential meters, positive (negative) contours are solid (dashed), and the bold contour is zero. Positive values are shaded (after Enfield and Mestas-Nuñez 1999).

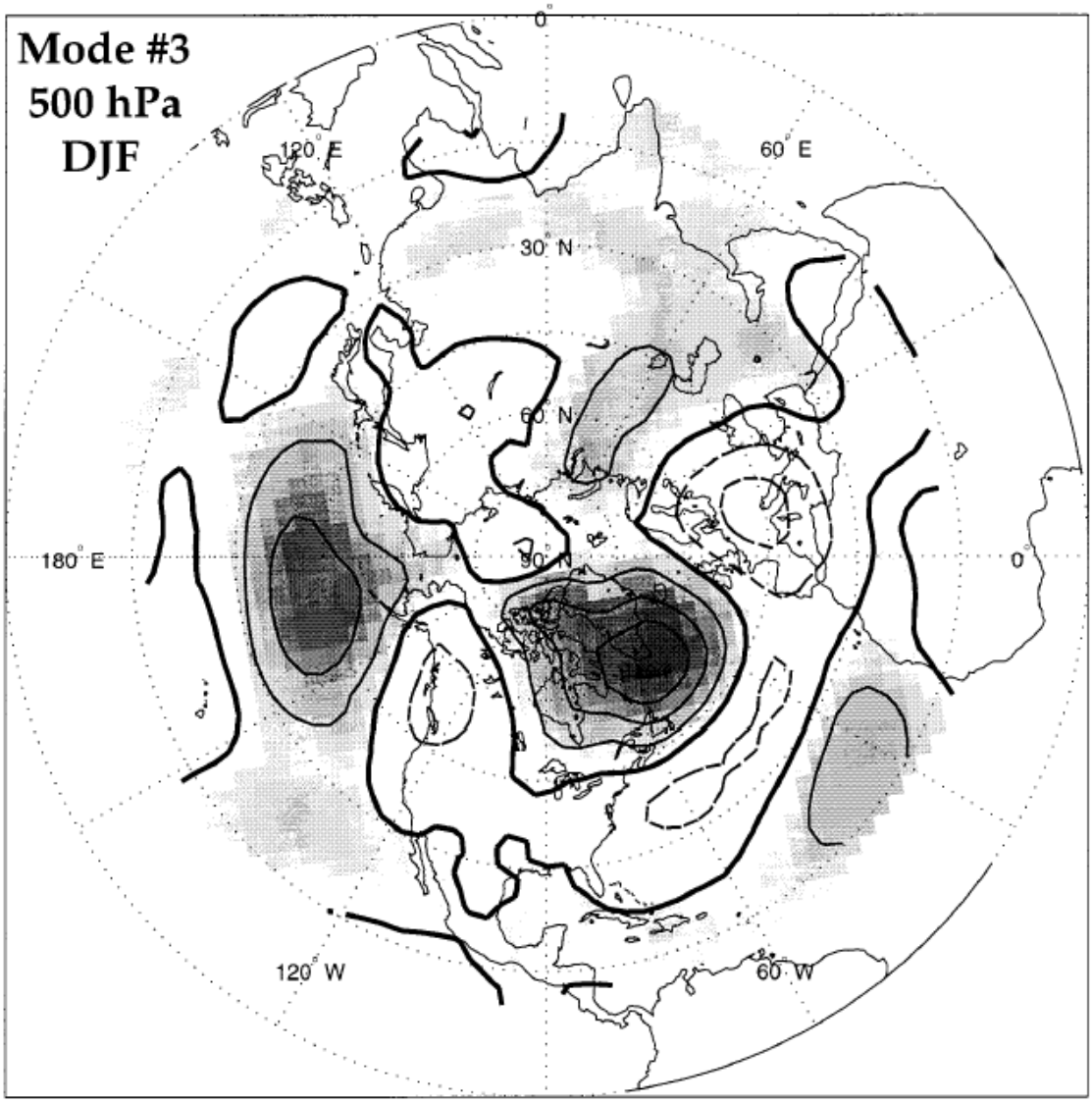

Fig. 61. As in Fig. 60 but with respect to the temporal reconstruction of the Atlantic decadal mode of SST anomaly variability (after Enfield and Mestas-Nuñez 1999).

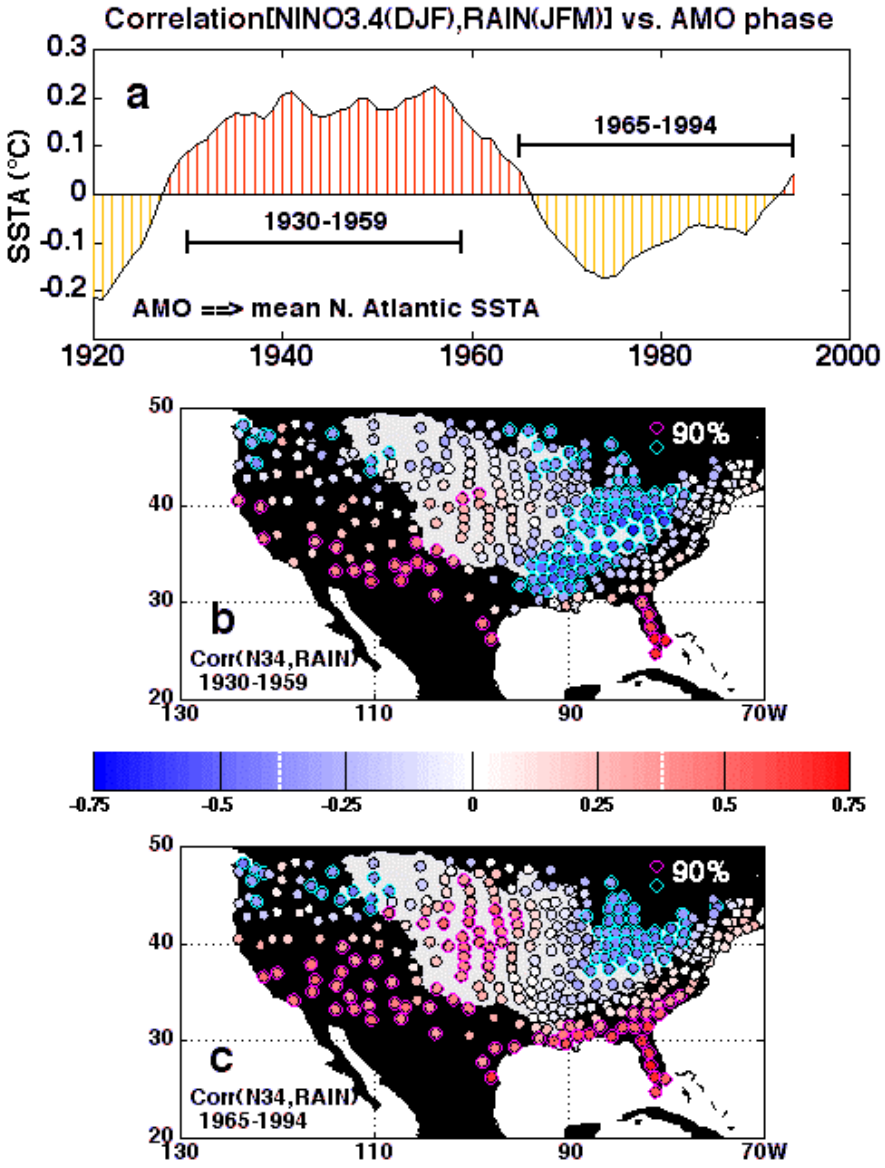

Fig. 62. (a) The Atlantic Multi-decadal Oscillation index showing two contrasting 30-year time periods for the calculation of ENSO-climate connections. (b) The correlation between Nino-3.4 SSTA index for Dec.-Feb. and the unsmoothed divisional rainfall for Jan.-Mar. during the 30 year period 1930-1959. (c) As in b, but for the 30 year period 1965-1994. The Mississippi basin is highlighted by light gray fill. The colorbar applies to both maps (after Enfield et al. 2001, see Appendix A for an abstract of this work).

References

Chelton, D. B., M. G. Schlax, D. L. Witter, and J. G. Richman, 1990: Geosat altimeter observations of the surface circulation of the Southern Ocean. *J. Geophys. Res.*, **95,** 17877-17903.

Cleveland and Devlin, 1988: Locally weighted regression: An approach to regression analysis by local fitting. *J. Am. Stat. Assoc.*, **83,** 596-610.

Enfield, D.B., and A.M. Mestas-Nuñez, 1999: Multiscale variabilities in global sea surface temperatures and their relationships with tropospheric climate patterns. *J. Climate,* **12**, 2719-2733.

Enfield, D.B., A.M. Mestas-Nuñez, and P.J. Trimble, 2001: The Atlantic multidecadal oscillation and its relation to rainfall and river flows in the continental U.S. *Geophys. Res. Lett.,* **28,** 2077-2080.

Hanson, K., and G. A. Maul, 1991: Florida precipitation and the Pacific El Niño, 1895-1989. *Florida Scient.,* **54**, 161-168.

Kaplan, A., M. A. Cane, Y. Kushnir, A. C. Clement, M. B. Blumenthal, and B. Rajagopalan, 1998: Analysis of Global Sea Surface Temperatures 1856-1991. *J. Geophys. Research*, **103,** 18,567-18,589.

Landsea, C. W., 2000: El Niño/Southern Oscillation and the Seasonal Predictability of Tropical Cyclones. In El Niño and the Southern Oscillation: Multiscale Variability and Global and Regional Impacts, H.F. Diaz and V. Markgraf, Cambridge University Press, p.149-181.

Mestas-Nuñez, A.M., and D.B. Enfield, 1999: Rotated global modes of non-ENSO sea surface temperature variability. *J. Climate,* **12**, 2734-2746.
Mestas-Nuñez, A.M and D.B. Enfield, 2001: Eastern Equatorial Pacific SST Variability: ENSO and Non-ENSO Components and their Climatic Associations. *J. Climate*, **14**, 391-402.

Trenberth, K.E., 1998: Progress during TOGA in understanding and modeling global teleconnections associated with tropical sea surface temperatures. *J. Geophys. Research*, **103,** 14,291-14,324.

Wang, C. and D. B. Enfield, 2001: The Tropical Western Hemisphere warm pool. *Geophys. Res. Lett.*, **28,** 1635-1638.

Wang, C. and D. B. Enfield, 2003: A further study of the tropical Western Hemisphere warm pool. *J. Climate*, submitted.

Appendix A

The Atlantic Multidecadal Oscillation and its Relation to Rainfall and River Flows in the Continental U.S.

David B. Enfield[1], Alberto M. Mestas-Nuñez[2] and Paul J. Trimble[3]

(*Geophysical Research Letters*, Volumen 28, Number 10, May 15, 2001)

[1] NOAA Atlantic Oceanographic and Meteorological Laboratory, Miami, Florida.

[2] Cooperative Institute for Marine and Atmospheric Studies, University of Miami, Miami, Florida

[3] South Florida Water Management District, West Palm Beach, Florida

Abstract. North Atlantic sea surface temperature for 1856-1999 contain a 65-80 year cycle with a 0.4 ˚C range, referred to as the Atlantic Multidecadal Oscillation (AMO) by *Kerr* [2000]. AMO warm phases occurred during 1860-1880 and 1940-1960, and cool phases during 1905-1925 and 1970-1990. The signal is global in scope, with a positively correlated co-oscillation in parts of the North Pacific, but it is most intense in the North Atlantic and covers the entire basin there. During AMO warmings, most of the United States sees less than normal rainfall, including Midwest droughts in the 1930s and 1950s. Between AMO warm and cool phases, Mississippi River outflow varies by 10% while the inflow to Lake Okeechobee, Florida varies by 40%. The geographical pattern of variability is influenced mainly by changes in summer rainfall. The winter patterns of interannual rainfall variability associated with El Niño-Southern Oscillation are also significantly changed between AMO phases.

Appendix B
Scientific Presentations

The Atlantic Multidecadal Oscillation and its Relationship to Rainfall and River Flows in the Continental U.S. (D. B. Enfield and A. M. Mestas-Nuñez). Greater Everglades Ecosystem Restoration Science Conference, December 11-15, 2000, Naples, Florida.

The multidecadal signal in global temperatures and its associated land-climate impacts. (A. M. Mestas-Nuñez and D. B. Enfield). 16th Biennial Conference of the Estuarine `Research Federation, November 4-8, 2001, St. Pete Beach, Florida.

Atlantic multidecadal variability and inter-american rainfall (D. B. Enfield and A. M. Mestas-Nuñez). American Geophysical Union 2001 Fall Meeting, 10-14 December, 2001, San Francisco, California